TECHNICKÁ UNIVERZITA V LIBERCI

FAKULTA TEXTILNÍ

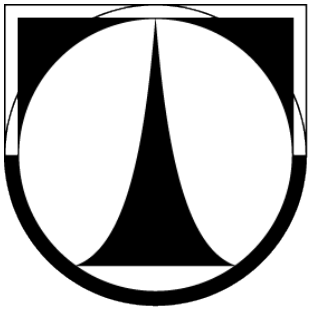

MONITOROVÁNÍ STRUKTURY TEXTILNÍCH ÚTVARŮ

HABILITAČNÍ PRÁCE

Souhrn uveřejněných vědeckých a odborných prací doplněný komentářem

Ing. Maroš Tunák, Ph.D.

Prosinec 2011

Obsah

1 Souhrn uveřejněných vědeckých a odborných prací

1.1 Publikace v recenzovaných časopisech

[1] Tunák, M. and Linka, A. Analysis of Planar Anisotropy of Fibre Systems by using 2D Fourier Transform. *Fibres and Textiles in Eastern Europe*, **15**(5-6), 2007, pp. 86–90. ISSN: 1230-3666. IF=0.629.

[2] Tunák, M. and Linka, A. Directional Defects in Fabrics. *Research Journal of Textiles and Apparel*, **12**(2), 2008, pp. 13–22. ISSN: 1560-6074. Excellent Paper Award 2008.

[3] Tunák, M., Linka, A., and Volf, P. Automatic Assessing and Monitoring of Weaving Density. *Fibres and Polymers*, **10**(6), 2009, pp. 830–836. ISSN: 1229-9197. IF=0.832.

[4] Tunák, M., Linka, A., and Volf, P. Load-sharing and Monte Carlo Models of Defects in a Bundle of Fibres. *Composites Science and Technology*, **69**(9), 2009, 1417–1421. ISSN: 0266-3538. IF=2.856.

[5] Tunák, M., Bajzík, V., and Testik, M. Monitoring Chenille Yarn Defects using Image Processing with Control Charts. *Textile Research Journal*, **81**(13), 2011, 1344–1353. ISSN: 0040-5175. IF=1.102.

1.2 Publikace v ostatních časopisech

[6] Tunák, M. and Linka, A. Methods for Recognition of Woven Structure Defects. *World Journal of Engineering*, **5**(1), 2008, 2 pages. ISSN: 1708-5284.

[7] Kula, J., Tunák, M., and Linka, A. Real-time Quality Control of Fabrics based on Multivariate Control Charts. *World Journal of Engineering*, **7**(1), 2010, 9 pages. ISSN: 1708-5284.

[8] Kula, J., Tunák, M., and Linka, A. Inspection System of Fabric based on Texture Segmentation utilizing Gabor Filters. *World Journal of Engineering*, **7**(1), 2010, 8 pages. ISSN: 1708-5284.

1.3 Příspěvek ve sborníku mezinárodní konference

[9] Tunák, M. and Linka, A. Applying Spectral Analysis to Automatic Inspection of Weaving Density. In: *STRUTEX 2004, Proceedings of 11th International Conference on Structure and Structural Mechanics of Textiles*. Liberec, Czech Republic, 2004, pp. 133–140. isbn: 80-7372-002-7.

[10] Tunák, M. and Linka, A. Fourier Analysis of Woven Composite Structures. In: *ICCE 12, 12th International Conference on Composites or Nano Engineering*. Tenerife, Spain, 2005.

[11] Tunák, M. and Linka, A. Planar Anisotropy of Fiber System by using 2D Fourier Transform. In: *STRUTEX 2005, Proceedings of 12th International Conference on Structure and Structural Mechanics of Textiles*. Liberec, Czech Republic, 2005, pp. 121–127. isbn: 80-7372-002-7.

[12] Tunák, M., Linka, A., and Volf, P. Stochastic Simulation of Deformation in Fabrics as Composite Reinforcement. In: *ECCM 12, 12th European Conference on Composite Materials*. Biarritz, France, 2006.

[13] Tunák, M. and Linka, A. Simulation and Recognition of Common Fabric Defects. In: *STRUTEX 2006, Proceedings of 13th International Conference on Structure and Structural Mechanics of Textiles*. Liberec, Czech Republic, 2006, pp. 363–370. isbn: 80-7372-135-X.

[14] Krupincová, G. and Tunák, M. Practical Approach to the Yarn Hairiness Determination. In: *CIRAT-2, 2nd International Conference of Applied Research on Textile*. Monastyr, Tunisia, 2006.

[15] Tunák, M., Linka, A., and Kalabishka, Y. Directional Defects in Fabrics. In: *TEXSCI 06, 6th International Conference Textile Science*. Liberec, Czech Republic, 2007. isbn: 978-80-7372-207-4.

[16] Tunák, M. and Linka, A. Methods for Recognition of Woven Structure Defects. In: *MMR07, Mathematical Methods in Reliability*. Glasgow, UK, 2007.

[17] Tunák, M. and Linka, A. Methods for Recognition of Woven Structure Defects. In: *ICCE 15, 15th International Conference on Composites or Nano Engineering*. Haikou, China, 2007.

[18] Tunák, M. and Linka, A. Analysis of Planar Anisotropy of Fibre Systems by using 2D Fourier Transform. In: *CEC 2007, 5th Central European Conference Fibre-grade Polymers, Chemical Fibres and Special Textiles*. Cracow – Bielsko-Biala, Poland, 2007.

[19] Tunák, M. et al. Automatic Detection of Fabric Defects. In: *JSM Proceedings, Classification Models with Applications to Quality Section, American Statistical Association*. New York, USA, 2009.

[20] Linka, A. and Tunák, M. Automatic On-line Detection of Defects in Fabrics. In: *EURISBIS09, European Regional Meeting of the International Society for Business and Industrial Statistics*. Cagliari, Italy, 2009.

[21] Kula, J., Tunák, M., and Linka, A. Real-time Defect Detection of Fabrics. In: *SMRLO10, Stochastic Models in Reliability Engineering, Life Sciences and Operation Management*. Beer Sheba, Israel, 2010.

[22] Kula, J., Tunák, M., and Linka, A. Real-time Quality Control of Fabrics based on Multivariate Control Charts. In: *TEXSCI 07, 7th International Conference Textile Science*. Liberec, Czech Republic, 2010, pp. 190–198. isbn: 978-80-7372-635-5.

[23] Techniková, L. and Tunák, M. Weaving Density Evaluation with the Aid of Image Analysis. In: *STRUTEX 2010, Proceedings of 17th International Conference on Structure and Structural Mechanics of Textiles*. Liberec, Czech Republic, 2010. isbn: 978-80-7372-664-5.

[24] Kula, J., Linka, A., and Tunák, M. Inspection System of Fabric based on Texture Segmentation utilizing Gabor Filters. In: *DEIT 2011, International Conference on Data Engineering and Internet Technology*. Bali, Indonesia, 2011. isbn: 978-1-4244-8581-9.

1.4 Příspěvek ve sborníku domácí konference

[25] Tunák, M. and Linka, A. Applying Spectral Analysis to Automatic Inspection of Weaving Density. In: *3mi, Moderní matematické metody v inženýrství*. Dolní Lomná, Czech Republic, 2006, pp. 205–211. isbn: 80-248-1224-X.

[26] Tunák, M. and Linka, A. Planar Anisotropy of Fibre Systems by using Matlab Image Processing Toolbox. In: *TCP2006, Technical Computing Prague 2006*. Prague, Czech Republic, 2006, 8 pages. isbn: 80-7080-616-8.

[27] Linka, A., Tunák, M., and Volf, P. Simulation and Recognition of Common Fabric Defects. In: *REQUEST06, Reliability, Quality and Estimation*. Prague, Czech Republic, 2007, pp. 239–249. isbn: 978-80-01-03709-6.

[28] Linka, A. and Tunák, M. Dostava tkaniny. In: *2THETA, Zajištění kvality analytických výsledků*. Komorní Lhotka, Czech Republic, 2007, pp. 172–178. isbn: 978-80-86380-37-7.

[29] Kula, J., Linka, A., and Tunák, M. Automatická vizuální kontrola textilních procesů. In: *REQUEST09, Reliability, Quality and Estimation*. Liberec, Czech Republic, 2009.

[30] Kula, J., Majdiak, P., and Tunák, M. Tvorba vzorovaných tapet pomocí rovinných grup symetrie. In: *3mi, Moderní matematické metody v inženýrství*. Dolní Lomná, Czech Republic, 2010, pp. 67–71. isbn: 978-80-248-2342-3.

[31] Bajzík, V. and Tunák, M. Detekce vad na žinylkové přízi pomocí regulačních diagramů. In: *2THETA, Zajištění kvality analytických výsledků*. Komorní Lhotka, Czech Republic, 2010, pp. 87–97. isbn: 978-80-86380-51-3.

1.5 Realizované technické dílo

[32] Kula, J., Tunák, M., and Linka, A. Zařízení pro vizuální monitorování kvality textilních struktur. Prototyp. 2009.

2 Komentář k publikacím

2.1 Úvod

V první kapitole je uveden souhrn uveřejněných vědeckých a odborných prací, ve kterých je autor této habilitační práce hlavním autorem, nebo spoluautorem. Souhrn prací obsahuje:

- 5 publikací v recenzovaných časopisech ([1–5]),
- 3 publikace v ostatních časopisech ([6–8]),
- 16 příspěvků ve sbornících mezinárodních konferencí ([9–24]),
- 7 příspěvků ve sbornících národních konferencí ([25–31]),
- 1 realizované technické dílo ([32]).

V přílohách k habilitační práci je uvedeno 8 vybraných publikací v zahraničních časopisech. Z toho 4 práce byly publikovány v časopisech s "Impact Factorem", jedna byla publikována v recenzovaném zahraničním časopise a obdržela ocenění "Excellent Paper Award 2008", ostatní byly publikovány v nerecenzovaném zahraničním časopise. Publikované práce je možné rozdělit do několika okruhů:

1. Směrová orientace vlákenných systémů,
2. Detekce defektů v plošných textiliích,
3. Automatický odhad dostavy tkaniny,
4. Monitorování kvality žinylkové příze,
5. Simulace deformace textilní výztuže.

Uvedené práce jsou tematicky přímo zaměřené na monitorování struktury textilních útvarů, ať plošných nebo lineárních, a to především s ohledem na kvalitu těchto útvarů. Většina z publikovaných prací je založena na použití metod obrazové analýzy pro monitorování struktury textilních útvarů.

Práce z okruhu směrové orientace vlákenných systémů se zabývají stanovením odhadu strukturní anizotropie nebo odhadu preference směrů textilních útvarů, který je důležitou součástí kvantitativního měření v textilní metrologii. U netkaných plošných textilních útvarů směrové uspořádání vláken zásadně ovlivňuje uspořádání vlákenného materiálu v ploše a s tím spojené mechanické a následně užitné vlastnosti těchto útvarů. Stanovením odhadu strukturní anizotropie se zabývá práce [1] uveřejněna v časopise *Fibers and Textiles in Eastern Europe* (viz Příloha 1).

Publikace z oblasti detekce defektů ve tkaninách se věnují tematice monitorování výskytu vizuálních a strukturních vad, jejich klasifikaci a stanovení polohy vady na plošném útvaru, což je důležitou součástí monitorování kvality v textilním průmyslu. V uvedených pracích byly navrženy algoritmy detekce vycházející ze statistického

a spektrálního přístupu k analýze textur. Metoda využívající pro automatickou detekci defektů statistické charakteristiky druhého řádu je navržena v práci [2] publikované v časopise *Research Journal of Textile and Apparel* (viz Příloha 2) a dále v práci [6] zveřejněné v *World Journal of Engineering* (viz Příloha 6). Automatická detekce, která je založená na spektrálních charakteristikách vycházejících z výkonového spektra byla uveřejněna v článku [8] v *World Journal of Engineering* (viz Příloha 8). K vlastnímu monitorování defektů je pak využita technika současného monitorování více charakteristik založená na vícerozměrných regulačních diagramech Hotellingova typu.

Stanovení dostavy tkaniny patří mezi rutinní činnosti v textilní metrologii. Za účelem stanovení odhadu dostavy tkaniny byly navrženy algoritmy pro automatické stanovení dostavy z obrazu tkaniny. Metodiku lze aplikovat i na detekci vad ve tkaninách způsobených změnou dostavy tkaniny opět s využitím nástrojů, které poskytuje statistická regulace procesu. Výsledky byly uveřejněny v časopise *Fibres and Polymers* (viz [3], Příloha 3).

V oblasti monitorování struktury lineárních textilních útvarů byla také řešena úloha použití regulačních diagramů pro detekci vad na žinylkové přízi. Mezi důležité parametry žinylkové příze patří stejnoměrná výška vlasu po celé délce příze, jelikož má silný vliv na její vzhled. Výška vlasové příze je monitorovanou charakteristikou jakosti. Modifikované EWMA regulační diagramy proto byly implementovány jako nástroj k monitorování a detekci defektů na tomto typu příze. Diagramy pomohly úspěšně odhalit různé typy běžných defektů vyskytujících se v přízi. Výsledky jsou uvedeny v časopisu *Textile Research Journal* (viz [5], Příloha 5).

Dále byly řešeny otázky kvalitativních parametrů textilních kompozitních výztuží a jejich chování při zatěžování. Textilní výztuž je modelována jako náhodné pole. V rámci modelování kompozitních výztuží byla studována i otázka modelování pevnosti svazku vláken při postupném zatěžování, jež je obdobou stanovení spolehlivosti systému složeného z paralelních komponent. Pro modelování byl použit Danielsův model a nástroje z teorie čítacích procesů. Výsledky získané simulací byly použity pro simulaci defektů textilní výztuže kompozitu a publikovány v *Composite Science and Technology* (viz [4], Příloha 4).

Habilitační práce obsahuje podrobný komentář k vybraným časopiseckým publikacím, který je rozčleněn podle jednotlivých okruhů. Závěrem je provedeno zhodnocení výsledků práce a doporučení pro další práci v oblasti monitorování struktury textilních útvarů.

2.2 Směrová orientace vlákenných systémů

Měření směrové orientace nebo odhad strukturní anisotropie objektových systémů na základě digitálních obrazů je důležitou součástí kvantitativního měření v textilní metrologii. Objekty rozumíme ty části obrazu, které nás z hlediska dalšího zpracování zajímají a odpovídají konkrétním objektům zobrazovaného světa. Objekty by měly být v kontrastu s pozadím obrazu (gradient obrazové funkce na hranici objektu a pozadí). V textilní praxi můžeme za objekty považovat vlákna, příze, řezy vláken a pod., systémy obsahující objekty mohou být rouna, vlákenné vrstvy, tkaniny, pleteniny, netkané textilie a např. nanovlákenné vrstvy. V současné době je zkoumání směrových vlastností prováděno převážně manuálně nebo s použitím specializovaného softwaru, kde odhad orientace je zatížen subjektivním pohledem.

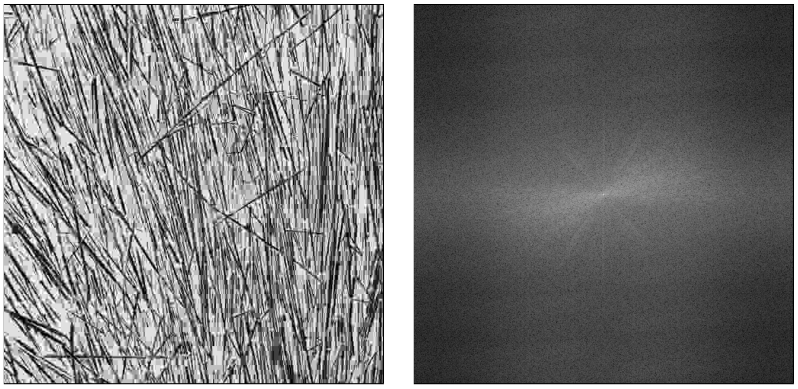

(a) (b)

Obrázek 2.1: (a) Brodatzova textura (D15), (b) odpovídající výkonové spektrum.

Charakteristikou anizotropie je úhlová hustota délek nitě $f(\alpha)$ směřujících do úhlového rozmezí $\alpha \pm \alpha/2$. Funkce $f(\alpha)$ se označuje jako směrová růžice. Experimentální grafická metoda pro odhad $f(\alpha)$ je popsaná v práci *Rataje a Saxla* [33]. Metoda využívá síť úhlů $\alpha_1, ..., \alpha_n$, umístěných na povrch sledovaného systému k sestrojení průsečíkové růžice (stanovené z počtu průsečíků sítě a vlákenných objektů). Směrová růžice je pak získána z průsečíkové růžice pomocí grafické konstrukce Steinerova kompaktu. Metoda je časově náročná a podle autorů i podle experimentů nestabilní, pokud je počet úhlů větší než 18.

Techniky založené na spektrálním přístupu, které nejprve převedou texturní obrazy do frekvenční oblasti, jsou vhodné pro popis směrovosti periodických nebo téměř periodických vzorů v monochromatických obrazech textury. Tyto techniky jsou založené na vlastnostech Fourierova spektra a popisují globální periodicitu úrovní šedi obrazu. Směr rozložení vysokých hodnot frekvenčních komponent ve frekvenční oblasti odpovídá převažujícím směrům objektů v obraze v prostorové oblasti. Naproti tomu náhodná textura způsobuje, že vysoké hodnoty frekvenčních komponent v obraze spektra jsou rozloženy isotropně a tvoří přibližně kruhový tvar. Výzkumem v oblasti směrové orientace založené na spektrálním přístupu se zabývali i jiní autoři, například *Josso et al.* [34], *Liu* [35], *Holota a Němeček* [36], *Tonar et al.* [37], *Kula* [38].

Nechť $f(x, y)$ je dvojrozměrná obrazová funkce, kde $x = 0, 1, 2, ..., m-1$ a $y = 0, 1, 2, ..., n-1$ jsou prostorové souřadnice a $f(x, y)$ je úroveň šedi obrazových bodů obrazu o velikosti mxn. Pro takový obraz je dvojrozměrná diskrétní Fourierova transformace (2DFT) dána vztahem [39]

$$F(u, v) = \sum_{x=0}^{m-1} \sum_{y=0}^{n-1} f(x, y)\, e^{-j\,2\,\pi(ux/m+vy/n)}, \tag{2.1}$$

kde, $u = 0, 1, 2, ..., m-1$ a $v = 0, 1, 2, ..., n-1$ jsou frekvenční proměnné. $F(0, 0)$ představuje počátek frekvenční oblasti. Dvojrozměrná inverzní diskrétní Fourierova transformace (2IDFT) má tvar

$$f(x, y) = \frac{1}{mn} \sum_{u=0}^{m-1} \sum_{v=0}^{n-1} f(x, y)\, e^{-j\,2\,\pi(ux/m+vy/n)}. \tag{2.2}$$

Jestliže $f(x, y)$ je reálná funkce, její transformace je funkce komplexní. Z důvodu vizuální analýzy transformace je vhodné vypočíst její spektrum $|F(u, v)|$ a zobrazit jako obraz. Výkonové spektrum (nebo výkonová spektrální hustota) je definovaná jako druhá

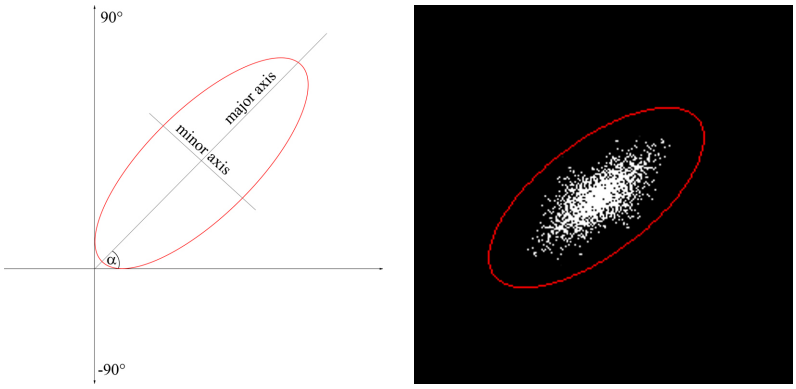

(a) (b)

Obrázek 2.2: (a) Elipsa, (b) oblast zájmu.

mocnina $|F(u,v)|$, tj.

$$P(u,v) = |F(u,v)|^2. \tag{2.3}$$

Pro účely vizualizace je vhodné zredukovat dynamický rozsah koeficientů logaritmickou transformací

$$Q(u,v) = log(1 + P(u,v)). \tag{2.4}$$

Příklad texturního obrazu z Brodatzovy databáze textur (D15) a odpovídající výkonové spektrum je zobrazen na obrázcích 2.1(a),(b).

Metodu pro odhad směrového rozložení objektů ve formě směrové růžice založené na spektrálním přístupu s použitím 2DFT navrhl *Tunák* v disertační práci [40] a publikoval v práci [1] (viz Příloha 1). Odhad anisotropie je vypočten jako suma frekvenčních komponent směrového vektoru v celém rozsahu úhlů. Odhad souřadnic směrového vektoru je proveden pomocí DDA algoritmu. Protože transformace reálné funkce $f(x,y)$ je komplexní číslo, jsou sečteny koeficienty Fourierova spektra $|F(u,v)|$ a vyneseny do polárního diagramu. Příklad odhadu anisotropie pro monochromatický obraz D15 z Brodatzovy databáze textur (obr. 2.3(a)) je uveden na obr. 2.3(c). Výhodou navržené metody je její rychlost a sledování orientace s úhlovým krokem 1°. V práci [1] jsou uvedeny příklady odhadu směrového rozložení pro simulované obrazy a monochromatické obrazy textilních struktur a práce [40] obsahuje zdrojové kódy algoritmu v programovém prostředí Matlab.

Jak už bylo zmíněno, směr frekvenčních komponent ve frekvenční oblasti koresponduje ze směrem hran objektů v prostorové oblasti. Další metoda pro odhad anisotropie navržena *Tunákem* vychází z transformace výkonového spektra do binárního obrazu prahováním, tím dojde k odsegmentování významných frekvenčních komponent. V takovýchto binárních obrazech uvažujeme shluk bílých pixelů jako oblast zájmu. Je možné určit vlastnosti jako délku hlavní, vedlejší osy a orientaci elipsy (úhel ve stupních v intervalu -90 až 90° mezi osou x a hlavní osou), která má stejný normalizovaný druhý centrální moment jako oblast zájmu (viz obr. 2.2). Orientace koresponduje s převládajícími směry objektů v prostorové oblasti. Porovnání výše zmíněných metod je uvedeno na obr. 2.3(a)-(d). Obr. 2.3(a) zobrazuje Brodatzovu texturu (D15), obr. 2.3(b) představuje směrovou růžici odhadnutou experimentální metodou dle *Rataje a Saxla* [33], na obr. 2.3(c) je odhad směrové růžice ve formě polárního diagramu dle *Tunáka* [1]. Elipsu zobrazenou červenou barvou, délku hlavní a vedlejší osy elipsy, a orientaci elipsy je možné vidět na obr. 2.3(d). Z obrázků je patrná shoda v převládajícím směru.

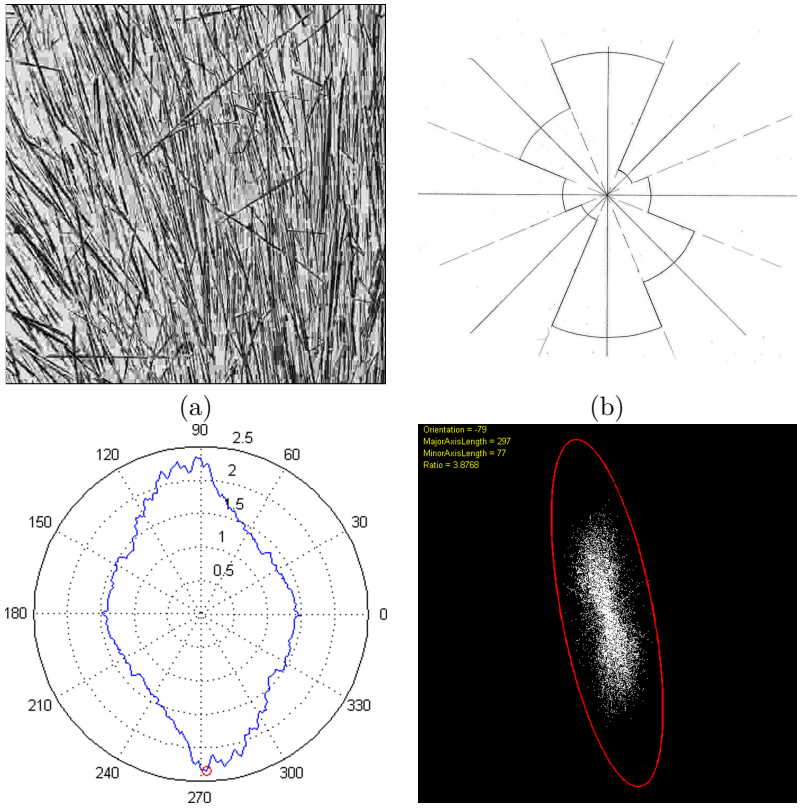

Obrázek 2.3: (a) Brodatzova textura (D15), (b) směrová růžice, (c) polární diagram, (d) orientace podle elipsy.

Obě autorem navržené metody provádí odhad směrového rozložení objektů pro monochromatický obraz jako celek. Ukazuje se, že pro textilní vlákenné systémy např. netkané textilie nebo nanovlákenné vrstvy by byla vhodnější podrobnější analýza. Myšlenka je založena na rozdělení obrazu na menší části a provedení analýzy pro takovéto oblasti. Obraz nanovláken o velikosti 1000x1000 pixelů vyrobených elektrostatickým zvlákňováním uvedený na obr. 2.4 (a) je rozdělen na menší podokna určité velkosti. Analýza směrového uspořádání je pak provedena pro každé podokno. Převládající orientace objektů pro každé podokno je reprezentována směrovým vektorem zobrazeným červenou barvou (při podmínce, že poměr hlavní a vedlejší osy elipsy je větší než 2). Kromě toho, orientace ve stupních je zobrazena jako mapa v šedé škále. Obr. 2.4(c),(d) představují šedotónovou mapu orientace pro podokna velikosti 20x20, resp. 10x10 pixelů. Je zřejmé, že oblasti zobrazené střední šedou, které neobsahují vektory směrů, reprezentují oblast bez preferovaného směru. Na obr. 2.4(e),(f) jsou vyznačeny vektory směrů v originálním šedotónovém obraze. Odpovídající distribuce směrů je uvedena ve formě histogramů a jádrových odhadů hustoty na obr. 2.4(g),(h). Odhady distribuce směrů jsou v korespondenci s odhadem anisotropie zobrazené formou polárního diagramu podle *Tunáka* [1] na obr. 2.4(b). Výsledky ukazují, že menší velikost podoken poskytuje přesnější výsledky. Další příklad nanovlákenné vrstvy, kde je vidět přechod mezi strukturou isotropní, bez preference směrů a orientovanou strukturou je uveden na obr. 2.5. Metodu pro hodnocení anizotropie nebo směrové orientace vlákenných nebo jiných objektových systémů za pomoci 2DFT je možné využít pro hodnocení plošných textilních struktur z pohledu jejich homogenity, vad a náhodných odchylek od struktury.

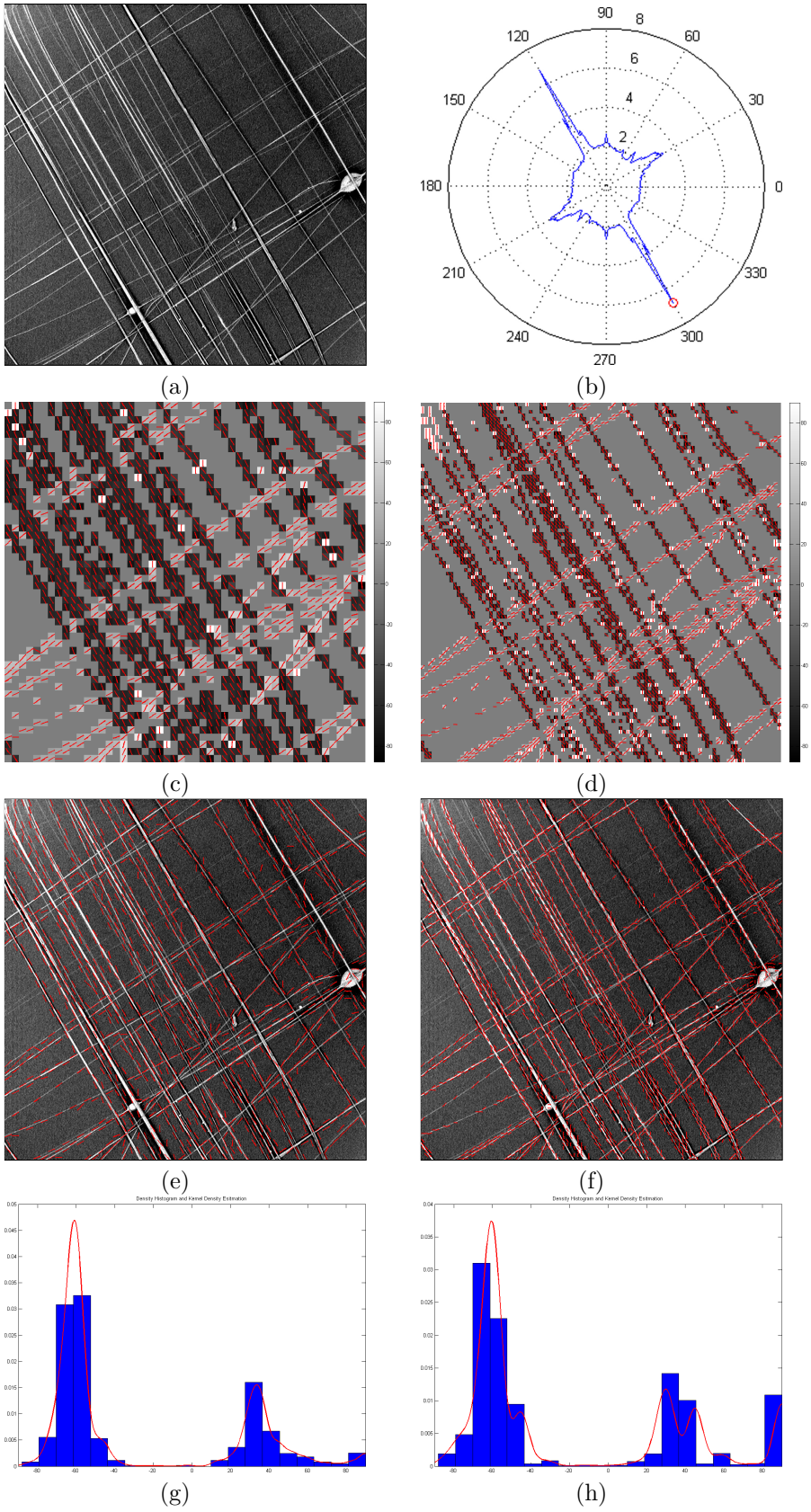

Obrázek 2.4: (a) Obraz nanovláken (1000x1000px), (b) polární diagram dle *Tunáka* [1],(c),(d) šedotónová mapa směrů (velikosti podokna 20x20 a 10x10 px), (e),(f) vektory směrů, (g),(h) histogramy a jádrové odhady hustoty rozdělení směrů.

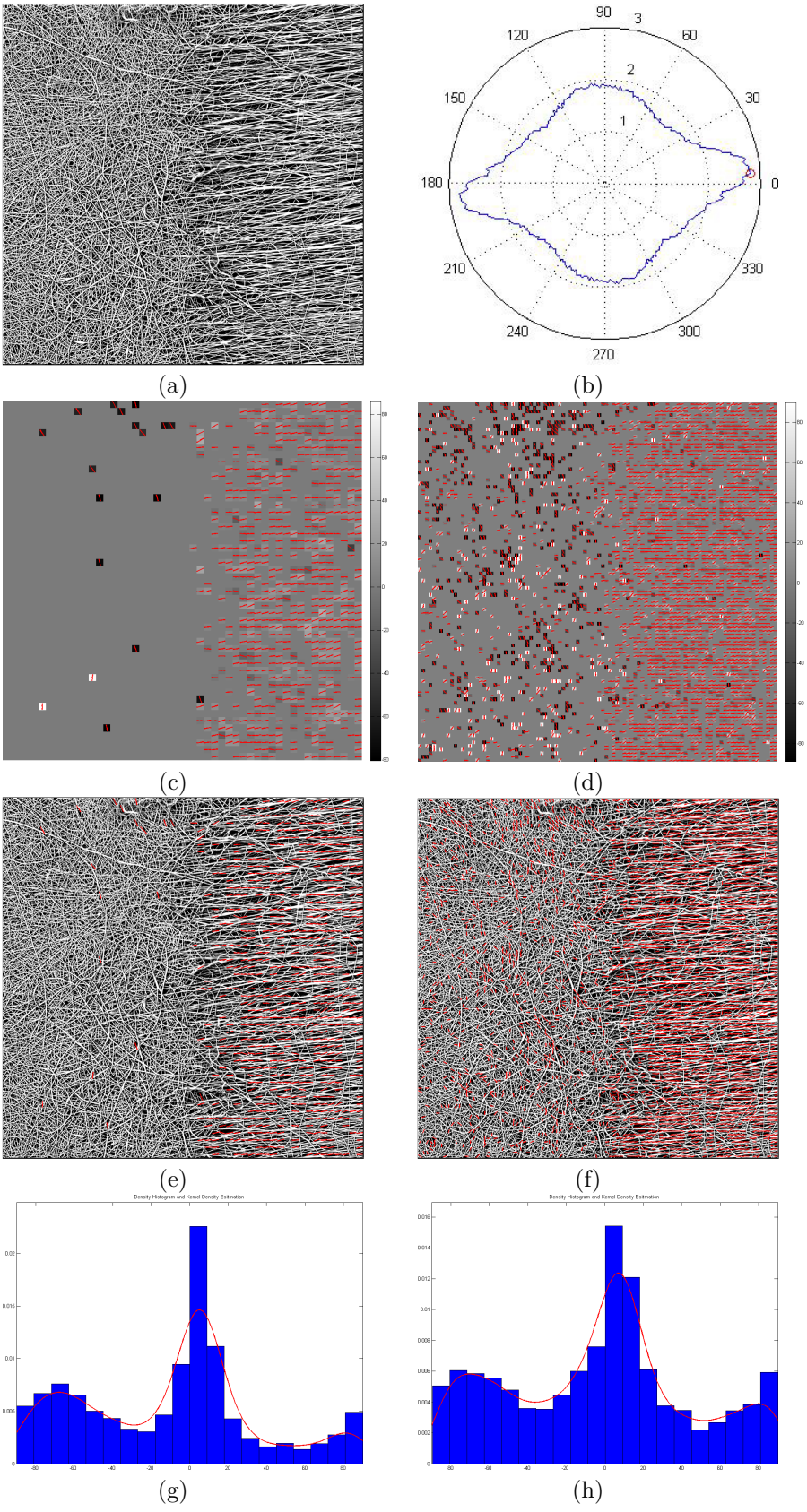

Obrázek 2.5: (a) Obraz nanovláken (2000x2000 px), (b) polární diagram dle *Tunáka* [1],(c),(d) šedotónová mapa směrů (velikosti podokna 40x40 a 20x20 px), (e),(f) vektory směrů, (g),(h) histogramy a jádrové odhady hustoty rozdělení směrů.

2.3 Detekce defektů v plošných textiliích

Vizuální kontrola textilií je důležitou součástí kontroly kvality v textilním průmyslu. Jejím účelem je dosažení maximální kvality textilních výrobků z pohledu vizuálních vad a odchylek, u tkanin také dané změnou periodické struktury. Z některých provedených studií (*Schicktanz*, [41]) vyplynulo, že cena textilních výrobků 2. jakosti je mezi 45-65% ceny výrobků 1. jakosti. Za účelem udržení vysoké kvality a standardů zavedených v textilním průmyslu musí textilní výrobci sledovat kvalitu svých výrobků, a to i několikanásobně opakovanou kontrolou. Monitorování kvality se dotýká i finální fáze výroby, která vyžaduje objektivní, spolehlivé, časově a finančně efektivní vyhodnocení. V současné době se vady detekují především subjektivní vizuální kontrolou plošných textilií prováděnou vyškoleným hodnotitelem, což je práce časově náročná a vyžaduje permanentní pozornost kontrolora. Takovéto zjišťování vad, kdy některé vady mají velikost jen pár milimetrů na velmi rozsáhlé inspekční ploše, poskytuje maximální přesnost něco kolem 70% (*Kumar* [42], *Chan a Pang* [43]). I toto je jedním z důvodů, proč má textilní průmysl zájem na nahrazení současných subjektivních postupů vhodným automatizovaným a z ekonomického hlediska efektivním řešením.

Výzkum v oblasti automatické inspekce plošných textilií existuje poměrně dlouhou dobu. Vývoj nových algoritmů pro rozpoznávání textilních vzorů nezávislých na pozici, velkosti, světlosti a orientaci je cílem mnoha výzkumných týmů. Nicméně v oblasti rozpoznávacích automatických systémů je stále prostor pro vývoj a zdokonalování těchto systémů. V současné době jsou na trhu s automatickým inspekčním systémem zastoupené firmy (*Elbit Vision System, Barco Vision's Cyclops, Shelton Vision Textile Inspection Systems, ComVis, Uster Zellweger*). Firmy garantují přesnost nalezení defektu v intervalu 70-90% v závislosti na typu materiálu a typu vad (*Kothari* [44]). Nevýhodou výše uvedených komerčních systémů je zatím velmi vysoká pořizovací cena a schopnost detekce vady jen na některých typech textilních materiálů. Nový typ sofistikovaného inspekčního systému by měl být použitelný na co možná nejširší spektrum materiálů, včetně vzorovaných materiálů a to nejenom textilních. Za tímto účelem bude třeba vyvinout zcela nové typy hybridních algoritmů (*Ngan et al.* [45]), které budou kombinovat stávající přístupy s novými moderními, které jsou založené například na grupách symetrie pro vzorované textury (*Ngan et. al* [46]).

Tunák se v disertační práci [40] zabýval metodami pro analýzu obrazu struktury textilie a monitorováním defektů ve tkanině. V práci byly použity postupy pro detekci vad resp. monitorování textury založené na texturních charakteristikách získaných především na základě statistického a spektrálního přístupu. Statistický přístup využívá texturní charakteristiky zejména vyšších řádů. Průkopníkem v této oblasti je *Haralick et. al*, který v práci [47] navrhl množinu 14 texturních charakteristik, za účelem klasifikace texturních dat. Charakteristiky jsou založeny na vzájemné prostorové závislosti úrovní šedi dvojic obrazových bodů a slouží k popisu charakterizace textury, jako např. homogenita, kontrast nebo přítomnost organizované struktury v obraze. Další charakteristiky popisují komplexnost a povahu přechodů úrovní šedi v obraze. Eficienci texturních charakteristik na klasifikaci textur získaných z databáze Brodatzových textur s využitím metody CART testoval *Carstensen* v práci [48]. Rozpoznáním defektů ve tkanině s využitím matic vzájemných šedotónových závislostí se zabývali *Kuo a Su* [49] a *Bodnarova et al.* [50].

Tunák et al. v práci [2] (Příloha 2) a [6] (Příloha 6) pomocí metody CART stanovil texturní charakteristiky s největší diskriminační silou, které pak byly použity pro

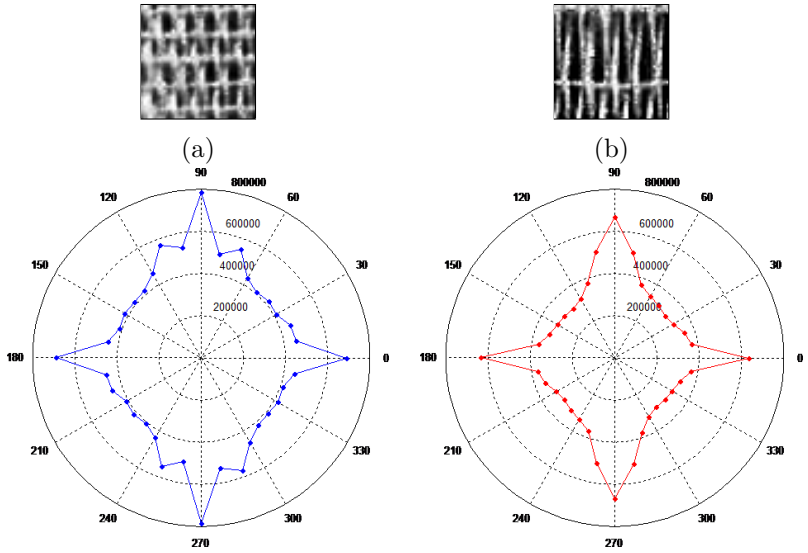

Obrázek 2.6: (a) Okno s obrazem neporušené části tkaniny, (b) okno s obrazem, který obsahuje poruchu, (c),(d) odhad směrového rozložení s krokem 10°.

detekci vizuálních defektů ve tkaninách. Studie ukázala, že za charakteristiky s největší rozlišovací sílou lze považovat charakteristiky energie, korelace, lokální homogenita a třetí a čtvrtý moment rozdělení hodnot součtů úrovní šedi. K vlastnímu testování algoritmů pro detekci vad ve tkaninách byl vytvořený dvojrozměrný model vazby tkaniny v plátnové vazbě se simulovanými běžnými defekty. Pro simulaci textilní struktury byl v Matlabu vytvořen program s využitím konvoluční věty s ohledem na typ vazby, dostavu a šířku modelové příze. Vstupními parametry simulace modelování struktury tkaniny byly: rozteč osnovních a útkových nití; průměr osnovních a útkových nití; úroveň šedi osnovních a útkových nití; hranice nití; stín nití a provázání, parametry náhodného šumu; šířka provázání a vazba. V práci [2] jsou uvedeny příklady simulovaných běžných defektů.

Spektrální přístup založený na 2DFT využívá charakteristiky získané ze spektra. V práci [8] (Příloha 7) byla k detekování využita sada 18 charakteristik pocházejících z *Tunákem et al.* navržené metody odhadu anisotropie [1]. Jestliže si představíme hodnoty vynesené v polárním diagramu jako vektor charakteristik $\mathbf{X}_i$, tyto charakteristiky lze využít pro hodnocení homogenity a odchylek od pravidelné struktury textilií. Obrazy stejné neporušené struktury tkaniny by měly mít přibližně podobné tvary odhadu směrové růžice, tj. téměř stejné hodnoty vektoru $\mathbf{X}_i$. Naopak, obraz struktury tkaniny, která obsahuje porušení, bude mít tvar odhadu směrové růžice a hodnoty $\mathbf{X}_i$ jiné. Pro ilustraci je uveden příklad na obr. 2.6. Obr. 2.6(a),(b) představují okna o velikosti 50x50 pixelů z obrazu tkaniny. Obr. 2.6(a) je obraz neporušené struktury, obr. 2.6(b) představuje obrázek tkaniny s defektem. Na obr. 2.6(c),(d) jsou korespondující odhady směrové růžice získané po úhlovém kroku 10°. Z obrázků je vidět rozdílnost tvarů odhadů, tj. hodnot vektoru $\mathbf{X}_i$. Tento fakt lze využít pro detekci vad, který může být pak realizovaný např. postupem regulace procesu pomocí Hotellingových regulačních diagramů.

U všech studovaných přístupů je k automatické detekci defektních oblastí využita technika současného monitorování více texturních charakteristik, individuální sledování těchto charakteristik může poskytovat nedostatečné výsledky. Proces monitorující kvalitu, která je charakterizována vektorem několika proměnných, je známý jako ví-

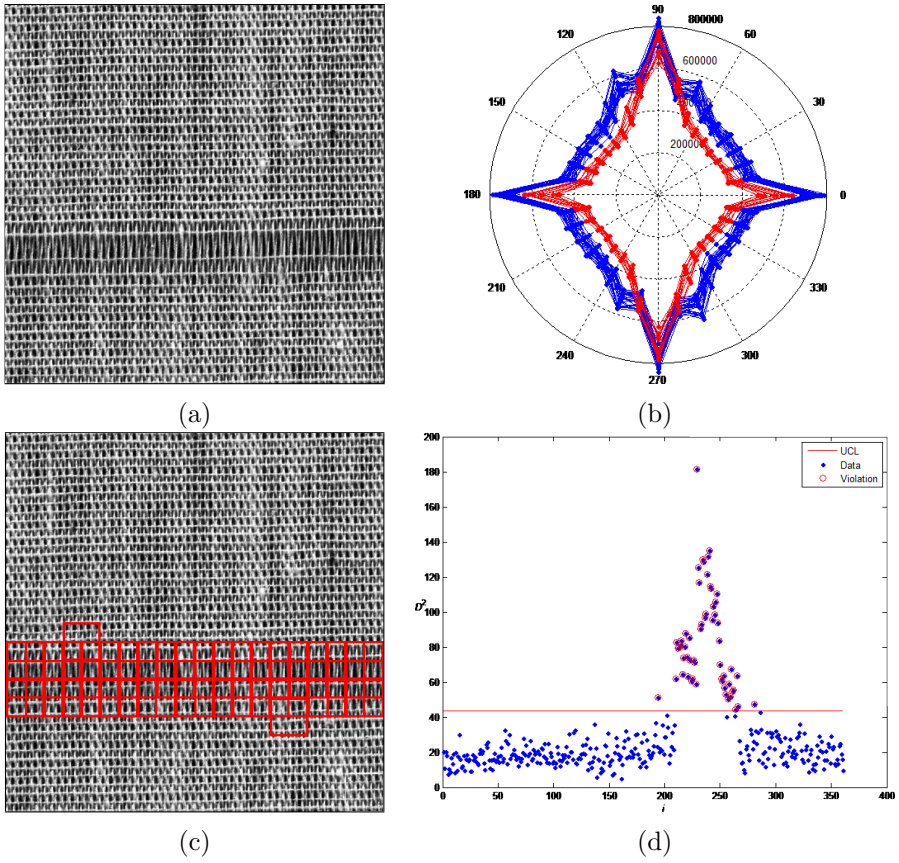

Obrázek 2.7: (a) Defekt v reálné struktuře, (b) odhady směrového rozložení s krokem 10°, kde červená barva zobrazuje odhad 10-ti oken s vadou a modrá zobrazuje odhad 50-ti oken z neporušené struktury, (c) výsledek realizace algoritmu, (d) graf i-té statistiky.

cerozměrná statistická regulace procesu. Nástrojem vícerozměrné statistické regulace procesu jsou Hotellingovy regulační diagramy, které využívají statistiky D^2 a jsou zobecněním Shewhartových regulačních diagramů. Při předpokladu, že data pocházejí s p-rozměrného normálního rozdělení se známým vektorem středních hodnot $\boldsymbol{\mu}$ a známou kovarianční maticí $\boldsymbol{\Sigma}$, potom testová statistika D_i^2 pro i-té individuální pozorování je ekvivalentní druhé mocnině Mahalanobisovy vzdálenosti [51]

$$D_i^2 = (\mathbf{X}_i - \boldsymbol{\mu})^T \boldsymbol{\Sigma}^{-1} (\mathbf{X}_i - \boldsymbol{\mu}), \tag{2.5}$$

kde $\mathbf{X}_i$ je i-té, $i = 1, 2, ..., m$ pozorování pocházející z p-rozměrného normálního rozdělení $N_p(\boldsymbol{\mu}, \boldsymbol{\Sigma})$. V řadě reálných situací se často potkáváme s případem, že vektor středních hodnot $\boldsymbol{\mu}$ a kovarianční matice $\boldsymbol{\Sigma}$ není známa apriori. Uvažujeme, že data jsou získána z procesu, u kterého předpokládáme stabilitu. Předpokládáme, že náhodný výběr z těchto dat pochází z p-rozměrného normálního rozdělení $N_p(\boldsymbol{\mu}, \boldsymbol{\Sigma})$, kde $\boldsymbol{\mu}$ a $\boldsymbol{\Sigma}$ není známa. Pro výběrový průměr a výběrovou kovarianční matici tohoto rozdělení platí

$$\overline{\mathbf{X}} = \frac{1}{m} \sum_{j=1}^{m} \mathbf{X}_i, \tag{2.6}$$

$$\boldsymbol{S} = \frac{1}{m-1} \sum_{j=1}^{m} (\mathbf{X}_i - \overline{\mathbf{X}})(\mathbf{X}_i - \overline{\mathbf{X}})^T. \tag{2.7}$$

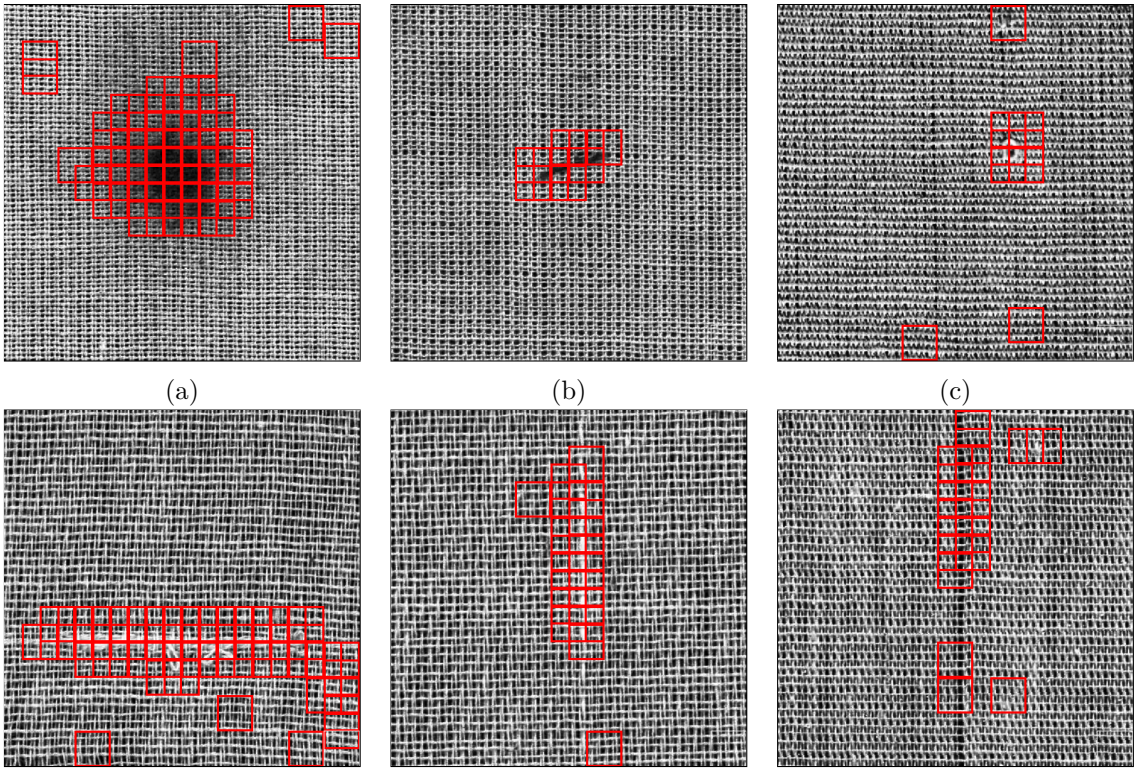

(a) (b) (c)

(d) (e) (f)

Obrázek 2.8: Výsledek algoritmu detekce na reálných vzorcích.

$\overline{\mathbf{X}}$ a $\boldsymbol{S}$ jsou nestranné odhady $\boldsymbol{\mu}$ a $\boldsymbol{\Sigma}$. Potom testová statistika pro vektor $\mathbf{X}_i$ má tvar

$$D_i^2 = (\mathbf{X}_i - \overline{\mathbf{X}})^T \boldsymbol{S}^{-1} (\mathbf{X}_i - \overline{\mathbf{X}}). \tag{2.8}$$

Pro monitorování individuálních pozorování, která následuje po počáteční kalibraci diagramů v trénovací fázi, má horní mez regulačního diagramu tvar

$$UCL = \frac{p(m+1)(m-1)}{m(m-p)} F_{p,m-p}(1-\alpha), \tag{2.9}$$

kde $F_{p,m-p}(1-\alpha)$ je $(1-\alpha)$ kvantil F-rozdělení s parametry p a $(m-p)$. Jestliže hodnota statistiky D_i^2 překročí horní regulační mez UCL pro danou hladinu významnosti α, pak je proces nestabilní, což v tomto případě zpravidla indikuje odchylku od běžné struktury textury.

Monitorování defektů bylo provedeno technikou posuvného okna o velikosti 50x50 pixelů, které se systematicky po kroku 25 pixelů posouvalo po celé ploše obrazu (simulace kontinuálního průběhu). Pro každé okno byla vypočtena i-tá testová statistika podle vztahu (2.8) a vynesena proti horní regulační mezi UCL. Jestliže i-tá hodnota testové statistiky byla mimo mez, okno bylo považováno za okno obsahující defekt. Vektor optimálních charakteristik $\overline{\mathbf{X}}$ je získán v trénovací fázi z náhodně vybraných oken v neporušené části textilie.

Příklad na obr. 2.7(a) zobrazuje defekt v reálné struktuře tkaniny, konkrétně útkový pruh (nedoraz). Na obr. 2.7(d) je vynesena i-tá testová statistika dle vztahu (2.8). Všechna pozorování (okna) nad horní regulační mezí jsou považována za okna obsahující defekt. Výsledek algoritmu je vidět na obr. 2.7(c), kde okna zobrazená červenou barvou jsou okna s defektem. Pro lepší představu jsou na obr. 2.7(b) zobrazené polární diagramy vypočtené po kroku 10°, kde červená barva představuje 10 zástupců

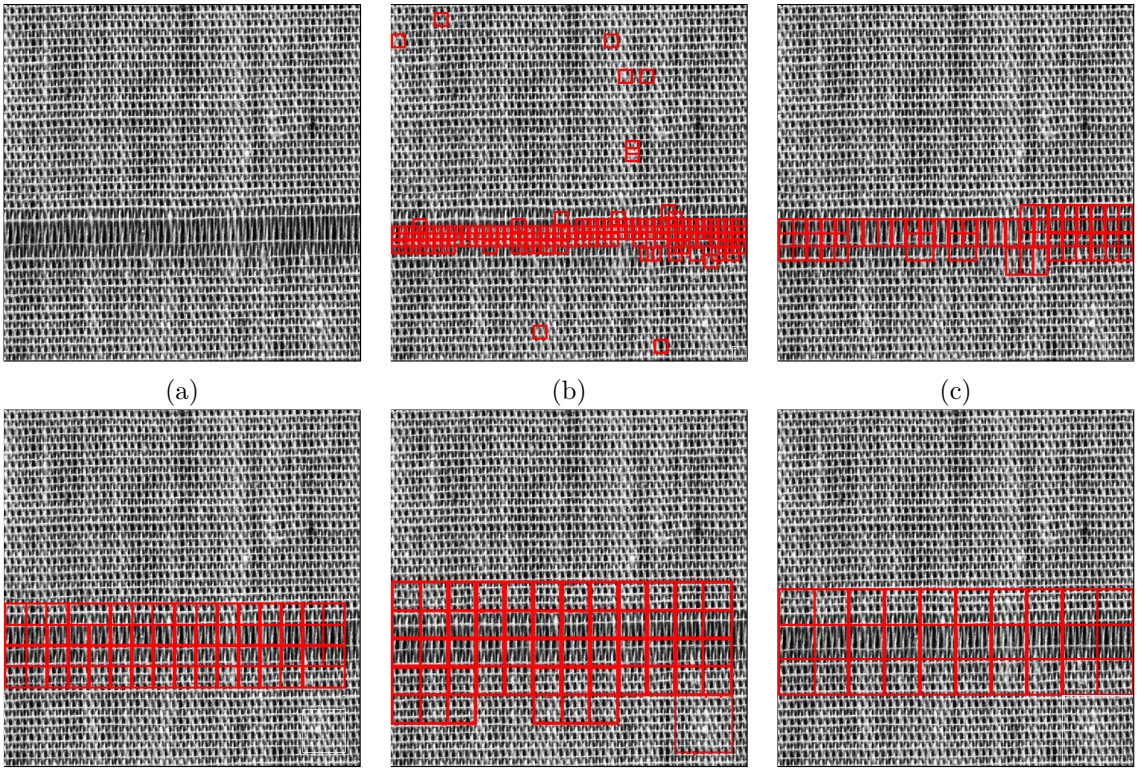

Obrázek 2.9: Výsledek algoritmu detekce s různou velikosti prohlížecího okna, (b) 20x20, (c) 40x40, (d) 60x60, (e) 80x80, (f) 100x100 pixelů.

(oken), které obsahují defekt a modrá barva představuje 50 oken s neporušené části tkaniny. Z obrázku je vidět podobnost tvaru polárních diagramů vypočtených z oken neporušené části, kdežto tvar diagramů příslušející oknům s defektem je jiný. Obrázky 2.8(a)-(f) zobrazují výsledek použití algoritmu detekce na obrazech reálných struktur, které obsahují běžné defekty. Detekce defektů založena na spektrálních charakteristikách získaných z Fourierova spektra vykazuje větší přesnost detekce vad. Užitím této metody můžeme detekovat vady spojené se změnou dostavy tkaniny a kontrastní nesměrové vady. V porovnání se statistickým přístupem se zlepšila účinnost detekce.

Dílčí výsledky byly prezentovány v pracích [13, 15–17, 19–22, 27, 29]. Postup monitorování defektů pomocí regulačních diagramů založený na texturních statistikách je velmi citlivý na pořízení trénovacího souboru dat (souboru dat z neporušené textury), tj. souboru dat, kdy je monitorovaný proces ve statisticky zvládnutém stavu. Ukazuje se, že například i velmi malé změny v průběhu získání digitálního obrazu (natočení snímaného vzorku, změna světelných podmínek při snímání, relativně malá změna povrchu) mohou mít velký vliv na parametry rozdělení vektoru texturních charakteristik získaných z výběru oken tohoto vzorku. Jako důležitý parametr se jeví také velikost prohlížecího okna, který má vliv na účinnost detekce (viz obr. 2.9). Nevýhodou u použití Hotellingových regulačních diagramů se však ukazuje poměrně veliký počet sledovaných jakostních znaků. U datových systémů vysoké dimenze s kolinearitami nemusí být použití těchto diagramů prakticky proveditelné. Běžně používanou metodou pro redukci dimenze dat je metoda hlavních komponent. Výhodou této metody je, že pouze několik latentních proměnných vystihuje téměř celou variabilitu původních proměnných. Při použití regulačního diagramu hlavních komponent založeného na Hotellingově statistice, kdy se do statistiky zahrne vliv jen několika hlavních komponent

vysvětlujících více jak 80% celkové variability dat, dojde při regulaci procesu k omezení false alarmů [52].

Navržené algoritmy detekce byly založeny na systematickém prohlížení statického obrazu tkaniny posuvným oknem. V reálném provozu je tkanina odtahována na válec rovnoměrnou rychlostí a finální monitorování kvality je prováděno na prohlížecích stolech, kde je tkanina převíjena na válec. V případě online kontroly jsou statické snímače obrazu rozmístěné rovnoměrně nad tkaninou po celé její šířce. V rámci úkolů Centra pro jakost a spolehlivost výroby (CQR) byl zkonstruován prototyp zařízení [32] na testování použitelnosti algoritmů pro detekci defektů plošných textilií k online detekci, které dovoluje převíjení nekonečného pásu plošné textilie a tím simulaci skutečného provozu. Zařízení se skládá z hliníkové konstrukce, převíjecích válců, hnacího motoru, osvětlení textilie a řádkové digitální kamery, která umožňuje sběr obrazových dat. Spolu se zařízením byla vytvořena softwarová aplikace k testování použitelnosti algoritmů pro online detekci defektů plošných textilií (viz [7], Příloha 7 a [8], Příloha 8). Z koncepčního hlediska je možné aplikaci chápat jako určitou platformu na jejímž základě je možné implementovat a ověřit vyvíjené metody pro detekci defektů a monitorování parametrů struktury textilních útvarů za podmínek, které se blíží podmínkám provozním.

2.4 Odhad dostavy tkaniny

V oblasti textilní metrologie je stanovení dostavy tkaniny činností, která se stále provádí převážně manuálně. Proto je v případě odhadu dostavy tkaniny snaha o jeho automatizaci. Je známo několik přístupů k úloze automatického stanovení odhadu dostavy tkaniny, například metoda profilové úrovně šedi pro stanovenení dostavy tkaniny (*Jeon a Jang* [53]), metoda pomocí rozložení obrazu prostřednictvím Wienerova (*Liqing et al.* [54]) nebo mediánového (*Yildirim a Baser* [55]) filtru, metoda vycházející se statistického přístupu založeném na maticích vzájemných šedotónových závislostí (*Lin* [61]). V oblasti stanovení dostavy a dalších konstrukčních parametrů tkaniny se několik autorů věnuje spektrálnímu přístupu založeném na 2D Fourierově transformaci obrazu textury textilie (*Wood* [56], *Ravandi a Toriumi* [57], *Xu* [58]). Jak už bylo zmíněno Fourierova transformace je vhodná pro popis periodických vzorů vzhledem k vztahu mezi pravidelnou strukturou v obraze v prostorové oblasti a významnými frekvencemi ve frekvenční oblasti. Dostavu tkaniny je možné získat nalezením těchto významných frekvencí.

Rekonstrukce obrazu využívající dvojrozměrnou Fourierovou transformaci byla aplikována na úlohu automatického určení dostavy tkaniny a automatické detekce defektů zapříčiněných změnou dostavy v práci *Tunáka et al.* [3] (Příloha 3). Informace o převažujících směrech v původním obraze je koncentrovaná v obraze spektra ve směrech s vysokými hodnotami frekvenčních komponent. Odstranění významných směrů, v tomto případě soustavy nití, je možné nastavením frekvenčních hodnot ve spektru odpovídajících dané soustavě nití na nulu. Obnovený obraz je pak získán použitím inverzní 2D Fourierovy transformace. Příklad na obr. 2.10(a) zobrazuje šedotónový obraz tkaniny v plátnové vazbě, obr. 2.10(b) je odpovídající výkonové spektrum. Obr. 2.10(c),(d) představují frekvenční komponenty v orientaci 0° a 90° a šířkou pásu 7 pixelů. Zbylé frekvenční komponenty jsou nastavené na nulu. Obnovené obrazy osnovní resp. útkové soustavy nití po provedení inverzní 2DFT jsou na obr. 2.10(e),(f). Z obnovených obrazů jednotlivých soustav nití je možné získat profil úrovní šedi, který je kolmý na

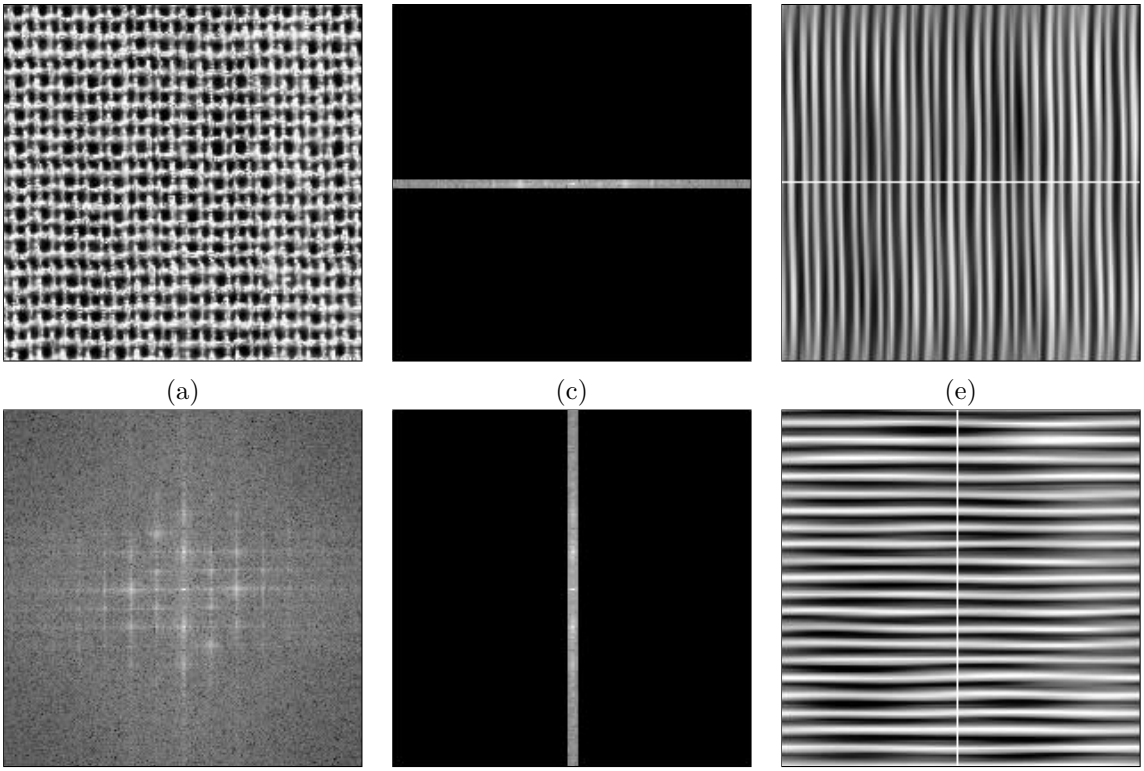

(a) (c) (e)

(b) (d) (f)

Obrázek 2.10: Obraz plátnové vazby, (b) výkonové spektrum, (c),(d) výřez ze spektra (e),(f) obnovené obrazy po inverzní 2DFT.

danou soustavu nití. Profil úrovní šedi si můžeme představit jako periodickou časovou řadu, kde vysoké hodnoty úrovní šedi představují nitě a nízké hodnoty úrovní šedi mezery mezi nitěmi. Základním nástrojem pro popis periodické časové řady je periodogram $I(\omega)$, který pro konečnou posloupnost náhodných veličin $y_1, ..., y_n$ definujeme jako funkci proměnné ω ve tvaru [59]

$$I(\omega) = \frac{1}{2\pi n} \left| \sum_{t=1}^{n} y_t e^{-it\omega} \right|^2, \qquad -\pi \leq \omega \leq \pi. \tag{2.10}$$

Periodogram slouží jako nástroj pro nalezení významných periodických složek v dané časové řadě. Objektivní metodou, která umožňuje statisticky rozhodnout, jaké hodnoty periodogramu můžeme opravdu považovat za významně velké ve srovnání s jeho ostatními hodnotami je Fisherův test periodicity [59, 60]. Nulová hypotéza ve Fisherově testu má tvar

$$H_0 : y_t = \epsilon_t, \tag{2.11}$$

tj. předpokládá se, že řada y_t neobsahuje žádnou periodickou složku a je přímo rovna bílému šumu ϵ_t s rozdělením $N(0, \sigma^2)$. Tato nulová hypotéza je testována oproti alternativní hypotéze, která je definovaná ve tvaru

$$H_A : y_t = \mu + \sum_{j=1}^{p} \alpha_j \cos(\omega_j t) + \beta_j \sin(\omega_j t) + \epsilon_t, \qquad t = 1, ..., n, \tag{2.12}$$

kdy se řada y_t chápe jako směs konečného počtu goniometrických funkcí s různými frekvencemi $\omega_1, ..., \omega_p$ s úrovní μ a s přidaným bílým šumem ϵ_t. Testová statistika ve

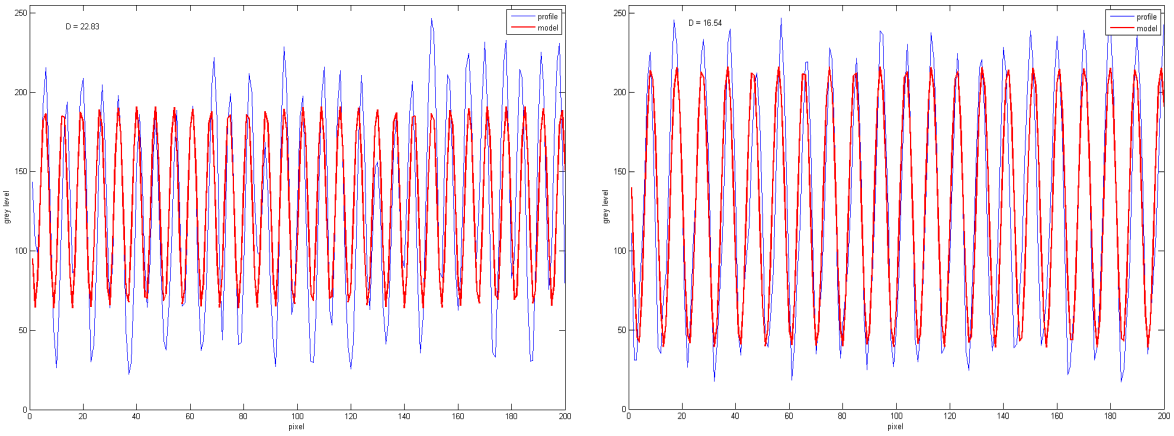

(a) (b)

Obrázek 2.11: Graf profilu úrovní šedi a graf modelu časové řady pro (a) osnovní a (b) útkovou soustavu nití.

Fisherově testu je založena na hodnotách periodogramu dané řady $y_1, ..., y_n$ vypočtených pro frekvence

$$\omega_j^* = \frac{2\pi j}{n}, \qquad j = 1, ..., m \qquad m \leq \frac{n-1}{2}. \tag{2.13}$$

Jestliže platí nulová hypotéza, potom by žádná z těchto hodnot periodogramu neměla být významně větší než zbývající hodnoty. Fisherův test vlastně odpovídá na otázku, jestli některé hodnoty periodogramu můžeme považovat za významně velké, což souvisí s výskytem periodických složek v řadě. Hodnoty periodogramu jsou normovány za účelem odstranění závislosti rozdělení na neznámé hodnotě σ_ϵ, a to $y_t = Y_t/s_y$, kde s_y je odhad směrodatné odchylky y_t, pokud je nulová hypotéza platná. Testová statistika je pak definovaná

$$W = \max_{j=1,...,m} I(\omega_j^*), \tag{2.14}$$

a nulová hypotéza se zamíta, jestliže $W > g_F$, kde g_F je kritická hodnota Fisherova testu na hladině významnosti α. Jestliže je pomocí Fisherova testu zjištěna významná periodická složku určité frekvence ω_{j0}^* (pro tuto frekvenci je $I(\omega_{j0}^*) = \max_{j=1,...,m} I(\omega_j^*)$, potom je možné testovat významnost další velké hodnoty periodogramu tak, že se hodnota $I(\omega_{j0}^*)$ vynechá a s ostatními hodnotami pracujeme analogicky jako předtím (hodnotu m nahradíme hodnotou $m-1$). Tato metoda umožňuje nalézt významné frekvence ω_j v modelu (2.12) na základě statistických postupů. Přitom μ, α_j, a β_j jsou neznámé parametry, které lze odhadnout například metodou nejmenších čtverců. Dostavu tkaniny je možné vyhodnotit na základě nalezení periodicity T (délky periody, po které se pravidelně opakují nitě jedné soustavy) v horizontálním a vertikálním směru obnoveného obrazu tkaniny. Jestliže známe rozlišení R (pixel/palec), při kterém byl obraz pořízený, je možné určit dostavu tkaniny D (počet nití/cm) podle

$$D = \frac{R/2.54}{T}, \tag{2.15}$$

kde $T = 2\pi/\omega_j^*$ a ω_j^* je první nejvýznamnější frekvence určená z Fisherova testu periodicity. Na obr. 2.11(a),(b) je modrou barvou vynesený profil úrovní šedi osnovních a útkových nití a červenou barvou model časové řady vypočtený ze vztahu (2.12) pro

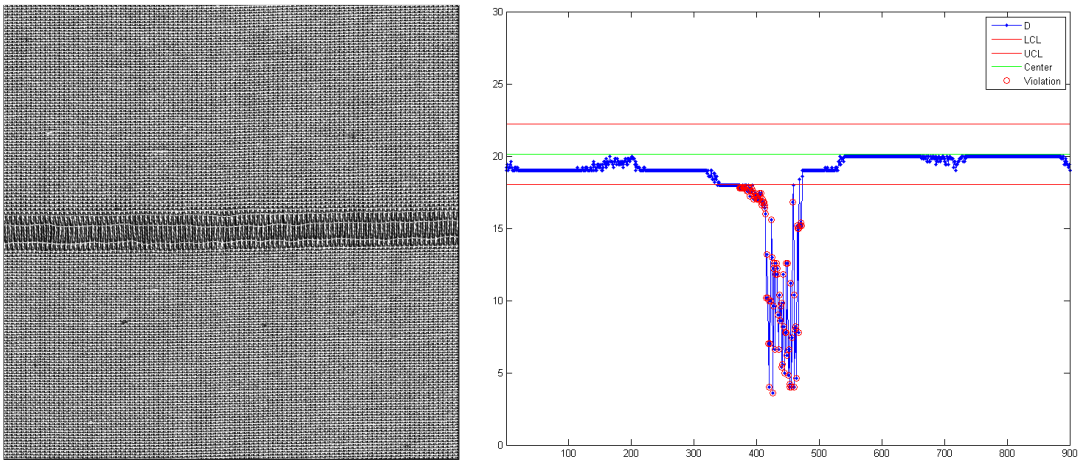

(a) (b)

Obrázek 2.12: (a) Obraz tkaniny s defektem, (b) regulační diagram pro dostavu.

nejvýznamnější frekvenci. Metoda byla testována na dvanácti vzorcích materiálu s plátnovou, keprovou a atlasovou vazbou. Celý proces je automatický, kde vstupní proměnou je rozlišení obrazu a výstupní proměnou je dostava tkaniny [9], [25].

Testování a ověřování efektivity vybraných metod automatického stanovení dostavy různých druhů tkanin je uvedeno v práci *Technikové a Tunáka* [23]. Pro zjištění dostavy prostřednictvím těchto metod byla vybrána sada vzorků s tkaninami v plátnové, keprové, atlasové vazbě a vzorované tkaniny. Mezi studované metody patřila metoda profilové úrovně šedi [53], metoda rozložení obrazu pomocí Wienerova filtru [54] a mediánového filtru [55], metoda matice vzájemného výskytu úrovní šedi [61] a metoda automatického určení dostavy pomocí 2DFT [3]. Výsledky ukázaly, že výpočetně a algoritmicky náročnější postupy nemusejí vždy vést k přesnějšímu výsledku stanovení dostavy. Zatím nebyla nalezena univerzální metoda stanovení dostavy, práce však navrhuje optimální metodu pro každý z typů vazeb.

Mnohé z běžných defektů, které se vyskytují ve tkaninách je spojeno se změnou dostavy tkaniny, převážně ve směru útku, které se rozkládají po celé šířce tkaniny. Navrženou metodu pro odhad dostavy tkaniny dle *Tunáka* [3] lze aplikovat i na detekci takovýchto vad. Myšlenka detekce defektů v útkovém směru je založena na sledování informace o hodnotě dostavy útku ve směru délky tkaniny. Za tímto účelem jsou použity regulační diagramy Shewhartova typu, které sledují změnu dostavy tkaniny v útkovém směru oproti očekávané hodnotě a indikují tak vadu struktury tkaniny. Algoritmus je učící, kde parametry regulačního diagramu jsou získány z obrazu tkaniny bez porušení. Algoritmus detekce je pak založen na systematickém výpočtu dostavy tkaniny po řádcích obrazové matice pro skupinu náhodně vybraných oken v každém řádku. Ve stejném řádku obrazu tkaniny je náhodně vybráno $n = 5$ oken o velikosti $100x100$ pixelů, které představují opakovaná měření stejné veličiny prakticky ve stejném čase. Pak v různých časech můžeme získat několik výběrů $V_1, ..., V_m$. Pro každý výběr V_j stejné velikosti n jsou určeny výběrové průměry x_{sj} a směrodatné odchylky s_j. Při předpokladu normality rozdělení $N(d, \sigma^2/n)$ výběrových průměrů x_s a nezávislosti výběrových průměrů je odhadem střední hodnoty d generální průměr definován vztahem [62]

$$d^* = \frac{1}{m} \sum_{j=1}^{m} x_{sj}, \tag{2.16}$$

a odhadem směrodatné odchylky je

$$\sigma^* = \frac{1}{mC_4} \sum_{j=1}^{m} s_j, \tag{2.17}$$

kde C_4 je konstanta zajišťující nevychýlenost. Regulační diagramy $\overline{x}$ využívají k posuzování stavu sledovaného procesu (v tomto případě hodnoty dostavy) aritmetické průměry x_{sj}. Ke své konstrukci vyžadují znalost parametrů d, σ^2 normálního rozdělení, nebo pouze znalost vhodných odhadů d^* a σ^{*2}. Regulační diagram $\overline{x}$ má pak centrální linii d^* a odhad regulačních mezí je dán

$$UCL, LCL = d^* \pm \frac{1.96\sigma^*}{\sqrt{n}}, \tag{2.18}$$

kde konstanta 1.96 představuje 97.5%-ní kvantil normovaného normálního rozdělení $u_{0.975}$, tj. 95% - ní pravděpodobnost s jakou se veličina vyskytuje v regulačních mezích, tj. proces je v požadovaném stavu (v tomto případě hodnota dostavy). Výběrové průměry x_{sj} odhadu dostavy jsou vynášeny do regulačního diagramu. Při překročení regulačních mezí je oblast považována za oblast, která vykazuje poruchu - odchýlení od periodicity struktury tkaniny.

Příklad regulačního diagramu pro monitorování dostavy tkaniny ve směru délky tkaniny je uveden na obr. 2.12, kde útkový pruh v půlce obrazu je způsoben absencí útkových nití, což můžeme pozorovat z regulačního diagramu, kde hodnoty dostavy útku jsou pod dolní regulační mezí LCL. Tyto příznaky indikují vadu nedostatečná dostava – útek (nedoraz), nebo přetržené útkové nitě. Tento přístup je zejména vhodný pro vady v útkovém směru, které jsou určitým způsobem spojeny se změnou dostavy, např. útkové pruhy nebo změna útkové dostavy. Některé další příklady monitorování dostavy jsou uvedeny v práci [3].

2.5 Monitorování kvality žinylkové příze

V oblasti monitorování struktury lineárních textilních útvarů byla řešena úloha sledování kvality a detekce vad žinylkové příze. Aplikací obrazové analýzy pro sledování parametrů lineárních vlákenných útvarů se zabývalo několik studií. *Barella* navrhl několik různých technik a algoritmů pro měření chlupatosti příze [63, 64]. Použití hranových operátorů pro stanovení chlupatosti ukázal *Guha et al.* v práci [65] a otázkou praktického určení chlupatosti s využitím obrazové analýzy se taky zabývá práce *Krupincové a Tunáka* [14]. Stanovení geometrických parametrů efektních přízí je popsáno v pracích *Xu* [66] a *Lia* [67].

Popis objektivní metody pro sledování homogenity a rozpoznání defektů jako indikátoru kvality žinylkové příze je uvedena v práci *Tunáka et al.* [5] (viz Příloha 5). Skaná žinylková příze sestává ze 2 typů přízí. Nosná (jádrová) příze o nekonečné délce provazuje kolmo kladené smyčky efektní příze. Smyčky efektní příze jsou po upevnění rozřezány a získá se tak vlas. Mezi důležité parametry žinylkové příze patří stejnoměrná výška vlasu po celé délce příze, jelikož má silný vliv na její vzhled. Byly získány monochromatické obrazy žinylkové příze a uložené jako obrazové matice o velikosti 1000x7500 pixelů. Předzpracování obrazu zahrnovalo prahování do binárního obrazu a morfologickou operaci otevření pro odstranění malých nežádoucích objektů v obraze (prach, nečistoty atd.). Následně byla z obrazu odečtena šířka příze v pixelech, která

byla použita jako jakostní znak při tvorbě regulačních diagramů. Datová sada obsahovala 7500 pozorování šířky příze ve směru její osy. Z důvodu vyhlazení byly data rozdělena na disjunktní po sobě následující sadu dat o velikosti 5 pixelů a průměry z této sady byly použity pro monitorování kvality žinylkové příze.

V trénovací fázi, kdy měření proběhlo na obraze žinylkové příze bez porušení bylo zjištěno, že výška vlasu jako monitorovaná charakteristika jakosti je vysoce autokorelovaná. Proto byl v práci *Tunáka et al.* [5] navržen autoregresní model prvního řádu AR(1), který se ukázal jako vhodný pro modelování autokorelační struktury. V práci jsou uvedeny grafy autokorelační a parciální autokorelační funkce, kde s rostoucí vzdáleností se autokorelace snižuje a pouze parciální autokorelace prvního řádu je statisticky významná. Data, která mají charakter časových řad můžou být modelována AR(1) modelem

$$x_t = c + \varphi x_{t-1} + a_t, \tag{2.19}$$

kde c je konstanta, $-1 < \varphi < 1$ je autokorelační koeficient prvního řádu, t je index, a je nezávislá, stejně rozdělená náhodná veličina $N(0, \sigma_a^2)$. Odhad procesu pro hodnotu $(t+1)$ založeném na minimu chyb kvadratické odchylky procesu je dán

$$\hat{x}_{t+1|t} = \varphi x_t, \tag{2.20}$$

a rezidua e_t je možné vypočítat podle

$$e_t = x_t - \hat{x}_{t+1|t}. \tag{2.21}$$

Protože procesní parametry nejsou známe, jsou odhadnuty v trénovací fázi z obrazu žinylkové příze v požadované kvalitě. Odhady parametrů AR(1) modelu jsou uvedeny v tabulce přiložené práce [5]. Použitím AR(1) modelu byly vypočteny rezidua, odpovídající autokorelační funkce a parciální autokorelační funkce. Ukázalo se, že navržený model dobře vysvětluje autokorelační strukturu a rezidua jsou rozdělená nezávisle. Modifikované EWMA regulační diagramy pak byly implementovány jako nástroj k monitorování a detekci defektů na přízi. *Testik* [68] navrhl modifikaci standardních EWMA regulačních diagramů, které jsou aplikovány na rezidua modelu časové řady, když procesní parametry časové řady nejsou známé, ale odhadované. Testové kriterium, které se vynáší do regulačního diagramu EWMA pro monitorování reziduí je definované

$$z_t = (1-\lambda) z_{t-1} + \lambda e_t, \tag{2.22}$$

kde $0 < \lambda \leq 1$ je váha a počáteční hodnota $z_0 = 0$, protože předpokládáme, že rezidua mají nulovou střední hodnotu. Regulační meze diagramu jsou nastaveny

$$\pm L\sigma_z, \tag{2.23}$$

kde L je šířka regulačních mezí a σ_z je směrodatná odchylka. Parametr $\lambda = 0.2$ a šířka regulačních mezí $L = 3$ byla nastavena při tvorbě modifikovaných EWMA regulačních diagramů. Podle *Testika* [68] rozpyl modifikovaných EWMA regulačních diagramů je dán

$$\sigma_z^2 = \sigma_a^2 \frac{(1-\nu)}{(1+\nu)} \left\{ 1 + \frac{1.6\nu\sqrt{(1-\phi^2)/n}}{(1-\nu\phi)} + \frac{(1+\nu\phi)}{n(1-\nu\phi)} \right\}, \tag{2.24}$$

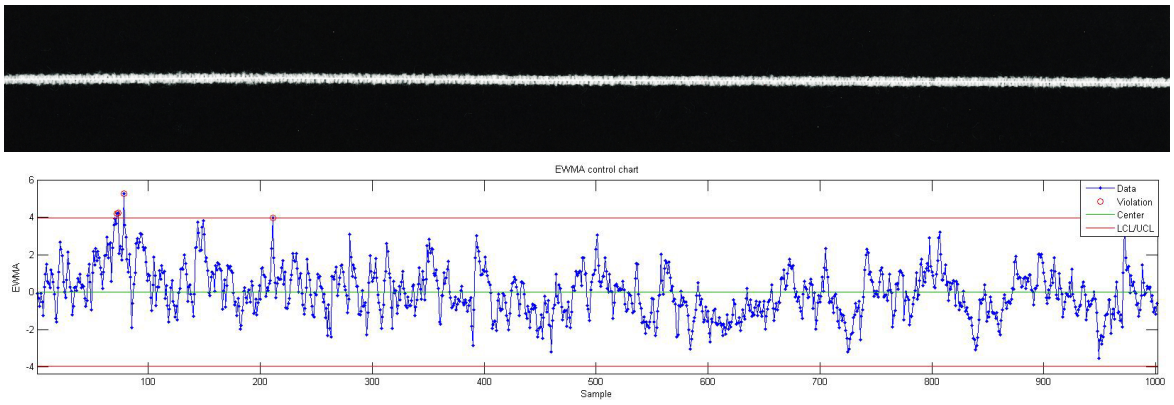

(a)

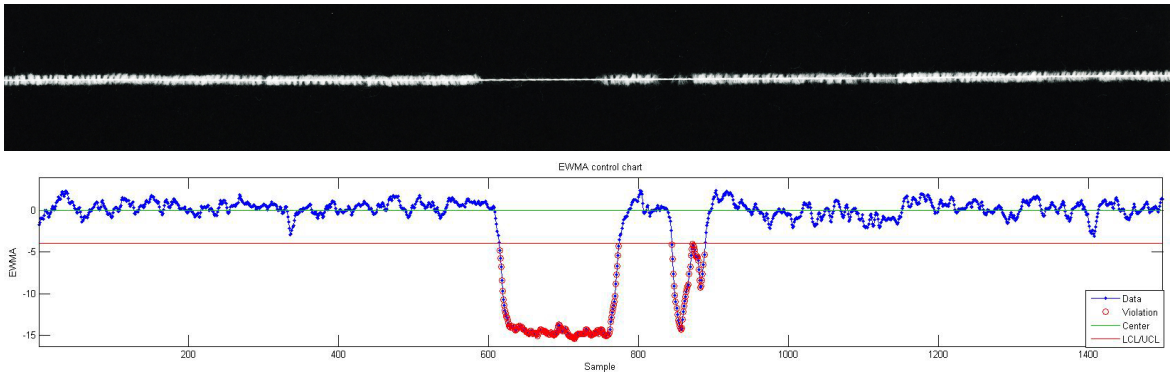

(b)

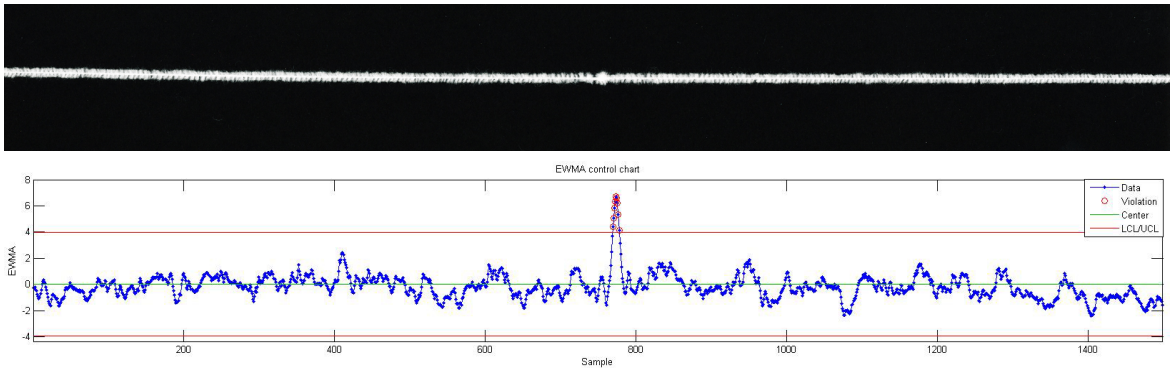

(c)

Obrázek 2.13: Modifikované EWMA regulační diagramy pro rezidua, (a) příze bez defektu, (b) prázdné místo, (c) nopek.

kde $\nu = 1 - \lambda$ a n je počet pozorování trénovací množiny použitých při odhadu parametrů AR(1) modelu. Tato praktická modifikace redukuje pravděpodobnost false alarmů. Diagramy úspěšně odhalily různé typy běžných defektů vyskytujících se v přízi (viz obr. 2.13(b),(c)). Obr. 2.13(a) zobrazuje EWMA regulační diagram trénovací sady, tj. obrazu příze bez porušení.

Laboratorní zařízení pro kontinuální pořizování obrazu a okamžitého vyhodnocování kvality textilií lze přizpůsobit pro monitorování kvality délkových textilií, v tomto případě žinylkové příze.

2.6 Simulace deformace textilní výztuže

Úlohu simulace deformace tkaniny jako textilní výztuže v kompozitech můžeme rozdělit do několika částí. Jednou z částí je modelování odolnosti svazku paralelních vláken proti rostoucí zátěži, jež je obdobou stanovení spolehlivosti systému složeného z paralelních komponent. Spolehlivostí budeme chápat odolnost systému proti zátěži způsobující poruchy jednotlivých komponent systému, v tomto případě za poruchy systému uvažujeme přetrhy jednotlivých vláken. Na rozdíl od houževnatých materiálů kompozitní materiály složené například s uhlíkových vláken jsou křehké a k popisu jejich chování je možné využít modely založené na konceptu nejslabšího článku. Poruchy komponent systému závisí od pevnosti materiálu, zátěže a chování struktury, která zahrnuje interakci mezi komponentami, okrajové podmínky atd. V práci [4] (viz Příloha 4) je uvažován systém složený z křehkých paralelních vláken a je modelována odolnost tohoto systému proti rostoucí zátěži. Výsledky z navrženého modelu lze využít pro simulaci deformace tkaniny a simulaci defektů ve tkanině.

Předpokládejme, že svazek vláken je zatěžován silou rostoucí od 0 až do přetrhu všech vláken, nebo do hodnoty S_{max}, kdy je experiment ukončen. V práci je použitý standardní popis z analýzy přežití, avšak místo doby přežití nás zajímá pevnost v tahu pro jeden pramen. Je uvažován Danielsův model přerozdělení síly působící na svazek mezi jednotlivá vlákna (*Belyaev a Rydén*, [69] *Volf a Linka* [70]). V tomto modelu se předpokládá, že síla působící na svazek je rovnoměrně přerozdělena mezi nepřetržená vlákna a pevnosti jednotlivých vláken jsou nezávislé, stejně rozdělené náhodné veličiny. V modelu je pozorována celková síla působící na svazek, přetržení vlákna vede k okamžitému přerozdělení síly působící na zbylé nepřetržené vlákna (z důvodu prudkého růstu síly působící na každé jednotlivé nepřetržené vlákno). Následně může dojít k přetržení několika dalších vláken (ne nutně všech, jejich pevnosti jsou náhodné veličiny). V tomto případě neznáme přesnou hodnotu síly, při které dojde k přetrhu jednotlivých vláken a ani pořadí ve kterém se trhají. V případě přetrhu více vláken známe pouze sílu, která způsobí přetrh prvního vlákna a interval síly, ve kterém dojde k přetrhu zbylých vláken. K registrování přetrhů při postupném zatěžování svazku vláken je využitý indikátorový proces v rámci modelu čítacího procesu.

Uvažujeme jedno vlákno a náhodnou veličinu U, která představuje pevnost v tahu. Předpokládáme, že náhodná veličina U má spojité rozdělení na intervalu $[0, \infty)$ s distribuční funkcí $F(u)$, hustotou $f(u)$ a intenzitou (rizikovou funkcí) $h(u) = f(u)/(1-F(u))$ definovanou na intervalu $u \in [0, S]$ takovou, že $F(S) < 1$. $H(t) = \int_0^t h(u)du$ označuje kumulativní intenzitu. Přetrh vlákna během rostoucího tahového napětí je popsáno dvěma náhodnými procesy, čítacím procesem $N^1(u)$ a indikátorovým procesem $I^1(u)$, které jsou standardní v analýze přežití. $I^1(u) = 1$ jestliže síla u působící na vlákno je pozorovatelná, jinak $I^1(u) = 0$. Speciálně, $I^1(u) = 0$, jestliže je vlákno přetrženo, jestliže je pozorování ukončeno a také pro hodnoty síly u během skokovitého růstu síly. Předpokládejme, že trajektorie $I^1(u)$ jsou zleva spojité. Pokud jde o $N^1(u)$, $N^1(0) = 0$ a $N^1(u)$ se zvětšují o 1 při hodnotě síly u_b, která způsobí přetrh vlákna a platí $I^1(u_b) = 1$.

Předpokládejme, že svazek je složen z m vláken a že přežití vláken (pevnost v tahu vláken) je popsaná nezávislými stejně rozdělenými náhodnými veličinami $U_j, j = 1, ..., m$ s rozdělením daným hustotou $f(u)$, distribuční funkcí $F(u)$, rizikovou funkcí $h(u)$ a kumulativní intenzitou $H(u)$. Síla působící na svazek je v každém okamžiku rovnoměrně přerozdělena mezi nepřetržená vlákna a struktura pozorovaných dat je uvedena v následujícím příkladu.

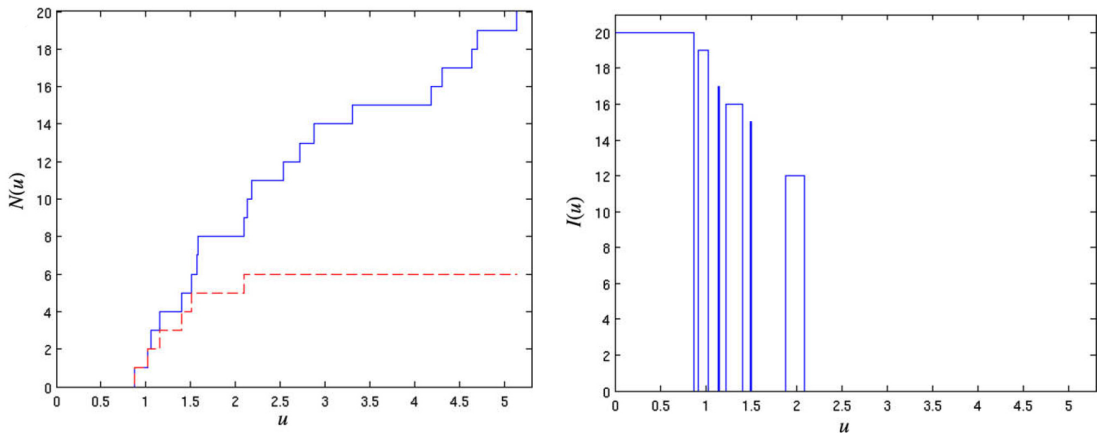

(a) (b)

Obrázek 2.14: (a) Čítací proces $N(u)$ a (b) indikátorový proces $I(u)$.

Představme si, že přetrhy vláken se objevují při třech globálních tahových silách působících na svazek, $0 < s_1 < s_2 < s_3 < S_{max}$ a že při síle s_1 a s_2 se přetrhne k_1 a k_2 vláken a zůstavajících k_3 vláken se přetrhne při síle s_3. Platí $k_1 + k_2 + k_3 = m$. Před prvním pozorovatelným přetrhem síla natahující každé vlákno byla rovna $u_1 = s_1/m$, v momentě druhého přetrhu byla rovna $u_2 = s_2/(m - k_1)$ a v okamžiku posledního přetrhu byla tato tahová síla působící na posledních $m - k_1 - k_2$ vláken $u_3 = s_3/(m - k_1 - k2) = s_3/k_3$. Byly pozorovány tři přetrhy (přetrhy pozorované při známé síle) způsobené sílou u_1, u_2 a u_3. Ostatní přetrhy byly způsobeny neznámými silami z intervalů $(u_1, \overline{u}_1 = s_1(m-k_1+1)), (u_2, \overline{u}_2 = s_2(m-k_1-k_2+1))$ a $(u_3, \overline{u}_3 = s_3)$, přičemž se jedná o k_1-1, k_2-1, k_3-1 vláken. Maximální síla je dostatečně velká (např. $S_{max} > S.m$), aby nedocházelo k předčasnému ukončení experimentů.

Uvažujme, že je testováno n identických, nezávislých svazků vláken. Označme U_{ij} náhodné veličiny (přežití), $N_{ij}(u), I_{ij}(u)$ označme odpovídající čítací a indikátorové procesy pro j-té vlákno i-tého svazku $(j = 1, 2, ..., m, i = 1, 2, ..., n)$. Dále označme

$$N_i(u) = \sum_{j=1}^{m} N_{ij}(u), \quad N(u) = \sum_{i=1}^{n} N_i(u), \quad I_i(u) = \sum_{j=1}^{m} I_{ij}(u), \quad I(u) = \sum_{i=1}^{n} I_i(u). \quad (2.25)$$

Nejběžnější odhad kumulativní intenzity poruch H_u (rozdělení pevnosti v tahu svazku) je Nelson-Aalenův odhad

$$\hat{H}_n(u) = \int_0^u \frac{dN(v)}{I(v)}, \quad (2.26)$$

kde definujeme $0/0 = 0$. Je patrné, že schopnost odhadu dobře aproximovat správné $H(t)$ závisí na indikátoru, tj. na pozorovatelnosti čítacího procesu pro všechny hodnoty síly u v sledovaném intervalu $[0, S]$.

Příklad svazku vláken složených z $m = 20$ vláken, kde předpokládáme, že pevnost v tahu (náhodná veličina U_{ij}) každého vlákna má Weibullovo rozdělení s kumulativní intenzitou

$$H(u) = \left(\frac{u}{\theta}\right)^{\beta} \quad (2.27)$$

a simulace přetrhu $n = 1000$ takovýchto svazků je uvedena v práci [4]. Výsledek simulace pro jeden takový svazek s parametry $\beta = 2$ a $\theta = 3$ je na obr. 2.14(a),(b). Globální

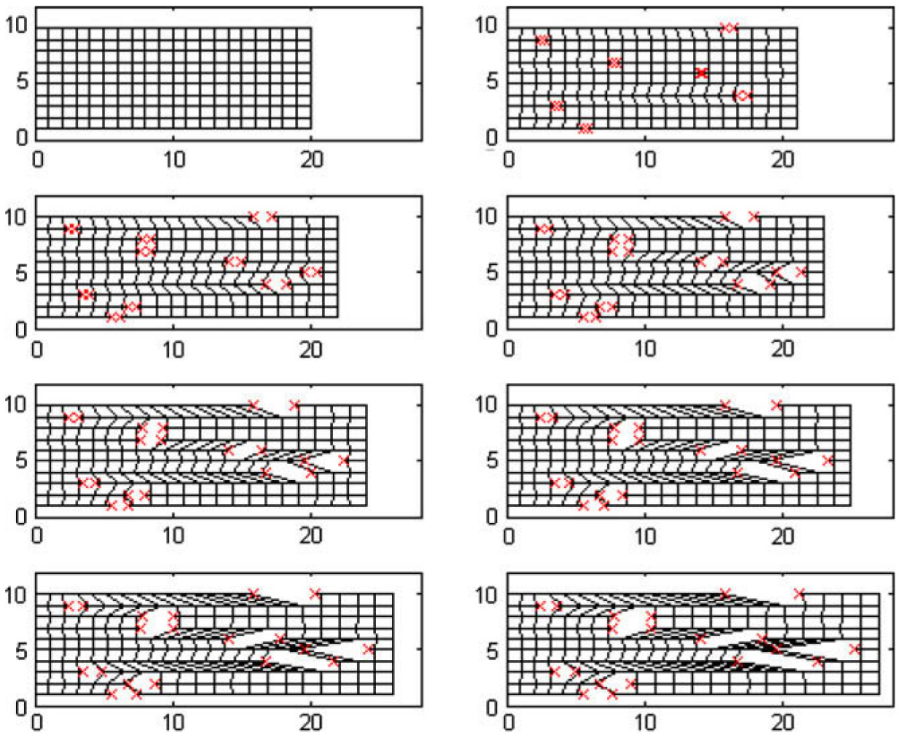

Obrázek 2.15: Simulace deformace do přetrhu všech vláken.

síla t při které se svazek přetrhne byla pozorována také. Byl obdržen výběr $n = 1000$ realizací t_i náhodné veličiny R - pevnosti v tahu svazku. Empirická distribuční funkce $\hat{F}_R(t) = \frac{1}{n}\sum I[t_i < t]$ konstruovaná z tohoto výběru a jiné empirické charakteristiky např. odhad kumulativní rizikové funkce $-\ln(1 - \hat{F}_R(t))$ a Nelson-Aalenův odhad stanovený za použití uspořádaného výběru

$$\hat{H}_R(t) = \sum_{i=1}^{n} \frac{I[t_i < t]}{n - (i) + 1} \tag{2.28}$$

jsou uvedeny na obrázcích v práci [4].

Na základě předchozí analýzy byla *Tunákem et al.* [4] navržena simulace procesu natahování a přetrhu svazku vláken. V simulaci se uvažuje každé vlákno jako sada uzlů a oblouků. V modelu se uvažuje tření mezi vlákny - odpor proti posunutí mezi jednotlivými vlákny, což je dalším zdrojem napětí. V tomto případě každé vlákno může prasknout víc než jednou. Simulace je prováděna ve smyslu změny pozice uzlů jenom v horizontálním směru. Celkové napětí je sumou napětí z jejich protažení (napětí je mocninnou funkcí protažení s exponentem větším než jedna) a tření (závisí lineárně on posunutí vlákna s ohledem na sousední vlákno). Jestliže celkové napětí překročí určitou hodnotu, vlákno praskne. Obr. 2.15 zobrazuje jeden takovýto experiment.

Uvedený model je možné využít pro simulaci defektu typu zátrh nebo díra. Síť tvořena sadou uzlů (vazné body) a ohebných oblouků (příze) představuje jednoduchý model tkaniny v plátnové vazbě. Defekt typu zátrh se projevuje jako lokální přemístění útkových nití, nitě nejsou v seskupení. Osnovní nitě jsou přetržené nebo velmi napnuté. Podobně defekt typu díra je místo, na kterém je několik sousedních osnovních a/nebo útkových nití přetržených. Je výsledkem chybějících částí nití různých velkostí a tvarů. Tyto typy defektů vznikají, když jedna nebo více útkových nití je zatržených prostřednictvím tlustého místa nebo uzlu a nitě jsou zadřené nebo přemístěné. V simulaci

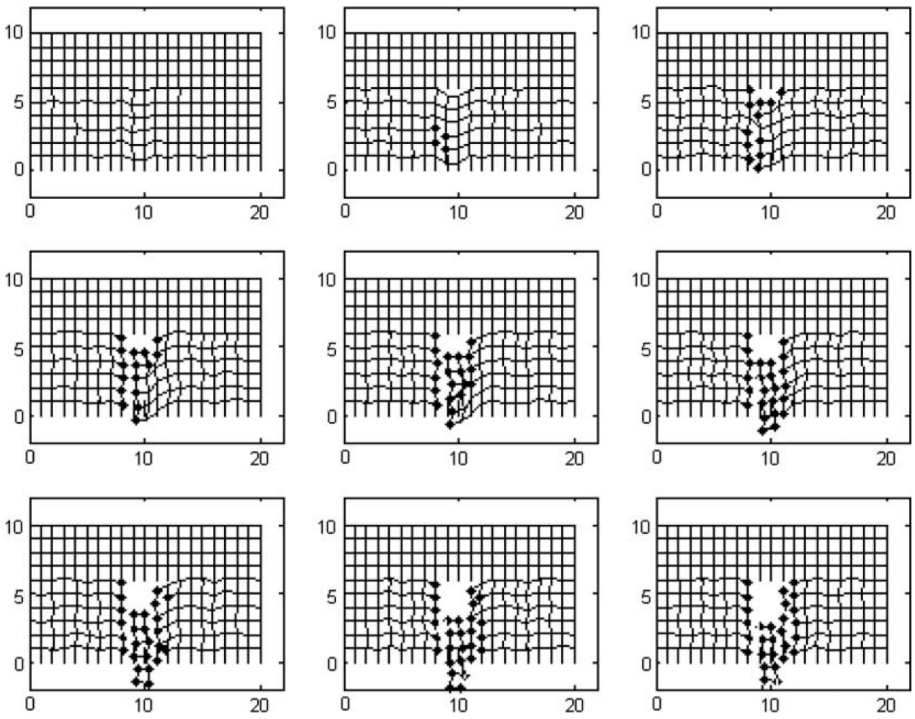

Obrázek 2.16: Přiklad simulace při působení vertikálního tlaku.

se předpokládá, že směr napětí je kolmý k útkové soustavě nití a hranice mríže jsou fixované. Napětí je přerozdělováno přes mříž, které způsobuje natahování a napětí v obloucích. Jestliže napětí překročí určitou hodnotu, oblouk (příze) praskne. V modelu se navíc uvažuje změna úhlu mezi oblouky, které spojují uzly a při překročení kritické hodnoty příze praskne. Obr. 2.16 zobrazuje příklad účinku verikálního tlaku působícího shora do centrálních uzlů mříže a výsledek simulace, když tlak postupně roste. Různé kombinace napětí způsobené změnou délky oblouků a úhlů mezi oblouky, spolu s kritickými hodnotami umožňují simulovat případy, které odpovídají reálným situacím.

2.7 Závěr

Obsahem habilitační práce je souhrn simulačních metod a metod obrazové analýzy pro monitorování struktury textilních útvarů. Obrazová analýza má v oblasti monitorování kvality velmi důležité místo, protože poskytuje informaci o geometrii, povrchu, defektech, o úpravách povrchu výrobku a jiných charakteristikách. Získané výsledky dokumentují, že uvedené postupy lze použít pro monitorování struktury lineárních a plošných textilních útvarů s ohledem na jejich kvalitu. Integrace navržených postupů a statistických regulačních diagramů do sofistikovaných systémů povede k vytvoření automatických vizuálních expertních systémů pro monitorování kvality těchto útvarů. Z výsledků práce lze učinit několik závěrů.

Fourierova transformace se ukázala jako vhodná pro stanovení strukturní anizotropie nebo směrové orientace vlákenných a jiných objektových systémů. U netkaných plošných textilních útvarů je nezbytně nutné zajistit stabilitu kvalitativních charakteristik těchto struktur. K tomuto účelu je nutné z těchto struktur odhadnout rozdělení směrového uspořádání vlákenného materiálu v ploše. V práci uvedené postupy umožňují tyto kvalitativní charakteristiky monitorovat.

V oblasti detekce defektů ve tkaninách bylo ověřeno, že algoritmus detekce založený na statistických charakteristikách druhého řádu je použitelný pro detekci vad ve tkaninách. Tímto postupem můžeme efektivně detekovat směrové, ale taky nesměrové typy vad. Algoritmus není vhodný pro vady, které nezpůsobují příliš velké změny struktury. Automatická detekce založena na spektrálních charakteristikách získaných z Fourierova frekvenčního spektra vykazuje větší přesnost detekce vad. Užitím této metody můžeme detekovat vady spojené se změnou dostavy tkaniny a kontrastní nesměrové vady. V porovnání se statistickým přístupem se zlepšila detekce u typů vad, které nezpůsobují příliš velkou změnu struktury. Algoritmy a postupy pro detekci defektů jsou efektivní jenom pro některé skupiny vzorů nebo materiálů a pro jiné skupiny selhávají. Pro pokrytí co největšího spektra skupin vzorovaných textur a materiálů bude třeba vyvinout zcela nové typy hybridních algoritmů, které budou kombinovat stávající přístupy s novými moderními, které jsou založené na grupách symetrie pro vzorované textury.

Metoda automatického zjišťování dostavy tkaniny může být také využita pro detekci vad, které jsou určitým způsobem spojené se změnou dostavy tkaniny. Vhodné je použití pro vady ve směru útku, které se rozkládají po celé šířce tkaniny. Myšlenka detekce defektů v útkovém směru je založena na sledování informace o hodnotě dostavy útku ve směru délky tkaniny. Změna hodnoty dostavy oproti očekávané hodnotě indikuje porušení struktury.

V oblasti monitorování kvality žinylkové příze se ukázalo, že navržené modifikované EWMA regulační diagramy úspěšně odhalily různé typy běžných defektů vyskytujících se v přízi. Ukazuje se, že podobně je možné použít tyto modely pro hodnocení chlupatosti, nerovnoměrnosti a vzhledu přízí a délkových textilních útvarů.

Na základě získaných výsledků lze konstatovat, že oblast analýzy obrazových dat a vícerozměrných regulačních diagramů je velmi perspektivní a moderní oblastí pro aplikace statistického řízení jakosti. Monitorování obrazu je přirozeným rozšířením monitorování profilů s rostoucí perspektivou v následujících 5-8 letech i s rostoucím počtem reálných aplikací v průmyslu. Přitom koncept statistického řízení jakosti v tomto přístupu hraje zásadní roli. Nejde jenom o zlepšení výkonnosti existujících metod či jejich aplikace na obrazová data. Především je nutné vyvinout zcela nové typy regulačních diagramů, které by odrážely prostorový charakter těchto dat a poskytly například i informaci a větší citlivost na situace, kdy některé vady jsou častější v některých částech plochy. Zejména se bude jednat o aplikace v textilním a materiálovém průmyslu. Nový typ sofistikovaného expertního inspekčního systému by měl být použitelný na co možná nejširší spektrum materiálů, včetně vzorovaných materiálů a to nejenom textilních.

2.8 Prohlášení

Rád bych na tomto místě poděkoval všem spoluautorům prací, které jsem prezentoval jako součást habilitační práce. Čestně prohlašuji, že ve všech prípadech byl můj podíl na přípravě, realizaci a interpretaci výsledků větší nebo stejný jako všech ostatních spoluautorů.

2.9 Použitá literatura

[33] Rataj, J. and Saxl, I. Analysis of Planar Anisotropy by Means of Steiner Compact: A Simple Graphical Method. *Acta Stereologica*, **7**(2), 1988, pp. 107–112.

[34] Josso, B., Burton, R., and Lalor, J. Texture Orientation and Anisotropy Calculation by Fourier Transform and Principal Component Analysis. *Mechanical Systems and Signal Processing*, **19**(2), 2005, pp. 1152–1161. issn: 0888-3270.

[35] Liu, Z. Q. Scale Space Approach to Directional Analysis of Images. *Applied Optics*, **30**(11), 1991, pp. 1369–1373. issn: 1559-128X.

[36] Holota, R. and Němeček, S. Recognition of Oriented Structures by 2D Fourier Transform. In: *Applied Electronics 2002*. Plzeň, Czech Republic, 2002. isbn: 80-7082-881-1.

[37] Tonar, Z. et al. Microscopic Image Analysis of Elastin Network in Samples of Normal, Atherosclerotic and Aneurysmatic Abdominal Aorta and its Biomechanical Implications. *Journal of Applied Biomedicine*, **1**, 2003, pp. 149–159. issn: 1214-021X.

[38] Kula, J. Segmentace objektů z obrazu vlákenné struktury na základě jejich orientace. In: *Workshop pro doktorandy FS a FT TUL*. Rokytnice nad Jizerou, Czech Republic, 2011. isbn: 978-80-7372-765-9.

[39] Gonzales, R. C., Woods, R. E., and Eddins, S. L. *Digital Image Processing using MATLAB*. Pearson Prentice-Hall, 2004.

[40] Tunák, M. *Detekce vad v plošných textiliích*. Disertační práce. Technická univerzita v Liberci, 2008.

[41] Schicktanz, K. Automatic Fault Detection Possibilities on Nonwoven Fabrics. *Melliand Textilberichte*, **74**, 1993, pp. 294–295. issn: 0341-0781.

[42] Kumar, A. P. *Automated Defect Detection in Textured Materials*. Ph.D. Thesis. The University of Hong Kong, 2001.

[43] Chan, C. and Pang, G. K. H. Fabric Defect Detection by Fourier Analysis. *IEEE Transactions on Industry Applications*, **36**(5), 2000, pp. 1267–1276. issn: 0093-9994.

[44] Kothari, V. Automatic Fabric Inspection. *Textile Review*, **5**(9), 2010, pp. 29–34.

[45] Ngan, H. Y. T., Pang, G. K. H., and Yung, N. H. C. Automated Fabric Defect Detection - A Review. *Image and Vision Computing*, **29**, 2011, pp. 442–458. issn: 0262-8856.

[46] Ngan, H. Y. T., Pang, G. K. H., and Yung, N. H. C. Motif-based Defect Detection for Patterned Fabric. *Pattern Recognition*, **41**(6), 2008, pp. 1878–1894. issn: 0031-3203.

[47] Haralick, R. M., Shanmugam, K., and Dinstein, I. Textural Features for Image Classification. *IEEE Transaction on Systems, Man and Cybernetics*, **3**(6), 1973, pp. 610–621. issn: 0018-9472.

[48] Carstensen, J. M. *Description and Simulation of Visual Texture*. Ph.D. Thesis. Technical University of Denmark, 1992.

[49] Kuo, C. F. J. and Su, T. L. Gray Relational Analysis for Recognizing Fabric Defects. *Textile Research Journal*, **73**(5), 2003, pp. 461–465. ISSN: 0040-5175.

[50] Bodnarova, A., Bennamoun, M., and Kubik, K. K. Suitability Analysis of Techniques for Flaw Detection in Textiles using Texture Analysis. *Pattern Analysis and Applications*, **3**, 2000, pp. 254–266. ISSN: 433-7541.

[51] Bersimis, S., Psarakis, S., and Panaretos, J. Multivariate Statistical Process Control Chart: An Overview. *Quality and Reliability Engineering International*, **23**(5), 2007, pp. 517–543. ISSN: 1099-1638.

[52] Ročková, K. *Monitorování defektů ve tkaninách pomocí Hotellingova regulačního diagramu a analýzy hlavních komponent*. Diplomová práce. Technická univerzita v Liberci, 2010.

[53] Jeon, Y. J. and Jang, J. Applying Image Analysis to Automatic Inspection of Fabric Density for Woven Fabrics. *Fibers and Polymers*, **6**(2), 2005, pp. 156–161. ISSN: 1229-9197.

[54] Liqing, L., Tingting, J., and Xia, C. Automatic Recognition of Fabric Structures Based on Digital Image Decomposition. *Indian Journal of Fiber and Textile Research*, **33**2008, pp. 388–391. ISSN: 0971-0426.

[55] Yildirim, B. and Baser, G. Processing Approach for Weft Density Measurement on the Loom. In: *STRUTEX 2009, Proceedings of 16th International Conference on Structure and Structural Mechanics of Textiles*. Liberec, Czech Republic, 2009. ISBN: 978-80-7372-542-6.

[56] Wood, J. E. Applying Fourier and Associated Transform to Pattern Characterization in Textiles. *Textile Research Journal*, **60**(4), , 1990, pp. 212–220. ISSN: 0040-5175.

[57] Ravandi, S. A. H. and Toriumi, K. Fourier Transform Analysis o Plain Weave Fabric Appearance. *Textile Research Journal*, **65**(11), 1995, pp. 676–683. ISSN: 0040-5175.

[58] Xu, B. Identifying Fabric Structures with Fast Fourier Transform Techniques. *Textile Research Journal*, **66**(8), 1996, pp. 496–506. ISSN: 0040-5175.

[59] Anděl, J. *Statistická analýza časových řad*. SNTL Praha, 1976.

[60] Cipra, T. *Analýza časových řad s aplikacemi v ekonomii*. SNTL Praha, 1986.

[61] Lin, J. J. Applying a Co-occurrence Matrix to Automatic Inspection of Weaving density for Woven Fabrics. *Textile Research Journal*, **72**(6), 2002, pp. 486–490. ISSN: 0040-5175.

[62] Meloun, M. and Militký, J. *Kompendium statistického zpracování dat*. Academia Praha, 2002.

[63] Barella, A. Yarn Hairiness. *Textile Progress*, **13**(1), 1983, pp. 1–57. ISSN: 0040-5167.

[64] Barella, A. The Hairiness of Yarns. *Textile Progress*, **24**(3), 1993, pp. 1–46. ISSN: 0040-5167.

[65] Guha, A. et al. Measurement of Yarn Hairiness by Digital Image and Signal Processing Methods. *Journal of The Textile Institute*, **101**(3), 2010, pp. 214–222. ISSN: 0040-5000.

[66] Xu, B. G. Automatic Measurement and Recognition of Yarns Snarl by Digital Image and Signal Processing Methods. *Textile Research Journal*, **78**(5), 2008, pp. 439–456. ISSN: 0040-5175.

[67] Liu, J., Xie, Z., and Gao, W. Automatic Determination of Slub Yarn Geometrical Parameters based on an Ameended Similarity-based Clustering Method. *Textile Research Journal*, **80**(11), 2010, pp. 1075–1083. ISSN: 0040-5175.

[68] Testik, M. C. Model Inadequacy and Residuals Control Chart fo Autocorrelated Process. *Quality and Reliability Engineering International*, **21**, 2005, pp. 115–130. ISSN: 0748-8017.

[69] Belyaev, Y. and Rzdén, P. *Non-parametric Estimators of the Distribution of Tensile Strengths for Wires*. Research Report. University of Umea, 1997.

[70] Volf, P. and Linka, A. On Reliability of System Composed of Paralle Units Subject to Increasing Load. *International Journal of Reliability, Quality and Safety Engineering*, **7**(4), 2000, pp. 271–284. ISSN: 0218-5393.

Příloha 1

[1] Tunák, M. and Linka, A. Analysis of Planar Anisotropy of Fibre Systems by using 2D Fourier Transform. *Fibres and Textiles in Eastern Europe*, **15**(5-6), 2007, pp. 86–90. issn: 1230-3666. IF=0.629.

Maroš Tunák,
Aleš Linka

Technical University in Liberec
Faculty of Textile Engineering
Department of Textile Materials
Studentská 2, 461 17 Liberec 1, Czech Republic
E-mail: maros.tunak@tul.cz
ales.linka@tul.cz

Analysis of Planar Anisotropy of Fibre Systems by Using 2D Fourier Transform

Abstract
This paper describes a simple method of description of the anisotropy of fibre systems using image analysis. The proposed method is based on Fourier transform which is in frequency domains displayed by high values of frequency components corresponding to major structural direction lines in the spatial domain image. The values of frequency components are summarised in directional vectors depending on their certain angle and transformed to a polar diagram and histogram. The polar diagram can be seen as an estimate of the rose of directions.

Key words: *anisotropy, fibre system, Fourier transform, rose of directions.*

Introduction

The article is aims to graphically describe the planar anisotropy of fibre or other planar systems based on image analysis. The method uses spectral techniques with the aid of two-dimensional Fourier transform. The objects are an important part of an image and represent real-world objects. These objects are either randomly placed or they prefer certain directional placement. The objects should be in contrast with the background (gradient of image function on the edges of the object and background). In textile experience, the objects are considered to be fibres, threads, cross – sections of fibres etc., systems containing objects can be webs, fibre layers, woven fabrics, knitted fabrics, nonwoven textiles etc.

The characteristics of planar anisotropy is the angular density of length of thread or fibres $f(\alpha)$, which defines the length of thread or fibres orientated to an angular segment $\alpha \pm \alpha/2$. Function $f(\alpha)$ or rather the polar plot of density $f(\alpha)$ is called the rose of directions. An experimental graphical method for the estimation of $f(\alpha)$ is described in [3]. This method uses the net of angles $\alpha_1 ... \alpha_n$ situated at the top of fibre system being monitored for the construction of the rose of intersections. The rose of directions as an estimate of function $f(\alpha)$ is then obtained from the rose of intersections through the graphical construction of the Steiner compact. The number limit of angles is $n \leq 18$.

The graphical method proposed is based on the spectral method of image analysis. The goal of this method is a fast graphical representation of the directional arrangement of objects (estimation of anisotropy $f(\alpha)$) in the form of rose of directions and histogram.

2D Fourier Transform (2DFT)

The spectral approach is based on two-dimensional (2D) Fourier transform (FT) and is suitable for describing the textured images. The dominating directions (gradient of image function) in the directional textures (spatial domain) correspond to the large magnitude of frequency components distributed along the straight lines in the Fourier spectrum (frequency domain). In contrast, the purely random texture causes, that the frequency components in the power spectrum are approximately isotropic and possess a near circular shape. The Fourier transform is rotation dependent, i.e. rotating the original image by an angle will rotate its corresponding frequency plane by the same angle. The transform of horizontal lines in the spatial domain image appears as vertical lines in the Fourier domain image, i.e. the lines in the spatial domain image and its transformation are orthogonal to each other [5]. Let $f(x,y)$ be the grey level at pixel coordinates (x,y). Let the size of spatial domain image be $M \times N$. For such an image the direct and inverse Fourier transforms are given

$$F(u,v) = \sum_{x=0}^{M-1} \sum_{y=0}^{N-1} f(x,y) e^{-j2\pi (ux/M + vy/N)} \quad (1)$$

$$f(x,y) = \frac{1}{MN} \sum_{u=0}^{M-1} \sum_{v=0}^{N-1} F(u,v) e^{j2\pi (ux/M + vy/N)} \quad (2)$$

where $u = 0, 1, 2, ..., N - 1$ and, $v = 0, 1, 2, ..., M - 1$ are frequency variables [4]. If $f(x,y)$ is real, its transform is, in general, complex. $R(u,v)$ and $I(u,v)$ represent the real and imaginary components of $F(u,v)$, the Fourier spectrum is defined as

$$|F(u,v)| = \sqrt{R^2(u,v) + I^2(u,v)} \quad (3)$$

The power spectrum $P(u,v)$ and the representation of $P(u,v)$ scaled to 8 - bit grey

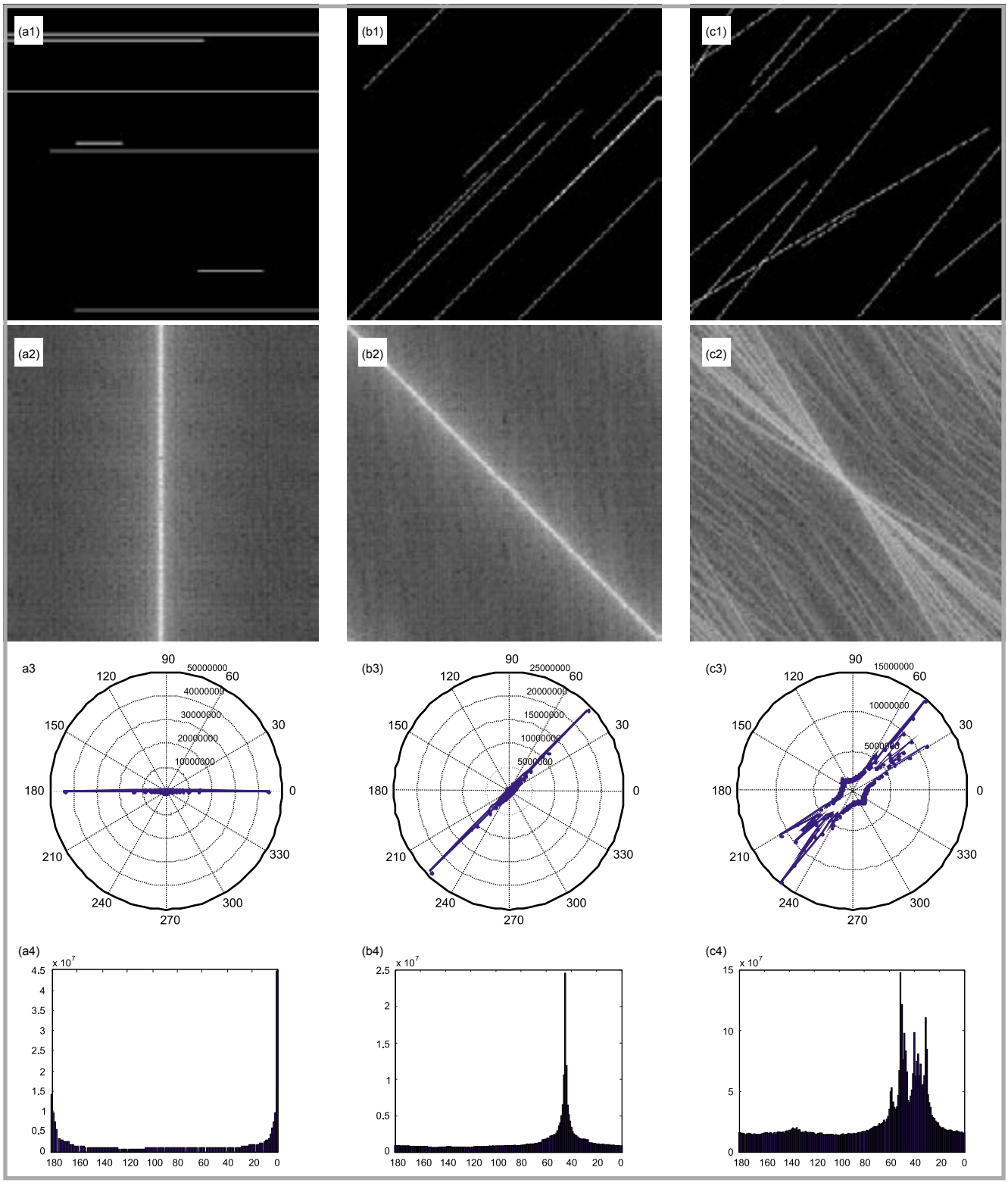

Figure 1. *(a1) - (c1) Binary images of simulated structural lines, (a2) - (c2) power spectrum as an intensity image, (a3) - (c3) polar plot of S_α, (a4) - (c4) histogram of S_α.*

levels is converted

$$P(u,v) = |F(u,v)|^2 \tag{4}$$

$$P(u,v) = \log(1 + |F(u,v)|^2) \tag{5}$$

If $f(x,y)$ is real, its Fourier transform is conjugated symmetrically around the origin, that is

$$F(u,v) = F^*(-u,-v) \tag{6}$$

which implies that the Fourier spectrum is also symmetric around the origin

$$|F(u,v)| = |F(-u,-v)| \tag{7}$$

Figures 1 (a1) - (c1) represent binary images of simulated structural lines in the 0° direction, 45° direction, in the interval 30° - 60°, respectively. The length, position and orientation of the lines were randomly generated from uniform distribution. Figures 1 (a2) - (c2) show power spectrums scaled into 256 grey levels.

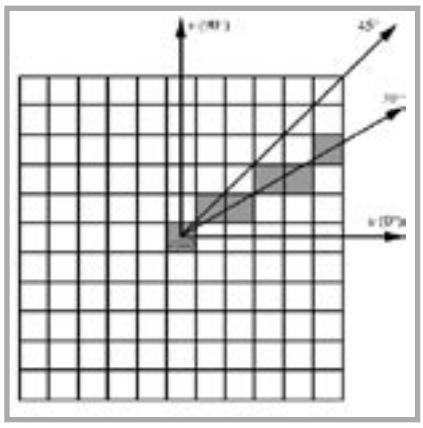

Figure 2. *Coordinates for directional vector dependent on α = 30°.*

As can be seen from these figures, information about the direction of major structural lines in the spatial domain is concentrated in the Fourier domain image as the direction of corresponding large magnitude frequency components (represented by white colour).

Assumptions

Let the image matrix be a square matrix of size $M \times M$. Let M be an odd number - it is convenient for the specification of the origin of the Fourier spectrum, and image matrix be scaled to 8 – bit grey levels (monochromatic image). All frequency components from the Fourier frequency spectrum are summarised together in the directional vector of certain angle α. Since the transform of real image function $f(x,y)$ is complex, the absolute magnitudes of frequency components $|F(u,v)|$ are obtained according to relation (3). The sum of frequency components S_α in the directional vector is given by

$$S_\alpha = \sum_{k=1}^{(M+1)/2} |F(u,v)| \qquad (8)$$

where α forms an angle between the directional vector and u axis, $|F(u,v)|$ is a frequency component of the directional vector at the coordinates (u,v) and M is the size of the image.

Computation of directional vector coordinates

As can be seen from equation (7), the Fourier frequency spectrum is symmetric around the origin; it is sufficient to add up the frequency components of directional vectors depending on α in the interval $(0, \pi)$, i.e. to specify that coordinates for the I. and II. quadrant. are symmetric around the ordinate (v axis, $\pi/2$), that is $(u,v) = (-u,v)$, therefore the determination of coordinates for I. quadrant suffices

$$\begin{aligned} 0 \le \alpha \le \frac{\pi}{4} \quad &\rightarrow \quad v = u\tan\alpha \\ \frac{\pi}{4} < \alpha \le \frac{\pi}{2} \quad &\rightarrow \quad u = \frac{v}{\tan\alpha}. \end{aligned} \qquad (9)$$

Here u is the abscissa axis or column number, v is the ordinate or row number and coordinates (u,v) are rounded to the closest integer, because the coordinates acquire an integer discrete value. The DC (Direct Current) component is the origin of frequency domain $F(0,0)$, and represents the origin of the system of coordinates. Figure 2 displays an example of coordinates for directional vector in I. quadrant, $\alpha = 30°$.

For an estimation of the rose of directions the magnitude of S_α is plotted onto the polar diagram and consequently into the histogram. The algorithm realising the method proposed was created in MATLAB programming language (Image Processing Toolbox). Input parameters are an image matrix and the output is the visualisation of the direction arrangement of objects in the form of a polar plot of S_α and histogram of S_α, which can be seen as the estimate of the rose of direction.

Figure 3 (a) displays the binary image of simulated structural lines from Figure 1 (c1) and corresponding estimate of the rose of direction achieved by means of the Steiner compact in six directions $\alpha_k = k\pi/6$ for $k = 1, \ldots, 5$. The red line in Figure 3 (c) displays the estimate of the rose of direction, also in six directions, and Figure 3 (d) in directions with one-degree step using image analysis with the aid of Fourier transform. Figures 1 (a3) - (c3) display the polar plot of S_α and represent the estimation of function $f(\alpha)$ (rose of directions), and Figure 1 (a4) - (c4) display the histogram of S_α for the binary images from the Figure 1 (a1) - (c1).

Figures 4 (a1) - (c1) show grey level images of nanofibres with a randomly distributed structure, captured by a screnning electron microscope. Figure 4 (a2) - (c.2) represent a corresponding power spectrum, Figure 4 (a3) - (c3) is a polar plot of S_α and Figure 4 (a4) - (c4) is the estimate of the rose of directions by means of the Steiner compact. As can be seen from the polar plot, the image struc-

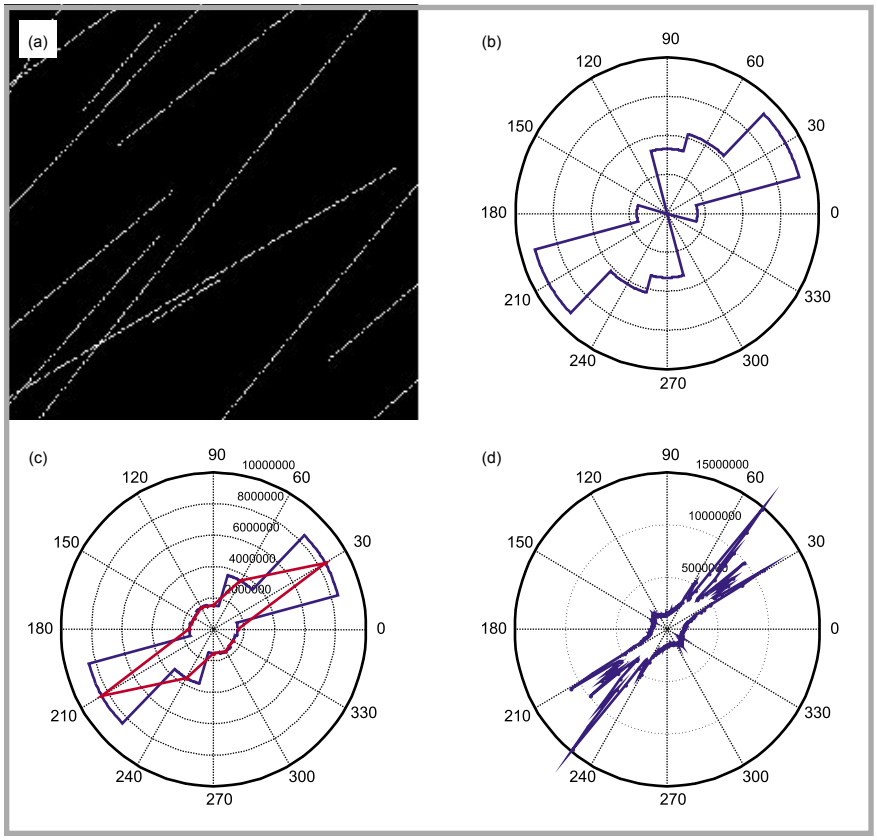

Figure 3. *(a) Simulated fibre system, (b) estimation of the rose of directions by means of Steiner compact, (c) estimation of the rose of directions by using the Fourier transform, plot with 30 degree step, (d) estimation of the rose of directions by using the Fourier transform, plotted with 1 degree step.*

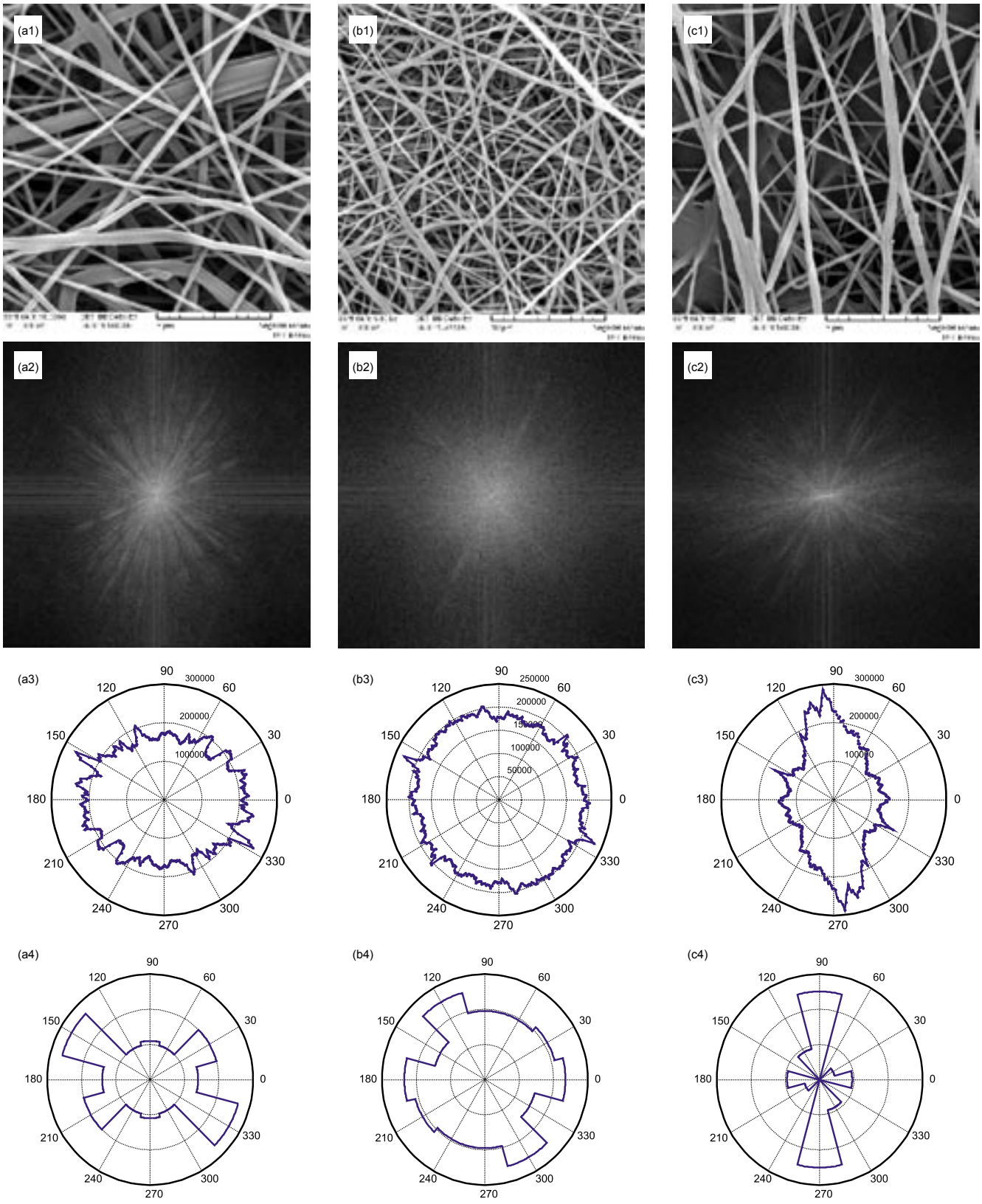

Figure 4. *(a1) - (c1) Textured images, (a2) - (c2) power spectrum as an intensity image, (a3) - (c3) polar plot of S_α, (a4) - (c4) estimation of the rose of directions by means of the Steiner compact.*

ture of the nanofibres in Figure 4 (a), and (b) is almost isotropic, but the structure in Figure 4 (c) shows a preference for the directional placement of fibres in a 90°- 120° direction.

Figure 5 (a1) is a grey level image of random Gaussian noise as an example of the isotropic system. The magnitudes of S_α are uniformly distributed along the whole spectrum of angles, which can be seen from the polar plot of S_α in Figure 5 (a2). Figure 5 (b1) displays a system of viscose fibres with preferred directions of orientation between the 0° - 30° and Figure 5 (c.1) is an image of a real fabric

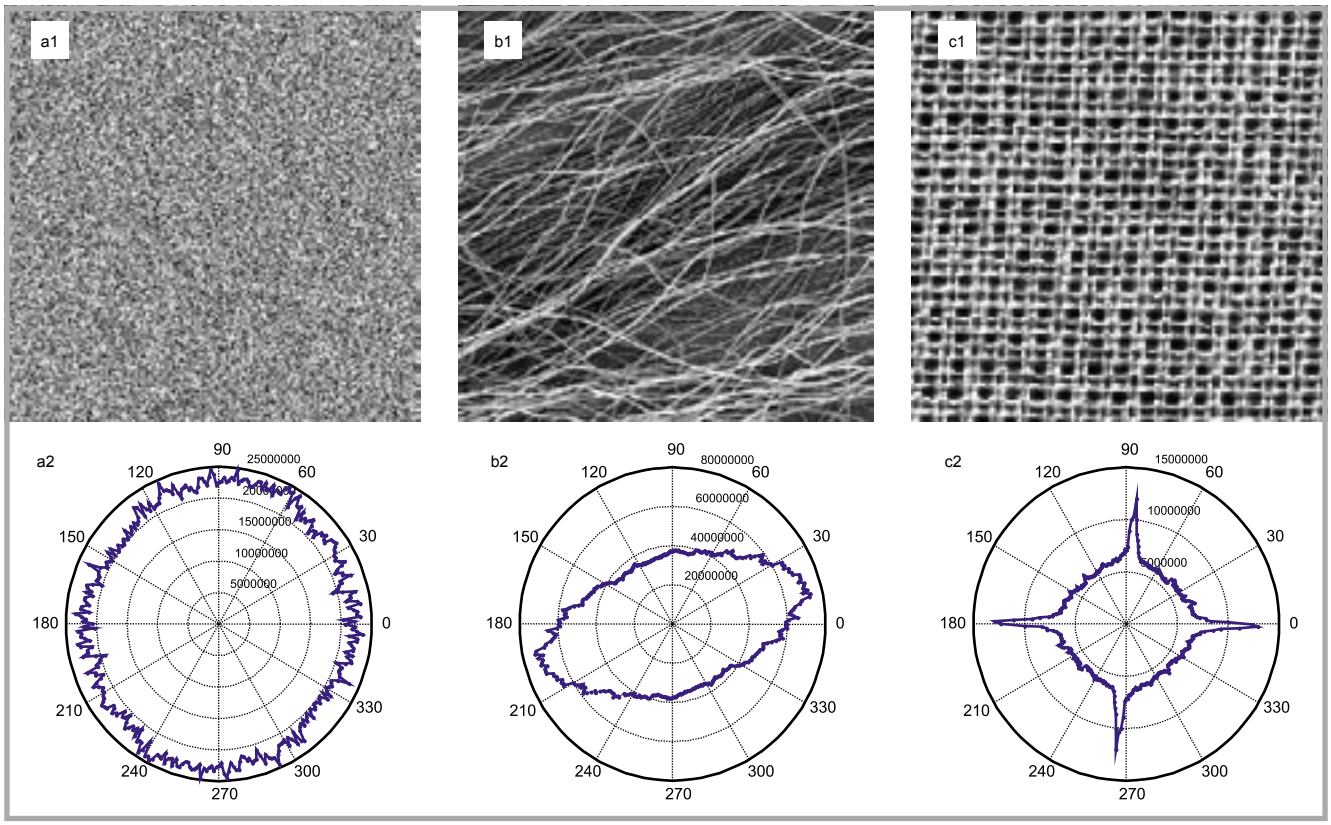

Figure 5. *(a.1) - (c.1) Textured images, (a.2) - (c.2) polar plot of S_α.*

in plain weave with a tilted warp set of yarns.

Conclusion

This paper presents a simple graphical method of planar anisotropy analysis for fibre systems. The advantage of this method is its fastness; results are directly available after the acquisition of image and application of algorithm. The visualization of anisotropy is obtained in the form of a polar diagram and histogram. The polar diagram can be seen as an estimate of the rose of directions or function $f(\alpha)$. It is possible to monitor directional vectors with an angular step of 1°. Method can be used for the analysis of anisotropy of other systems, too.

Acknowledgement

This work was supported by project MSMT CR No. 1M06047 and by the Czech Science Foundation under grant No. 106/03/H150.

References

1. *Baddeley A., Jensen E. B. V.; Stereology for Statisticians. Chapman & Hall/CRC, New York, 2005.*
2. *Stoyan D., Kendall W. S., Mecke J.; Stochastic Geometry and its Applications. John Wiley & Sons, 1995.*
3. *Rataj J., Saxl I.; Acta Stereologica, Vol. 7/2 (1988) pp. 107-112.*
4. *Gonzales R. C., Wood R. E.; Digital Image Processing. 2nd edition, Prentice-Hall, 2002.*
5. *Tsai D. M., Huang T. Y.; Image and Vision Computing, Vol. 18 (1999) pp. 49 – 62.*
6. *Karkkäinen S., Jensen E. B. V.; Image Anal. Sterol., Vol. 20(2001) pp. 199-202.*

Received 15.11.2007 Reviewed 15.01.2008

Příloha 2

[2] Tunák, M. and Linka, A. Directional Defects in Fabrics. *Research Journal of Textiles and Apparel*, **12**(2), 2008, pp. 13–22. issn: 1560-6074. Excellent Paper Award 2008.

Directional Defects in Fabrics

Maroš Tunák and Aleš Linka*
Technical University in Liberec, Department of Textile Materials, Czech Republic,
maros.tunak@tul.cz, ales.linka@tul.cz

ABSTRACT

This paper deals with a procedure that recognizes common defects occurring in woven fabric. Images of woven fabric are considered as having a directional texture due to their periodical nature. We used a statistical approach based on the analysis of periodicity of texture images in horizontal and vertical directions. These periodicities correspond to the periodicity of second-order grey level statistical features obtained from a grey level co-occurrence matrix. A set of five significant features is extracted from the matrix: energy, correlation, homogeneity, cluster shade and cluster prominence. The presence of a defect over texture causes regular structure changes and consequently, statistical changes. Detection algorithm is based on the sliding window technique; the window is moved over the whole image area. We counted the test statistic for every window and the multivariate control charts are used as a tool for judging the existence of defects. The results show that the statistical approach is suitable for detection of directional defects or changes in regular structure in analysed simulated and real fabrics.

Keywords: Texture, Statistical approach, Grey level co-occurrence matrix, Defect detection

1. Introduction

In the textile industry, the current inspection process for the quality of textiles still depends on human visual inspection. It is time consuming and repetitive activity requiring permanent attention in order to detect defects. Accordingly, there are many human mistakes in this process and human visual inspections can only catch around 70% of significant defects. Therefore, the textile industry is concerned with replacing human visual inspection with a suitable automated visual inspection.

Lately, the task of automatic detection of fabric defects has attracted the attention of many research teams. Although there are many different approaches in dealing with the automatization of defect detection, it is mostly still performed manually. A frequently used approach for texture analysis is based on statistical properties obtained from grey level co-occurrence matrices (GLCM). The standard set of statistical features was originally introduced for the first time by Haralick et al. (1973).

Proposed features were used for identifying regions in photomicrographs of sandstones, an aerial photograph or satellite images. The performance of 15 GLCM features was tested in CART classification of Brodatz textures by Carstensen (1992).

Simultaneously, the most important features were determined. Selected Brodatz textures contained deterministic and stochastic textures; some of them were textile textures. The automatic inspection of weaving density is based on the co-occurrence matrix algorithm presented by Lin (2002).

There are a few articles dealing with the problem of defect detection in woven fabric based on the grey level co-occurrence matrix. Recognition of fabric defects, including broken warps, broken wefts, holes and oil stains by applying the co-occurrence matrix and grey relational analysis was described by Kuo (2003).

An overview of defect detection techniques for detecting the presence of defects including statistical techniques was presented in the paper by Bodnarova (2000).

* Corresponding author. Tel.: (+420) 48 535 3548; Fax: (+420) 48 535 3542
E-mail address: ales.linka@tul.cz

The modelling of woven fabric structure based on the two dimensional discrete convolution theorem can be found in Chan (2000) and Escofet (2001).

Due to the periodical nature of woven fabrics, their images are homogenously structured and can be considered as texture images. These periodicities correspond to the periodicity of second-order grey level statistical features obtained from grey level co-occurrence matrices. Presence of a defect over the periodical structure of woven fabric causes changes in periodicity and consequently, changes of statistical features. We especially focus on the recognition of common directional defects associated with the change of weaving density or defects that appear as thickly distributed along the width or height of an image. In this paper, we will introduce detection algorithm for automated visual inspection based on a statistical approach. In the experimental part, we will test algorithm for recognition of simulated defects and finally, we will show a few examples of recognition on real samples too.

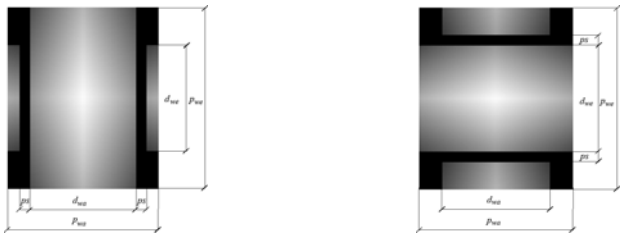

(a) (b)

Fig. 1. (a) Warp interlacing point, (b) weft interlacing point.

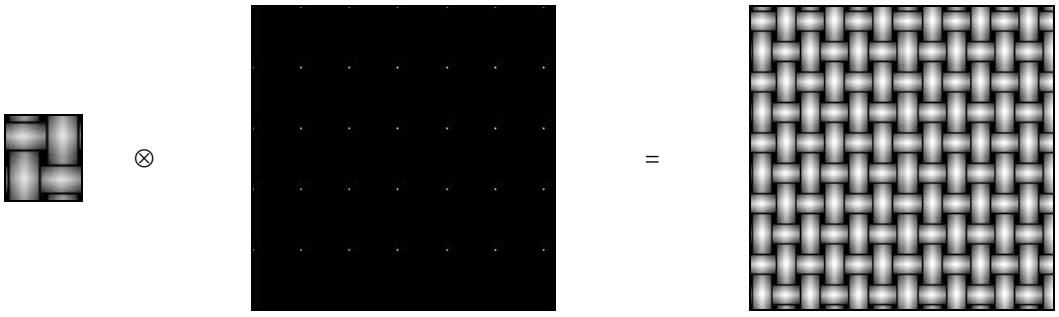

(a) (b) (c)

Fig. 2. (a) Convolution mask, elementary unit, (b) pattern of repetition, (c) result of convolution.

2. Simulation of a Plain Weave

The convolution of an elementary unit (pattern of repetition) and grid or pattern of repetition in the spatial domain for a plain weave simulation was used. Let $h(x,y)$, $g(x,y)$ and $b(x,y)$ be the input image, output image and convolution mask, respectively, and convolution denoted by $\otimes$. At each point (x,y), the response of the mask at that point is the sum of products of the filter coefficients and the corresponding neighbourhood pixels in the area spanned by the mask (see Gonzales, 2002; Escofet, 2001).

$$g(x,y) = b(x,y) \otimes h(x,y) = \sum_{m=0}^{x} \sum_{n=0}^{y} b(m,n) h(x-m, y-n). \quad (1)$$

Figures 1 (a) and (b) display an image of warp and weft interlacing points respectively. The yarns are represented by white, the space among them by black. Warp and weft interlacing points can be generated on the basis of input parameters, where p_{wa}, p_{we} represent warp and weft spacing, and d_{wa}, d_{we} define warp and weft diameter in pixels.

The woven fabric was composed by two sets of

mutually perpendicular and interlaced yarns. The weave pattern or basic unit of the weave was periodically repeated throughout the whole fabric area with the exception of the edges. The simulated output image of a periodic structure in a plain weave $g(x,y)$ can be simulated as a convolution of an elementary unit $b(x,y)$ and an input image of pattern of repetition $h(x,y)$.

The elementary unit (pattern of repetition in this case) was created by the formation of warp and weft interlacing points, depending on the type of weave. For the simulation of common woven fabric defects in this paper, we used plain weave only. The result of the convolution theorem can be seen in Figure 2 (c), which represents a grey level image of plain weave in a spatial domain. The size of the image is 200 x 200 pixels; the number of grey levels is 256. Warp and weft yarn diameter is set to 12 pixels, warp yarn spacing to 16 pixels, weft yarn spacing to 20 pixels and parameter *sp* to 1 pixel.

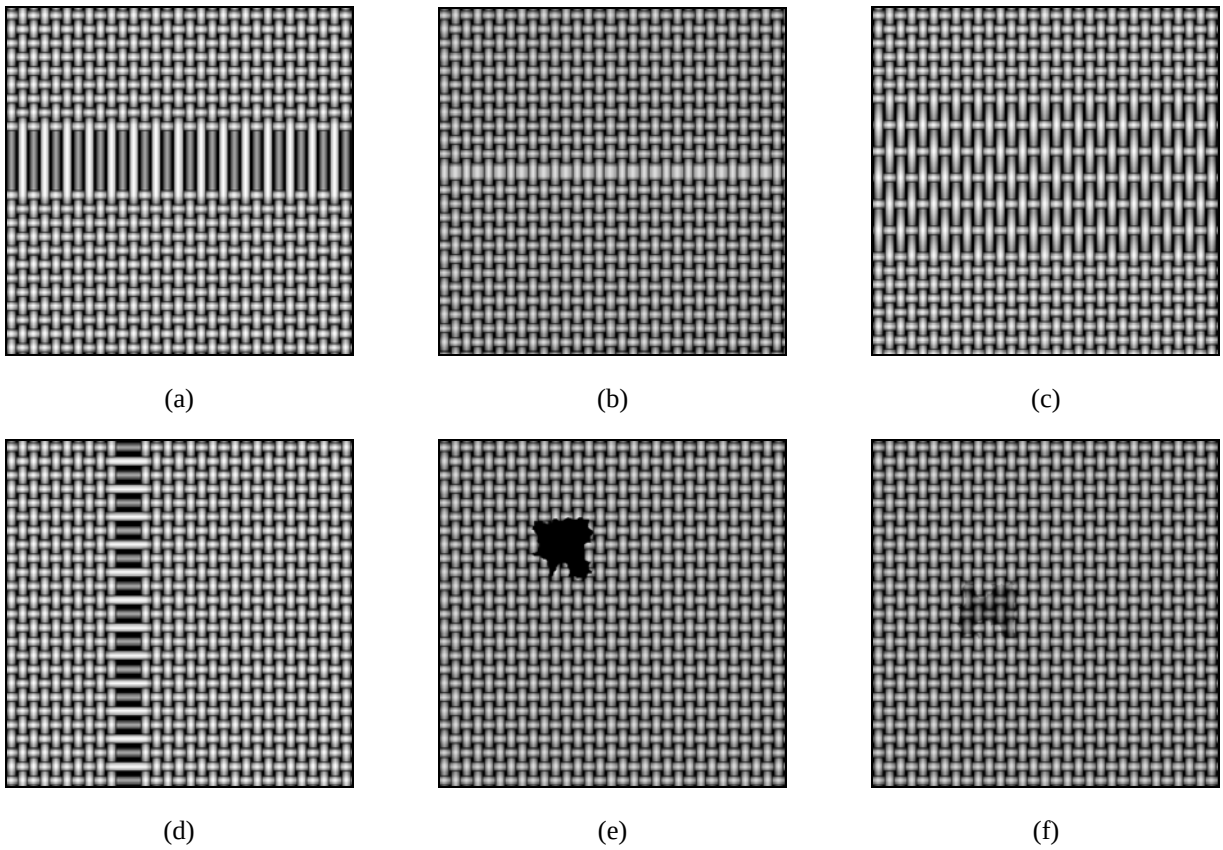

Fig. 3. (a) - (f) Simulated defects in a plain weave.

3. Simulation of Woven Fabric Defects

Many different types of defects can be introduced during fabric manufacturing. Our focus is on a few examples of some of the common woven fabric defects. According to ITS Publishing (1996), woven fabric defects can be split into three basic categories: the weft direction defects, warp direction defects and defects with no directional dependence. Some of the weft direction defects are: irregular weft density (insufficient, excessive), double pick, weft yarn defect, broken or short pick. Defects in the warp direction are: broken end, double end and warp yarn defect. Defects with no directional dependence involve the following: stains, holes, foreign bodies. Defected images were modelled by using algebraic operations on simulated images of plain weave structure and in some cases, removing some of the rows or columns.

Position, size and shape of defects were randomly generated from uniform distribution. The algorithm and graphical user interface in the MATLAB software was created for realization. A few examples of simulated common fabric defects in a plain weave can be seen in Figures 3 (a) - (f). Figures 3 (a) - (c) represent weft direction defects:

broken picks, weft yarn defect, irregular weft density (insufficient). Figure 3 (d) displays the warp direction defect: broken end. No directional defects: holes and stains, can be seen in Figures 3 (e) and (f).

4. Second Order Grey Level Statistics

Texture statistics are frequently classified into first-order, second-order and high-order statistics. First-order statistics refer to the marginal grey level distribution and can be derived from the grey level histogram, e.g. mean, variance, energy etc. The first-order statistics are highly dependent on the lighting conditions and in common practice, there should be elimination of the influence of first-order statistics by making the grey level histogram match a specific distribution. For example, a match to a uniform distribution is called histogram equalization.

This approach destroys any spatial information of texture pattern and only retains their brightness information. Second-order grey level statistics refer to the joint grey level distribution of pairs of pixels and it is based on grey level co-occurrence matrices (GLCM). The GLCM are full representation of the second-order grey level statistics and retain both spatial arrangement and relative brightness information.

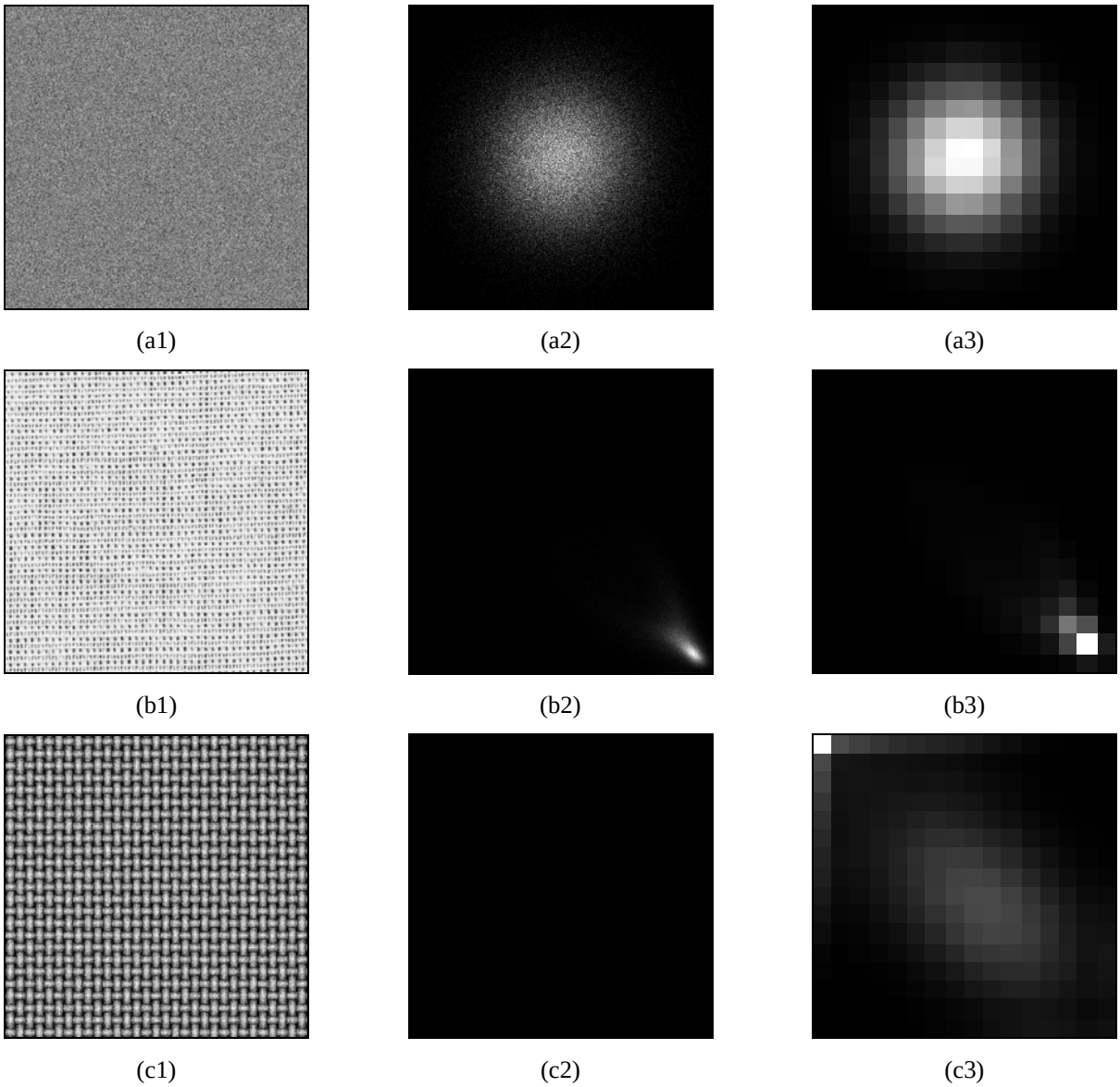

Fig. 4. a1) - (c1) Texture images, (a2) - (c2) GLCM-256 grey levels, (a3) - (c3) GLCM-16 grey levels, $d = 1$, $\theta = 0°$.

5. Grey Level Co-Occurrence Matrices

The size of textured digital image $f(x,y)$ is mxn and its grey level resolution is G. GLCM is a square matrix with a size equal to the number of grey levels G contained in the texture image and is defined with respect to two parameters: d, the distance between two pixels and θ, the position angle between two pixels (x_1, y_1) a (x_2, y_2).

As can be seen in Figure 5, there are four directions for the directional position angle: the horizontal direction $\theta = 0°$, the right diagonal direction $\theta = 45°$, the vertical direction $\theta = 90°$ and the left diagonal direction $\theta = 135°$. The four kinds of relative positions R between the two pixels can be defined in Haralick (1973) and Lin (2002).

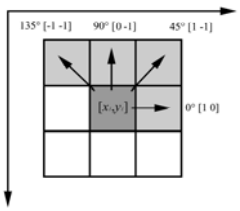

Fig. 5. Relative position angle between two pixels for $d = 1$.

$\theta = 0°$	$R_H\,(d)$:	$x_2 - x_1 = d$	$y_2 - y_1 = 0$,
$\theta = 45°$	$R_{RD}\,(d)$:	$x_2 - x_1 = d$	$y_2 - y_1 = -d$,
$\theta = 90°$	$R_V\,(d)$:	$x_2 - x_1 = 0$	$y_2 - y_1 = -d$,
$\theta = 135°$	$R_{LD}\,(d)$:	$x_2 - x_1 = -d$	$y_2 - y_1 = -d$,

The relationship between a pixel pair and co-occurrence probability of grey levels i and j with respect to parameters d and θ can be given by

$$
\begin{aligned}
P(i,j,d,0^o) &= f(x_1,y_1)=i, f(x_2,y_2)=j\ \},\\
P(i\,j,d,45^o) &= \#\{R_{PD}(d), f(x_1,y_1)=i, f(x_{2,}\,y_2)=j\ \},\\
P(i,j,d,90^o) &= \#\{R_V\,(d), f(x_1,y_1)=i, f(x_2,y_2)=j\ \},\\
P(i,j,d,135^o) &= \#\{R_{LD}(d), f(x_1,y_1)=i, f(x_2,y_2)=j\ \}.
\end{aligned}
$$

Symbol # {} denotes the probability sum of occurrence on all events in parentheses. P is a function of the four parameters i, j, d, θ, and the matrix formed with them is referred as the grey level co-occurrence matrix, $\boldsymbol{c}$, c_{ij} is the element of matrix. Let N be the total number of pairs, then $C_{ij}=c_{ij}/N$ denotes the elements of the normalized GLCM, $\boldsymbol{C}$. Normalized GLCM represents the joint probability occurrence of pixel pairs with a defined spatial relationship having grey level values i and j in the image.

There are two ways that it is possible to define co-occurrence matrices; namely, directional and rotationally invariant. For the construction of a rotationally invariant co-occurrence matrix, we can pool co-occurrence matrices with a fixed distance d and different angles surrounding the pixel of interest. Directional co-occurrence matrix captures directional information. We considered only pairs of pixels that are at a certain distance apart.

Examples in Figures 4 (a1) - (c1) display texture images of size 500 x 500 pixels with number of grey levels $G = 256$. Figures 4 (a2) - (c2) show directional grey level co-occurrence matrices computed with parameters $d = 1$, $\theta = 0°$. Matrices are visualised in the form of grey level images, where the frequency of occurrence is represented by grey level (zero occurrence - black, maximal occurrence - white).

If we do not wish to have such a large and sparse matrix, we may reduce the number of grey levels. Figures 4 (a3) - (c3) represent grey level co-occurrence matrices for the original images scaled to grey levels $G = 16$ computed with the same parameters. As can be seen from the figures, GLCM for original image of random Gaussian noise is isotropic, whereas GLCM for periodical structures show anisotropic occurrence. Many features can be computed from the normalized GLCM. Standard set of features contains 15 features (see Carstensen, 1992).

We used CART (Classification and Regression Trees) techniques for reduction of all features and determination of the most important features. On the basis of classification results, we have chosen a set of five significant features. The sum of the squares of normalised GLCM elements returns *Energy* (measure of uniformity of image):

$$\varepsilon = \sum_{i=0}^{G-1}\sum_{j=0}^{G-1} C_{ij}^2. \qquad (2)$$

Correlation is a measure of grey level linear dependencies in the image:

$$\rho = \sum_{i=0}^{G-1}\sum_{j=0}^{G-1}\frac{(i-\mu_x)(j-\mu_y)C_{ij}}{\sigma_x\sigma_y}. \qquad (3)$$

Homogeneity or *inverse difference moment* measures the closeness of the distribution of elements in the GLCM to the GLCM diagonal

$$IDM = \sum_{k=0}^{G-1}\frac{D_k}{1+k^2}. \qquad (4)$$

Cluster shade and *cluster prominence* are given by:

$$A = \sum_{k=0}^{2G-2}(k-SA)^3 S_k, \qquad (5)$$

$$B = \sum_{k=0}^{2G-2}(k-SA)^4 S_k. \qquad (6)$$

6. Defect Recognition in Simulated Structures

The detection algorithm was tested first for simulated structures of woven fabric in a plain weave with randomly generated defects. On the base of relations (2) - (6), we evaluated a set of p = 10 features for m = 1000 randomly placed windows of size 50 x 50 pixels in images of simulated structures without defects. Five features were extracted from GLCM with parameters d = 1 and θ = 0° (weft direction dependence) and five features from GLCM with parameters d = 1 and θ = 90° (warp direction dependence).

We obtained m samples of p – dimensional normal distribution. Then we evaluated Hotelling's multivariate control charts, which are a direct multivariate equivalent of the Shewhart $\overline{X}$ charts (based on Mahalanobis distance), for the process mean with an upper control limit as shown in Zamba (2006).

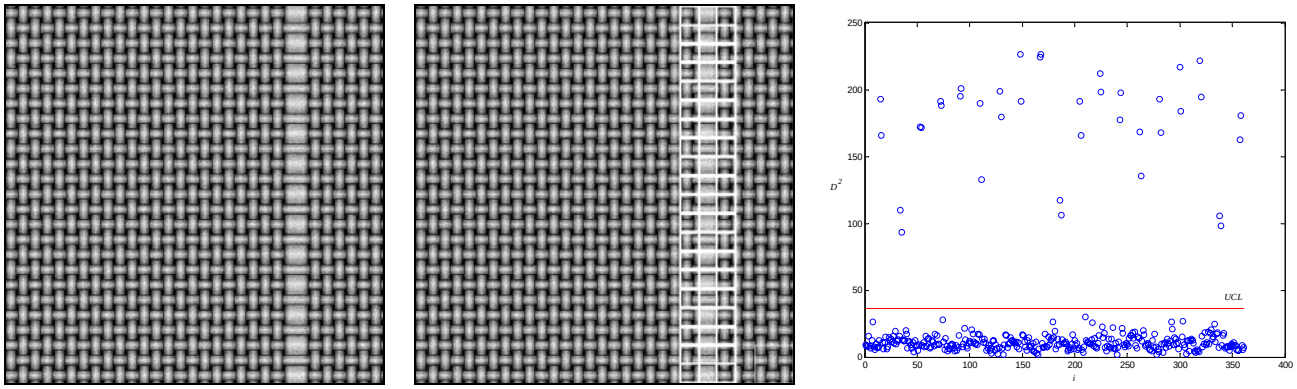

(a) (b) (c)

Fig. 6. (a) Warp yarn defect, (b), result of applied algorithm, (c) plot of the test statistic against control limit.

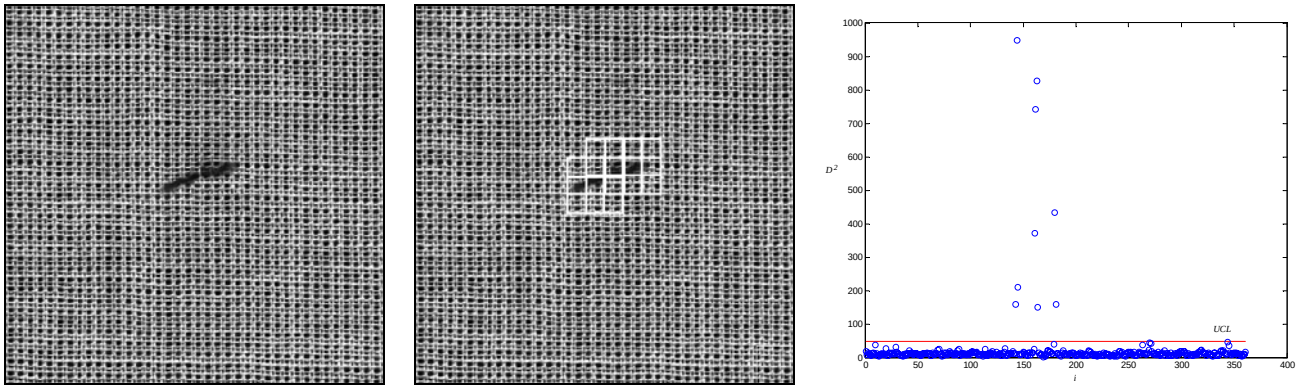

(a) (b) (c)

Fig. 7. (a) Foreign body defect, (b), result of applied algorithm, (c) plot of the test statistic against control limit.

$$UCL = \frac{p(m+1)(m-1)}{m(m-p)} F_{1-\alpha,p,m-1}, \qquad (7)$$

where $F_{1-\alpha,p,m-1}$ is the (1 - α) percentile of the F-distribution with p and (m-p) degrees of freedom, m is number of multivariate observation and p is number of variables. Then we applied algorithm to detection of defects in simulated structure. We counted the test statistic for i-th individual observation of features extracted from the sliding window moved over the whole image in this form:

$$D_i^2 = (\mathbf{X}_i - \overline{\mathbf{X}})' S^{-1} (\mathbf{X}_i - \overline{\mathbf{X}}) \qquad (8)$$

where $\overline{\mathbf{X}}$ is the mean and S is the variance-covariance matrix. $\mathbf{X}_i$ represents 10 values of features in window i. If D_i^2 is greater then the upper control limit computed from the "learning sample", for a given level of significance, a window is considered as the window containing the defect. Size of images is set to 500 x 500 pixels; Gaussian noise of mean 0 and variance 0.0025 is added to the images, a = 0.001 is used. A sliding window of size 50 x 50 pixels is moved systematically over the whole image area with the step of size 25 pixels.

Windows with detected defects or imperfections remaining in the image are displayed in a white colour. In Figure 6 (a), a simulated warp yarn defect (thick yarn) can be seen. Figure 6 (c) shows the plotting of individual testing statistics against the upper control limit. Figure 6 (b) represents the results of detection algorithm, where white windows are observed outside the control and considered as containing defects. Figures 8 (a) - (f) display the results of algorithm applied to simulated images of common woven fabric defects similar to Figure 3. As we can see from the figures, the process is suitable for detection and localization of directional defects in simulated samples.

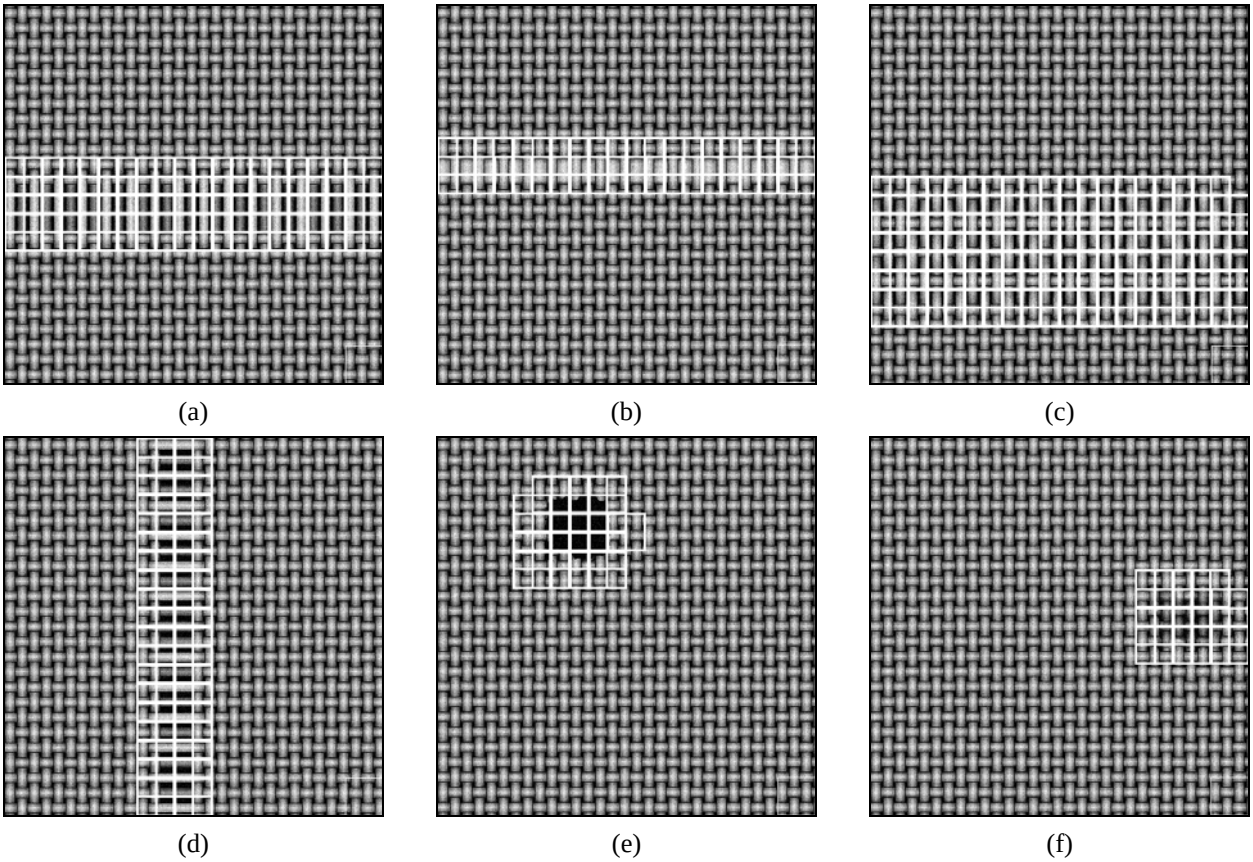

Fig. 8. Result of the algorithm applied to simulated samples, white windows indicate defect.

7. Directional Defect Detection

The same algorithm was tested for detection in real samples, in a plain and twill weave. Images were captured by a flat scanner with a resolution of 400 dpi in 256 grey levels and stored in an image matrix with a size of 500 x 500 pixels. Equalization was used for contrast enhancement. The *UCL* was counted from the image of the structure without defects. A sliding window was set again to a size of 50 x 50 pixels, $a = 0.001$ was used. In a similar way, in Figure 7 (a), it can be seen that the foreign body is the no directional defect. Figure 7 (b) shows the results of applied detection algorithm, where windows framed by white colour are windows with a test statistic greater then the upper control limit in Figure 7 (c).

Figures 9 (a) - (f) show a few examples of recognizing before and after defects in real structures. Examples in Figures 9 (a) - (c) represent real directional defects: irregular weft density (insufficient), irregular weft density (excessive) and double pick. Figure 9 (d) displays the results of algorithm for warp directional defect: warp yarn defect. Figures 9 (e) and (f) show examples of no directional defects: a stain and hole.

A few samples were in a plain weave, for example in Figures 9 (a1), (e1) and (f1) and the other in the twill weave in Figures 9 (b1) - (d1). The method has been also tested in other real cases.

8. Conclusion

Recognition algorithm based on second-order statistical features extracted from a grey level co-occurrence matrix is suitable for detection of common woven fabric defects. By using this method, we can detect defects associated with the change of weaving density or defects that appear thickly, distributed along the width or height of an image, as well as for no directional defects.

Algorithm is tested first for simulated structures of woven fabric with randomly generated defects, where the convolution theorem is used for the mathematical modelling of woven fabric structures. For practical reasons of uncomplicated modelling of woven structure and common woven fabric defects, only the plain weave is used for simulated samples.

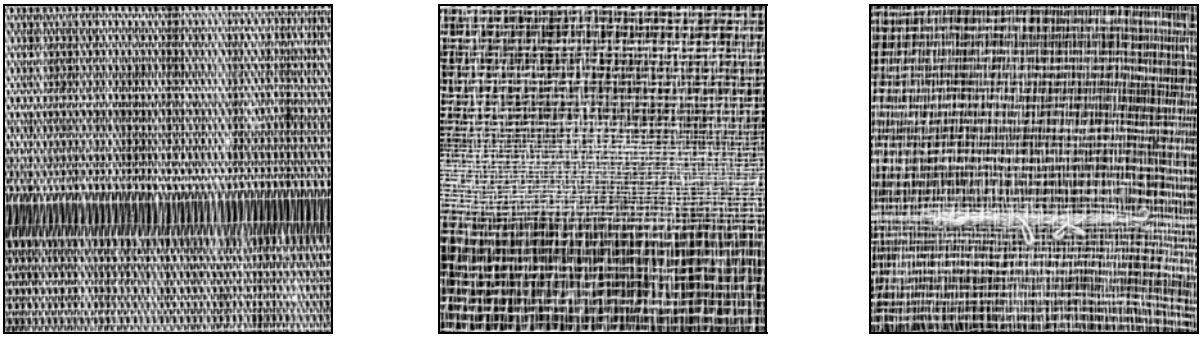

(a1) (b1) (c1)

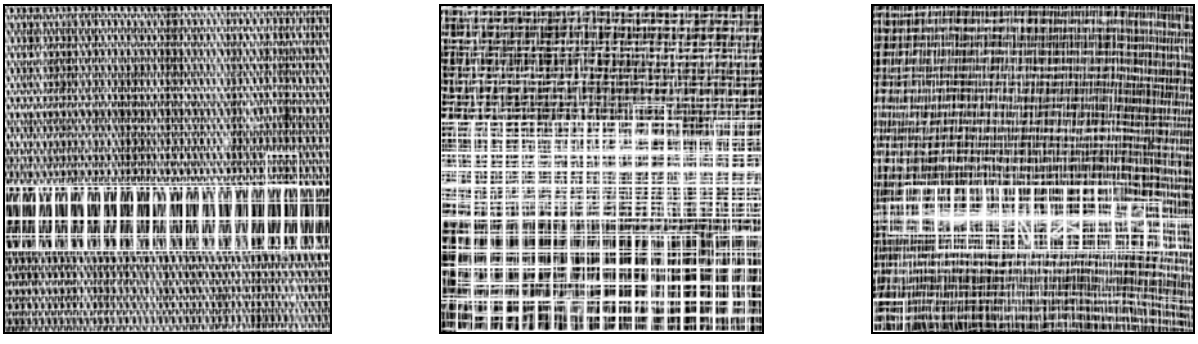

(a2) (b2) (c2)

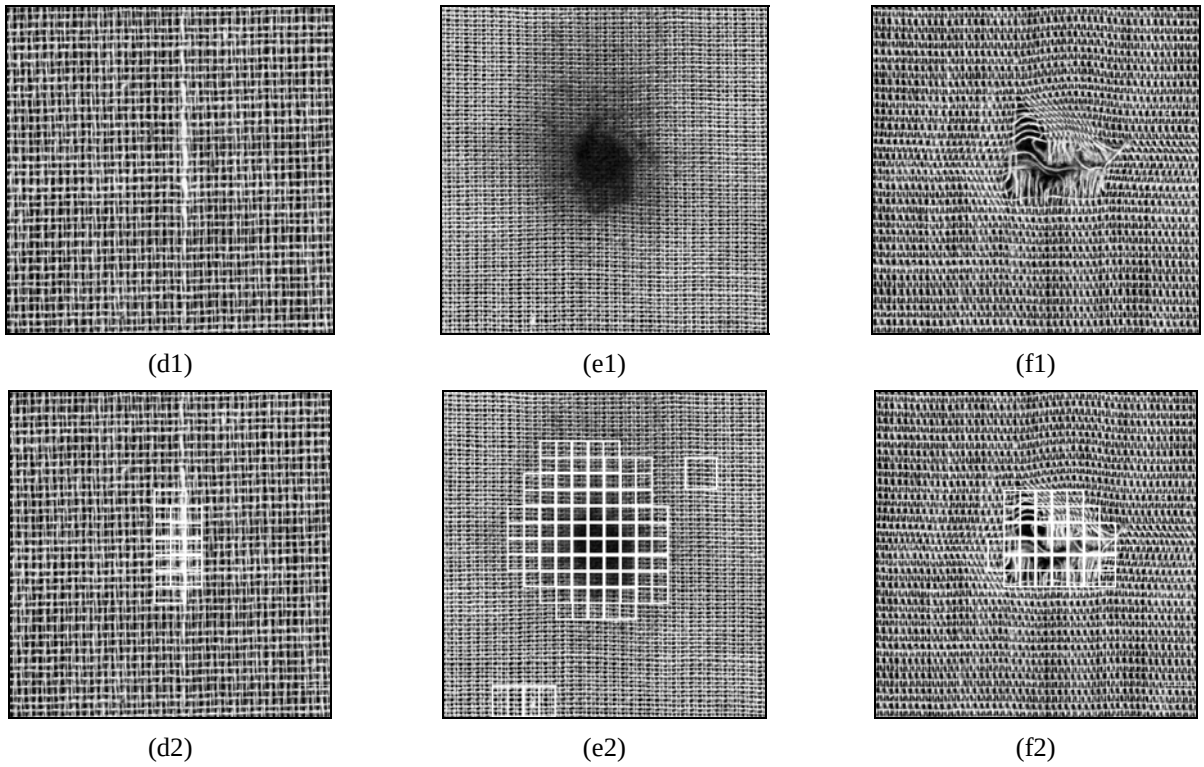

Fig. 9. (a1) - (f1), Defected images before the (a2) - (f2) result of the algorithm applied to real samples, white windows indicate defect, imperfection.

Another reason is the determination of second order features with high discriminatory power which are nominated as the most important features. We extracted five of the most significant features from GLCM with parameters corresponding to weft direction and five features obtained from GLCM with parameters corresponding to the warp direction Then we used the sliding window technique for detection and localization of defects or changes of regular structure.

The idea is based on the finding of the optimal second order features corresponding to a certain structure. We used Hotelling's multivariate control charts for upper control limit determination from the structure without defect as a learning sample.

Consecutively, we executed automated inspection in samples containing defects. We computed and compared the test statistics for every window with upper control limit. Exceeding of control limit indicates changes in regularity of structure. The same process was used for real samples. The results show that the process is suitable for simple simulated samples as well as for real samples with different structures.

The upper control limit is as a rule, acquired by training on a non-defective part of fabric. From this point of view, the parameters of structure (e.g. yarn diameter, yarn spacing, the complexity of weave) do not matter. The algorithm is applicable and appropriate for undyed or uni-colour fabrics. On the other hand, the selection of window size can be important.

Multivariate control charts are useful tools to integrate the multiple texture features and judge the existence of defects. The advantages of automated visual inspection are objectivity and independence on the human inspectors. This method is relatively fast and it can be used as an online visual inspection of quality. In this paper, we used the inspection window moving systematically over the whole image area and the image is static. In the case of online inspection, the fabric moves while the image camera can be static.

It will be reasonable to devise an optimised method, which defines appropriate parameters for a given structure (e.g. the size of a sliding window). It means that the algorithm will detect the parameters on the training data set and then

these parameters will be used for defect detection in real fabric structures. Other approaches (i.e. spectral, structural) can be tested as well.

Acknowledgements

This work was supported by the project MSMT CR No. 1M06047 and the Czech Science Foundation under grant No. 106/03/H150.

REFERENCES

[1] Bodnarova, A., Bennamoun, M. & Kubik, K.K. 2000, 'Suitability Analysis of Techniques for Flaw Detection in Textiles using Texture Analysis', *Pattern Analysis & Applications*, vol. 3, pp. 254 - 266.

[2] Carstensen, J.M. 1992, *Description and Simulation of Visual Texture*, Ph.D. Thesis. Lyngby, Technical University of Denmark.

[3] Chan, C. & Pang, G.K.H. 2000, 'Fabric Defect Detection by Fourier Analysis', *IEEE Trans. on Industry Applications*, vol. 36, no. 5, pp. 1267 – 1276.

[4] Escofet, J., Millán, M.S. & Ralló, M. 2001, 'Modelling of woven fabric structures based on Fourier image analysis', *Applied Optics*, vol. 40, no. 34, pp. 6170 – 6176.

[5] Gonzales, R.C. & Wood, R.E. 2002, *Digital Image Processing*. 2nd edition, Prentice-Hall, New Jersey.

[6] Haralick, R.M., Shanmugam, K. & Dinstein, I. 1973, 'Textural Features for Image Classification', *IEEE Transaction on Systems, Man. and Cybernetics*, vol. 3, no. 6, pp. 610 – 621.

[7] ITS Publishing 1996, *Catalogue of types of fabric defects in grey goods*, 3rd ed., Schlieren/Switzerland.

[8] Kuo C.F.J. & Su, T.L. 2003, 'Gray Relational Analysis for Recognizing Fabric Defects', *Textile Research Journal*, vol. 73, no. 5, pp. 461 – 465.

[9] Lin, J.J. 2002, 'Applying a Co-occurrence Matrix to Automatic Inspection of Weaving Density for Woven Fabrics', *Textile Research Journal*, vol. 72, no. 6, pp. 486 – 490.

[10] Zamba, K.D. & Hawkins, D.M. 2006, 'A Multivariate Change-Point Model for Statistical Process Control', *Technometrics*, Nov 2006; vol. 48; no. 4, pp. 539 - 549.

Excellent Paper Award of Year 2008

Vol. 12 No. 1 2008

Effect of UV Curable Pretreatments on the Color Quality of Inkjet Printed Polyester Fabrics

Qinguo Fan, Hongxia Xue and Yong K. Kim
University of Massachusetts Dartmouth, North Dartmouth, MA, U.S.A

Vol. 12 No. 2 2008

Directional Defects in Fabrics

Maroš Tunák and Aleš Linka
Department of Textile Materials, Technical University in Liberec, Czech Republic

Vol. 12 No. 3 2008

Analysis of Supply Chain Strategies Used by The United States Textile and Apparel Industries

Matt Berdine[1], Erin Parrish[2], Nancy L. Cassill[3], William Oxenham[3] and Michelle R. Jones[3]
[1]Lands' En d, Dodgeville, Wisconsin, USA
[2]East Carolina University, Greenville, North Carolina, USA
[3]College of Textiles, North Carolina State University, Raleigh, North Carolina, USA

Vol. 12 No. 4 2008

Dyeing Properties of Natural Dyes Extracted from Turmeric and their Comparison with Reactive Dyeing

Saima Umbreen[1], Shaukat Ali[1], Tanveer Hussain[2] and Rakhshanda Nawaz[1]
[1]Department of Chemistry, University of Agriculture, Faisalabad, Pakistan
[2]Department of Textile Chemistry, National Textile University, Faisalabad, Pakistan

Characterization of Electroless Ni-P Plated Polyester Fabric

S.Q. Jiang, X.M. Tao, C.W.M. Yuen, C.W. Kan and R.H. Guo
Institute of Textiles and Clothing, The Hong Kong Polytechnic University, Hung Hom, Kowloon, Hong Kong, China

Příloha 3

[3] Tunák, M., Linka, A., and Volf, P. Automatic Assessing and Monitoring of Weaving Density. *Fibres and Polymers*, **10**(6), 2009, pp. 830–836. issn: 1229-9197. IF=0.832.

Fibers and Polymers 2009, Vol.10, No.6, 830-836 DOI 10.1007/s12221-009-0830-1

Automatic Assessing and Monitoring of Weaving Density

Maroš Tunák*, Aleš Linka, and Petr Volf[1]

Department of Textile Evaluation, Technical University of Liberec, Czech Republic
[1]Department of Applied Mathematics, Technical University of Liberec, Czech Republic
(Received October 17, 2008; Revised March 30, 2009; Accepted April 11, 2009)

Abstract: Image restoration using the spectral approach is applied to the problem of automatic assessing of weaving density. A restored image of one set of yarns is obtained with the aid of two dimensional discrete Fourier transform. From the line profile of restored images Fisher's test of periodicity find out the significant periodical components of specific frequency and defines model of time series. On the basis of frequency of model, the weaving density can be computed automatically. This method is then used for detection of defects associated with the change of weaving density, i.e. the weft direction defects. The detection is based on monitoring of weaving density in direction of length of fabric. Change of weaving density value against expected value indicates failure of regular structure. Control charts were used as a tool for judge the existence of failure or defects of regular structure.

Keywords: Weaving density, Spectral approach, Fourier transform, Control chart, Defect detection

Introduction

In textile industry there is a standard practice to measure weaving density (number of warp and weft yarns per unit length) by manual operations. It is a time consuming manual activity requiring permanent attention of human inspector. Therefore, textile industry takes concern in replacing human inspection by a suitable automated assessing and monitoring of weaving density.

Several approaches to this problem are known. A few articles deal with the automatic inspection of weaving density with the aid of a direct image analysis. Automatic inspection of weaving density based on the co-occurrence matrix algorithm was presented in [1]. The co-occurrence matrices in weft and warp direction for several displacements were counted from grey level images of woven fabric. Feature contrast was obtained from such matrices and weaving density was calculated from figure where the feature contrast against distance pixels is plotted. This method is suitable only for fabric in a plain weave.

Some papers deal with the spectral approach based on Fourier transform [2-4]. Fourier transform is useful to describe periodic patterns in grey level images due to the relationship between the regular structure in the spatial domain and its Fourier spectrum in the frequency domain. Significant frequencies in frequency domain correspond to periodicities of structure in spatial domain. Weaving density can be obtained by finding such frequencies in Fourier spectrum.

The grey line profile method is introduced in paper [5]. Method is simple and can be applied for various weaves. However, the direction of warp and weft yarns must be in parallel way with the axes of the image of fabric. This can be achieved for instance with the aid of Hough transform, as shown in [6].

*Corresponding author: maros.tunak@tul.cz

In the present paper we use the spectral approach based on the Fourier transform. We demonstrate its easy and reliable use for different textile structures, too. Application of this method enables us not only to monitor weaving density in direction of length of fabric but also to detect defects associated with the change of weaving density of weft yarns. To this end, an automated procedure has been developed and their results are presented. Moreover, the spectral method is less sensitive to possible rotation of image. The paper is organized as follows: First, the method of spectrum analysis and detection of main frequency components is recalled. Then, the spectral approach is used for assessing the weaving density in a fabric. Finally, the same approach is utilized to the detection of sites with defects - changed density. Proposed procedures are illustrated on examples dealing with real plain weave fabric.

2D Fourier Transform

The spectral approach is based on two-dimensional discrete Fourier transform (2D DFT). The Fourier spectrum is ideally suited for describing the directionality of periodic patterns in grey level images of texture. The directional characters of grey level images clearly correspond to high-energy frequency components in the Fourier spectrum. Let $f(x, y)$ be a two-dimensional function, where x and y are the spatial coordinates and the amplitude of f at any pair coordinates is the grey level of the image of size mxn. The 2D DFT of $f(x, y)$ and its inverse 2D IDFT are given by following equations [7]

$$F(u,v) = \sum_{x=0}^{m-1}\sum_{y=0}^{n-1} f(x,y)e^{-j2\pi(ux/m+vy/n)} \quad (1)$$

and

$$f(x,y) = \frac{1}{mn}\sum_{u=0}^{m-1}\sum_{v=0}^{n-1} F(u,v)e^{j2\pi(ux/m+vy/n)} \quad (2)$$

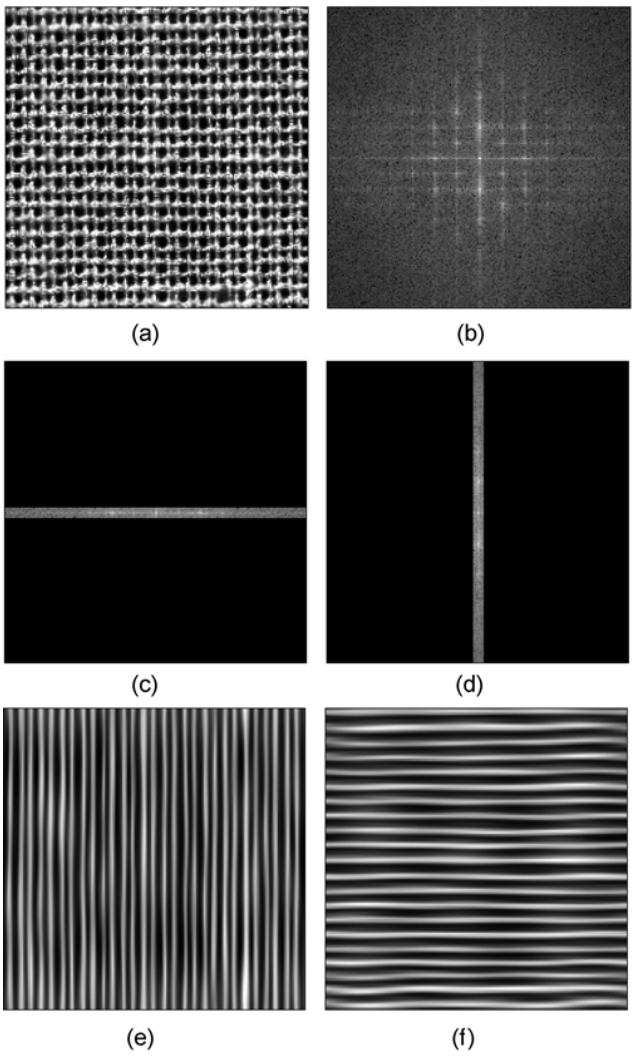

Figure 1. (a) Image of plain weave fabric, (b) power spectrum after logarithmic transformation, stripe of orientation (c) $\varphi=0^{\circ}$, and (d) $\varphi=90^{\circ}$ with width $\Delta w=7$ pixels and (e), (f) restored images after 2D IDFT.

where $u = 0, 1, 2, \ldots, n-1$ and, $v = 0, 1, 2, \ldots, m-1$ are frequency variables. The power spectrum $P(u, v)$ is defined as the square of the magnitude. To display power spectrum in 8-bit grey level depth, $P(u, v)$ is converted to

$$P(u,v) = \log(1 + |F(u,v)|^2) \tag{3}$$

Information about major structural direction lines in the spatial domain image is concentrated in the Fourier domain image as a direction of high-energy peaks. The set of yarns (directional lines of texture) can be removed by detecting of corresponding high-energy frequency components in Fourier domain image and setting them to zero. Then, after the inverse FT transform of such a reduced spectrum we obtain an image where only one set of yarns remain. Example in Figure 1(a) represents the grey level image of woven fabric in a plain weave with the size 200×200 pixels, Figure 1(b) shows corresponding power spectrum after the log transformation. Figure 1(c) and (d) display the power spectra where the high-energy frequency components in orientation $\varphi=0^{\circ}$ and $\varphi=90^{\circ}$ with width $\Delta w=7$ pixels remain and the frequency components out of this stripe was set to zero. As can be seen from Figure 1(e) and (f) restored images after the 2D IDFT contain only warp set or weft set of yarns, respectively. Hence, restored images can be used for automatic assessing of weaving density.

Fisher's Test of Periodicity

This part deals with the problem of evaluation a main spectrum frequency, which is consequently used for the weaving density assessing. Woven fabrics are periodically structured, due to the characteristics of the weaving process used in their formation. Grey levels along a line perpendicular to a set of yarns can be obtained from the restored images. Pixel values along such a line form a periodical time series, where the high values represent yarns and low values spaces between the yarns. The elementary characterization of periodical time series is the periodogram $I(\omega)$. For a finite sequence of random variables $y_1, \ldots, y_n$ it is defined as a function of variable ω in the form [8]

$$I(\omega) = \frac{1}{2\pi n}\left|\sum_{t=1}^{n} y_t e^{-it\omega}\right|^2, \quad -\pi \le \omega \le \pi \tag{4}$$

The periodogram is a statistical tool for finding significant periodic components in time series. One statistical method for testing of periodicity in a time series is provided by the Fisher's test of periodicity [8]. Fischer's test defines significant frequencies in model of time series and the weaving density of fabric can be evaluated. The null hypothesis in Fisher's test is given as

$$H_0: y_t = \varepsilon_t \tag{5}$$

i.e. it is assumed that the series y_t does not contain any periodical components and it is equal to white noise e_t with distribution $N(0, \sigma_\varepsilon^2)$. The alternative hypothesis is defined as

$$H_A: y_t = \mu + \sum_{j=1}^{p} (\alpha_j \cos(\omega_j t) + \beta_j \sin(\omega_j t)) + \varepsilon_t, \; t = 1, \ldots, n \tag{6}$$

where time series is a combination of a finite number of goniometrical functions of different frequencies $\omega_1, \ldots, \omega_p$ with level μ and added white noise ε_t. Fisher's test is based on periodogram values of given time series $y_1, \ldots, y_n$ computed for frequencies

$$\omega_j^* = \frac{2\pi j}{n}, \quad j = 1, \ldots, m, \quad m \le \frac{n-1}{2} \tag{7}$$

If the null hypothesis is valid, then any of these periodogram values are not significantly larger than values of noise. Actually, the Fisher's test replies to a question whether there are some significantly large periodogram values. This is connected with the presence of periodical components in the time series. The periodogram values are standardized in order to eliminate distribution dependence on unknown value of σ_ε. Namely, we standardize y_t to Y_t/s_y, where s_y estimates the standard deviation of y-s provided the null hypothesis is valid (see [8]). Then the test statistic is given by

$$W = \max_{j=1,\ldots,m} I(\omega_j^*) \tag{8}$$

and null hypothesis will be rejected if $W > g_F$, where g_F is the critical value of Fisher's test on significance level α. If the Fisher's test finds out a significant periodical component with specific frequency ω_{j0}^* (for this frequency $I(\omega_{j0}^*) = \max_{j=1,\ldots,m} I(\omega_j^*)$ holds), it is possible to search for possible another large significantly periodogram value: The value $I(\omega_{j0}^*)$ is omitted and the method is repeated (the value m is replaced by the value $m-1$). This method defines all significant frequencies ω_j of model (6) by using the statistical test. Unknown parameters μ, α_j, and β_j can than be estimated by the least square method.

Monitoring of Weaving Density

The weaving density of fabric can consequently be evaluated by finding the main periodicity in restored image of sets of yarns. Namely, the weaving density D is obtained from the equation

$$D = \frac{R/2.54}{T} \tag{9}$$

where R is the image resolution (pixel per inch), $T = 2\pi/\omega_j^*$ and ω_j^* is the first most significant frequency determined

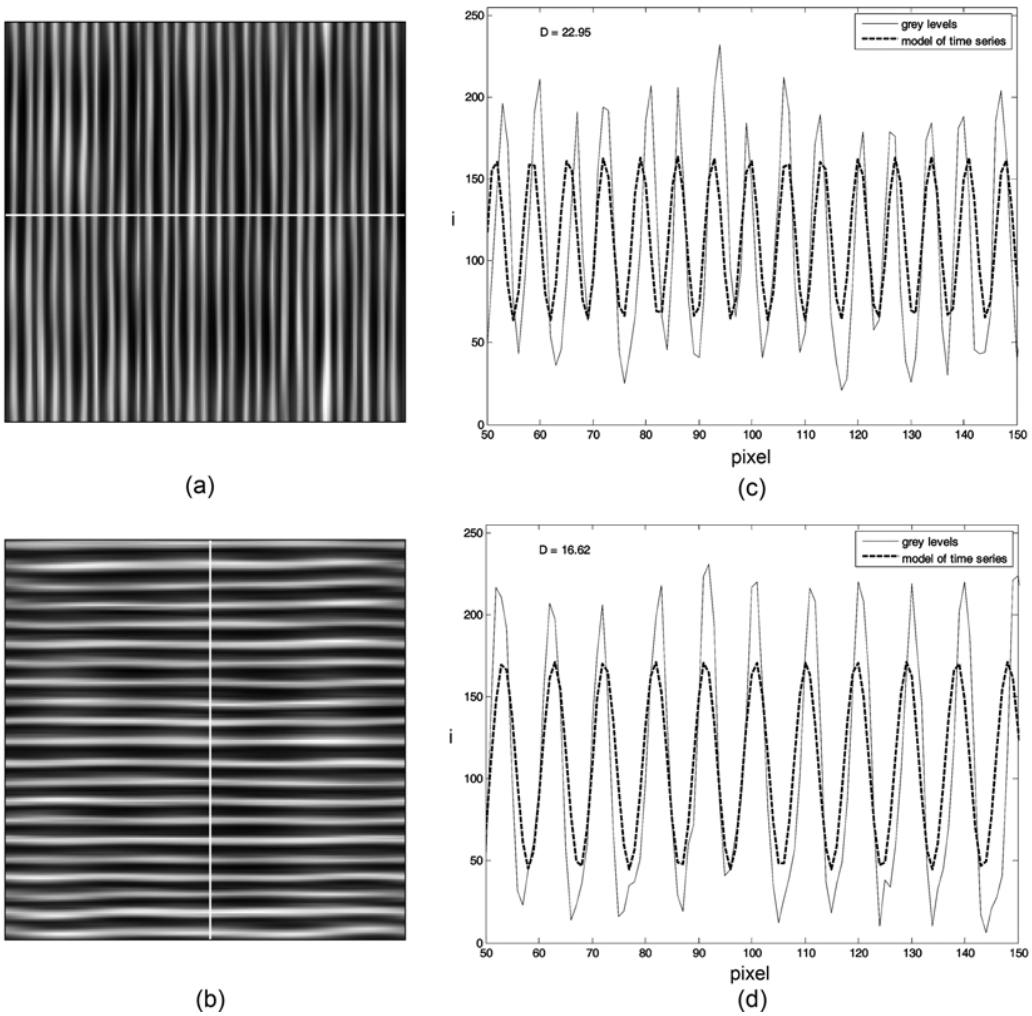

Figure 2. Restored images of (a) warp and (b) weft set of yarns after 2D IDFT, (c), (d) line profile of grey levels, model of time series for first most significant frequency.

from Fisher's test of periodicity. Example in Figure 2(a) and (b) shows restored images of warp and weft yarns after 2D IDFT of a fabric in a plain weave from Figure 1(a). Blue solid line in Figure 2(c) and (d) corresponds to grey level values along the lines selected in the middle of restored images (lines are shown in figures (a) and (b), too). Red dashed line represents the fitted model evaluated for the first most significant frequency ω_j^* from equation (6). Figures show good approximation of the model to real profile. Using equation (9), we then calculated the value of the weaving density for warp yarn, with result 22.95 yarns per centimetre. Density of warp yarns measured by ravelling is 23.0 yarns/cm. Similarly, the density of weft yarns measured by proposed spectral analysis method was 16.62 yarns/cm, while the measurement by ravelling yielded 15.5 yarns/cm.

Method of automatic assessing of weaving density was tested on twelve solid samples. Eight samples were in plain weave, two samples in twill weave and two samples in satin weave. Images were captured by flat scanner with resolution 400 dpi in 256 grey levels and stored as image matrices. Equalization was used for contrast enhancement. Table 1 contains results of weaving density measurement by ravelling method (average of 5 measurements) and spectral method in plain (P1-P8), twill (T1, T2) and satin weave (S1, S2). The results show good accuracy of examined spectral method. Proposed method was also tested on images of plain weave fabric with check pattern. The whole process is automatic, input variable is the resolution of image R (pixel per inch) and output value is the weaving density D (yarns per centimetre). The method is relatively fast and non-destructive.

Defect Detection

A lot of common directional defects in woven fabrics are associated with the change of weaving density in a specific region, for example irregular weft density (insufficient, excessive), broken pick etc. The idea of weft direction defects detection is based on monitoring of weaving density in direction of length of fabric. Change of weaving density value against expected value indicates failure of regular structure. In order to detect such a change, we propose the application of control charts (namely the X-bar charts) approach. It will be used in the following manner:

Table 1. Results of weaving density measurement

Sample code	Weave	Density, yarns/centimetre (warp×weft) ravelling method	Density, yarns/centimetre (warp×weft) spectral method
P1	Plain	23.0×15.5	22.95×16.62
P2	Plain	23.0×20.5	22.95×18.99
P3	Plain	23.5×24.0	22.95×23.74
P4	Plain	22.3×9.0	22.95×8.70
P5	Plain	22.3×13.4	22.95×13.45
P6	Plain	22.4×17.2	22.95×18.20
P7	Plain	22.8×22.2	22.95×22.16
P8	Plain	22.7×23.2	23.74×23.74
T1	Twill	23.7×21.9	22.95×22.16
T2	Twill	23.0×21.7	23.74×22.16
S1	Satin	22.9×22.0	22.95×22.16
S2	Satin	23.0×21.6	23.74×21.37

In a row of fabric image n windows are randomly selected. In each window the weaving density D is evaluated by the automatic method described in the preceding parts. Those values, from the point of view of the control chart construction, represent n observations in one subgroup of repetitive measurement obtained practically in the same time. Then, when fabric is shifted, we obtain consecutive subgroups $V_1, \ldots, V_m$ of the same size n. Subgroup averages $\bar{x}_i$ and estimates of standard deviations $\bar{s}_i$ are computed for every subgroup V_i, from corresponding values D_{ji}, $j = 1, \ldots, n$, $i = 1, \ldots, m$. We assume that the distribution of subgroup averages is normal $N(\mu, \sigma^2/n)$ and variables D_{ji} are mutually independent. The unknown process mean μ is estimated by $\bar{\bar{x}}$ (see [9]), where

$$\bar{\bar{x}} = \frac{1}{m}\sum_{i=1}^{m}\bar{x}_i \tag{10}$$

the process standard deviation s is estimated by

$$\hat{\sigma} = \frac{1}{m c_4}\sum_{i=1}^{m}\bar{s}_i \tag{11}$$

where the constant c_4 is tabulated for different values of n. The $\bar{X}$ chart is then used for checking whether the process variability is in the state of statistical control. In other words, we check whether the values of weaving density along the fabric length are stabilized around the central line $\bar{\bar{x}}$. The upper control limit (UCL) and lower control limit (LCL) for an $\bar{X}$ chart are given as

$$UCL, LCL = \bar{\bar{x}} \pm \frac{K\sigma}{\sqrt{n}} \tag{12}$$

where constant K represents $100(1-\alpha/2)$ percentile of the standard normal distribution and α is the level of significance.

It is seen that the construction of control limits (a training phase) requires non-overlapping windows, both in each subgroup and between subgroups. Then, when using the procedure in praxis, we may relax the condition of independent subgroups, i.e. we allow them to overlap. On the other hand, if values in one subgroup are dependent, it is better to use the chart for individual values [9], hence here for subgroup averages $\bar{x}_i$.

Real Data Examples

The method has been tested on real specimen of fabric. Figure 3(a) presents an image of woven fabric in a plain

weave of size 1000×1000 pixels. Defect, weft stripe, occurs approximately in the middle of image and is extended across the full width of the fabric.

From the spectral approach the density of weft yarns was evaluated for n=5 randomly selected windows of size 100×100 pixels in the same row of image matrix. It was done for m=1000 subgroups in the image of woven fabric without defects. The distribution of subgroup averages was approximately normal. From equation (11) the estimation of

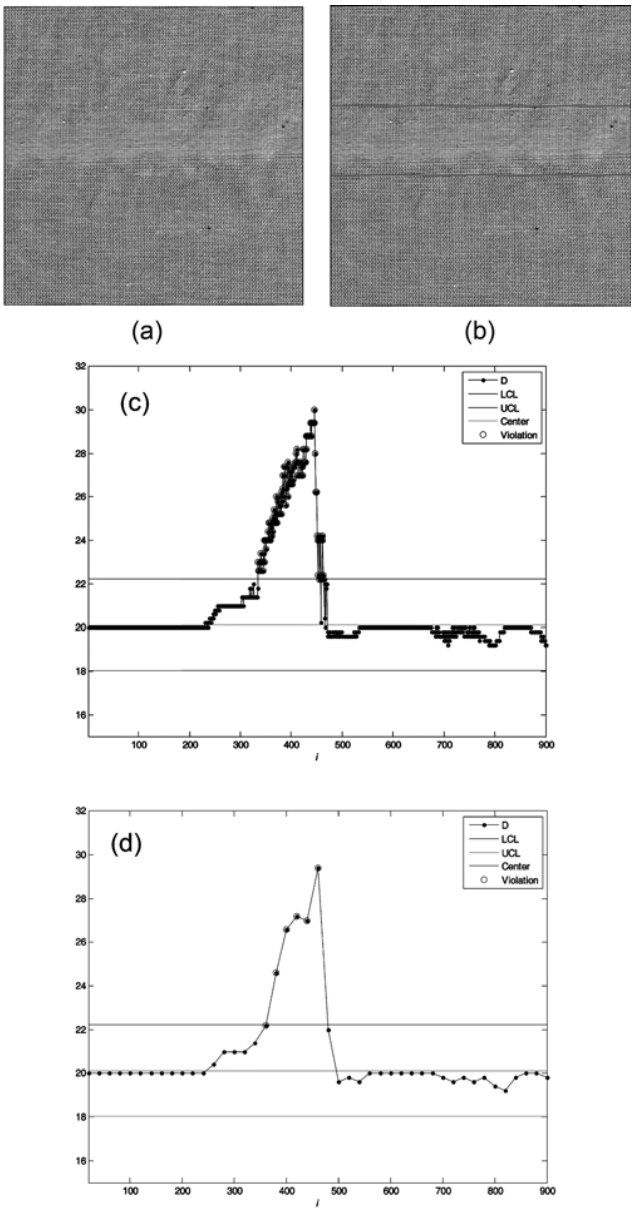

Figure 3. (a) Image of woven fabric in a plain weave with defect weft stripe, (b) defective region, (c) control chart for weaving density of weft yarns (1 pixel shift in vertical direction), and (d) control chart for weaving density of weft yarns (20 pixel shift in vertical direction).

standard deviations was counted, consequently upper and lower control limit for level of significance α=0.05 were obtained from (12). The constant c_4=0.94 in this case. The weaving density of weft yarns for fabric in plain weave in all following figures is $\bar{\bar{x}}=CL$=20.12, lower control limit LCL=18.03 and upper control limit UCL=22.21.

Then we applied monitoring process for image in Figure 3(a). Weft yarn density was counted for subgroups of n=5 windows randomly selected in every row - they were shifted mutually, in vertical direction, by 1 pixel. Subgroup averages are then plotted into the control chart. They are represented by blue dots in Figure 3(c). Green line represents the central line and red lines are lower and upper control limits. Violation of upper control limit, points out to a higher concentration of weft yarns (excessive weft yarn density) in region approximately between 335-th and 465-th pixel. Defective region is displayed in Figure 3(b). In praxis, larger shift, for example by half of window-width is quite sufficient for defect detection and reduces the amount of computations. Figure 3(d) shows control charts of subgroup averages for 20 pixels shift in vertical direction.

Figure 4(a1)-(a3) illustrates other three types of weft direction defects: (a1) insufficient weft density, (a2) change of weft density (insufficient) and (a3) change of weft density (excessive). Original images are of size 1000×1000 pixels, but displayed images are cutout of size 500×500 pixels for better details visibility. Figure 4(b1)-(b3) represents again control charts for weaving density of weft yarns. First example in Figure 4(a1) shows low values of weft density below the lower control limit in region from 190-th to 280-th pixel. This indicates the defect of insufficient weft density or broken pick which can be caused by absence of one or several weft threads and visible as a partially transparent place in the fabric. Low values of weft density from 200-th pixel can be seen from Figure 4(b2). Decreasing values characterize again irregular weft density, insufficient weft density in this case. Inverse case can be seen in Figure 4 (b3). Increasing values of weft density from 90-th pixel indicate the defect of excessive weft density.

Conclusion

Image restoration method using the two-dimensional Fourier transform was applied for the task of automatic assessing of weaving density and detection of defects in fabric. The whole process of density evaluation is automatic, where the input variables are image matrix and resolution of image, output value is the weaving density. We compared the weaving density of weft and warp yarns measured by proposed spectral method and measured by ravelling. The results show that the method is suitable for real samples with different structure. The algorithm was tested for solid samples, but it could be used for adorned fabric too. In that case, yarns in restored images have different grey level

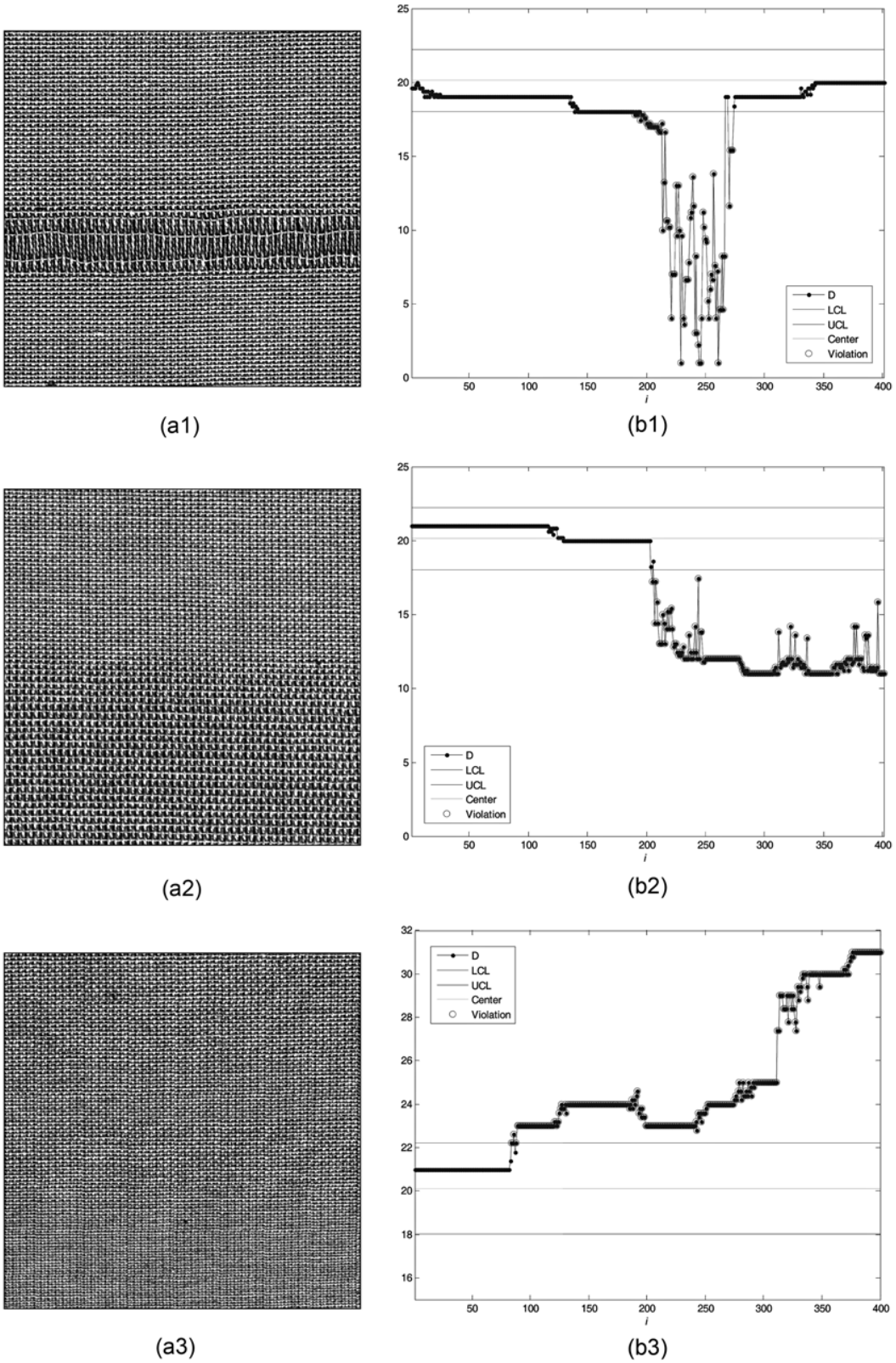

Figure 4. (a1)-(c1) Images of woven fabric in a plain weave with weft direction defects, (b1)-(b3) control charts for weaving density of weft yarns.

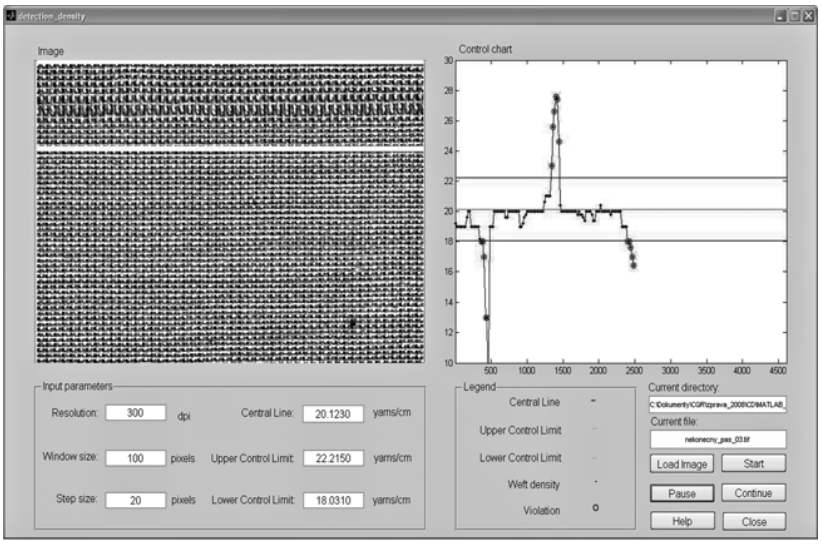

Figure 5. Graphical user interface for monitoring of weaving density.

values depending on colour or pattern. Some transformation can be used for elimination of this non-uniformity. We used top-hat transformation followed by histogram equalisation for contrast enhancement. This procedure was tested on images of plain weave fabric with check pattern.

The advantage of proposed method is that it can be used for woven fabric where sets of yarns are not mutually perpendicular, i.e. with a tilted set of yarns.

Further, it was shown how the method of automatic assessing of weaving density can be used for monitoring and detection of defects associated with the change of weaving density. This method is suitable for detection of weft directional defects which are extended across the full width of the fabric, for example insufficient weft density, excessive weft density, broken pick etc. The idea of detection is based on monitoring of weft yarns density in direction of length of fabric. Change of weaving density against expected value indicates changes in regularity of structure. Control charts were used as a tool for detection of sites of potential defects. The method is rather reliable and computation fast, so that it is convenient for the on-line fabric inspection under real conditions. In this paper the fabrics was inspected in windows moving systematically over the whole image area, while the image was static. In the case of on-line inspection the fabric moves while the image camera could be static. The procedure is at present time implemented for laboratory on-line experiments. For this reason the graphical user interface for monitoring weaving density was created in MATLAB environment which can be seen in Figure 5.

Acknowledgement

This work was supported by the projects of MSMT CR No. 1M06047 and No. LC06024.

References

1. J. J. Lin, *Text. Res. J.,* **72**, 486 (2002).
2. J. E. Wood, *Text. Res. J.,* **60**, 212 (1990).
3. S. A. H. Ravandi and K. Toriumi, *Text. Res. J.,* **65**, 676 (1995).
4. B. Xu, *Text. Res. J.,* **66**, 496 (1996).
5. Y. Jeong and J. Jang, *Fiber. Polym.,* **6**, 156 (2005).
6. Y. Jeong, *Text. Res. J.,* **78**, 304 (2008).
7. R. C. Gonzales and R. E. Woods, "Digital Image Processing", 2nd ed., Prentice-Hall, NJ, USA, 2002.
8. T. Cipra, "Time Series Analysis, with Applications in Economy" (in Czech), SNTL, Praha, 1986.
9. T. P. Ryan, "Statistical Methods for Quality Improvement", J. Wiley, New York, 1989.

Příloha 4

[4] Tunák, M., Linka, A., and Volf, P. Load-sharing and Monte Carlo Models of Defects in a Bundle of Fibres. *Composites Science and Technology*, **69**(9), 2009, 1417–1421. issn: 0266-3538. IF=2.856.

Composites Science and Technology 69 (2009) 1417–1421

Contents lists available at ScienceDirect

Composites Science and Technology

journal homepage: www.elsevier.com/locate/compscitech

Load-sharing and Monte Carlo models of defects in a bundle of fibres

M. Tunák [a,*], A. Linka [a], P. Volf [b]

[a] Department of Textile Evaluation, Technical University of Liberec, Liberec, Czech Republic
[b] Department of Applied Mathematics, Technical University of Liberec, Liberec, Czech Republic

ARTICLE INFO

Article history:
Received 4 December 2007
Received in revised form 24 April 2008
Accepted 7 September 2008
Available online 16 September 2008

Keywords:
A. Fabrics/textiles
A. Textile composites
B. Stress/strain curves
C. Probabilistic methods
C. Modelling

ABSTRACT

Two methods for modelling and random simulation of progressive deformation and breaks in a bundle of parallel fibres are proposed. First, a stochastic load-sharing reliability model of a parallel system and of its resistance against a stress is utilized. The method of its statistical analysis is presented, too. In order to improve certain limitations of such model, a complementary method based on the Monte Carlo simulation is introduced. The bundle of fibres is modelled as a grid consisting of a set of nodes and connecting arcs. The deformation and breaks are caused by an external load stretching the grid. The first objective is to find an optimal, stabilized, states of the grid corresponding to each load level. Optimal configuration is found with the help of Markov Chain Monte Carlo (MCMC) procedures. In order to model the breaking process, the load is increased sequentially. It is shown that the model is applicable also to other structures, namely to the plain weave fabric and its defects simulation. The results with bundle of fibres are compared with real stress–strain curves. The parameters for simulation were selected in such a way that obtained stress–strain curve corresponds to a real experiment with carbon fibres.

1. Introduction

In contrast to metal structures that generally exhibit ductile behaviour, composite materials tend to be brittle. That is important feature, because they can be described by theories based on the weakest link concept. In general, the failure of component depends on the material strength, on loading and the structural behaviour, which also includes interaction between components, boundary conditions and so on. The joint effect of probabilistic description of loading, structural response and material strength is dealt with by reliability analysis of composite material structures (see [4] for review).

In the present contribution we first model strength of bundle composed from *m* fibres as the reliability (survival) of a system composed from a set of parallel components. We will consider a model of redistribution of load among the fibres, namely the Daniels load-sharing model (see [1] or [2]). In this model it is assumed that the applied load is distributed equally among the surviving (unbroken) fibres and further, the breaking strengths of individual fibres are independent and identically distributed random variables. The model neglects the interactions between fibres, which arise when the fibres are twisted to form a yarn or they are set in matrix to form composite. Daniel's model provide links between the probabilistic theory of brittle materials, such as glass, carbon or Kevlar, and bundles of fibres, tow and strands, which are used as the reinforcement phase in many composites. Thus, the theory allows for prediction of the characteristics of reinforcing bundles in composite.

However, as it has been said, the model neglects several important features of real bundles, as the interaction between fibres or possible piece-wise character of fibres, which is typical for fibres used in composites, but also for textile yarns. The Monte Carlo approach described in part 3 is able to incorporate also these aspects. The bundle is still composed from parallel fibres (which could be a limitation of the model), however it allows to consider interrupted fibres, their friction or other interaction, and also a local load-sharing in large bundles. After a proper modification the model is applicable also to other fibres structures. The part 4 shows its adaptation to the case of a plain weave fabrics and its progressive deformation. In both cases, the structure is modelled as a grid consisting of a set of nodes and connecting flexible (to some extent) arcs. In the case of bundle, one set of arcs represents the interaction among fibres. The deformation and break of arcs are caused by an external load stretching the grid. The objective is to find optimal, stabilized, states of the grid, for each load level, and to simulate sequence of fibres breaks. Hence, the problem can be reformulated as the problem of optimal configuration of a random field of points with local dependencies, which is one of typical problems solved with the aid of Monte Carlo Markov Chains (MCMC) procedures. To do so, the prior distribution of nodes is given by local conditional distributions, further; the potential function is defined as a tension in grid arcs. Optimal configuration then can be found with

* Corresponding author.
E-mail addresses: maros.tunak@tul.cz (M. Tunák), ales.linka@tul.cz (A. Linka), petr.volf@tul.cz (P. Volf).

0266-3538/$ - see front matter © 2008 Elsevier Ltd. All rights reserved.
doi:10.1016/j.compscitech.2008.09.004

the help of Metropolis–Hastings algorithm, possibly accompanied with simulated annealing. The method complements the one described in [3]. An example dealing with the stretching a bundle of fibres shows that the parameters of our simulation procedure can be selected in such a way that obtained results are comparable with real experimental stress–strain curves of sequential breaks of fibres.

2. The model for counting process of breaks of fibres

Let us imagine that the fibre bundle is stretched by a load increasing from 0 up to the level breaking the bundle (i.e. all its fibres) – or up to a given maximal load $S_{\max}$ when the experiment is terminated. This testing experiment is relatively fast, so that the time of duration of the tension does not play any role. Therefore, we use more or less standard survival analysis approach, however, instead the time, the tensile strength is the variable of interest.

The global load affecting the bundle is observed. However, as the break of a fibre leads to an immediate redistribution of the force to the other fibres (so that to the abrupt increase of the force affecting each individual fibre), the consequence is the break of several of remaining fibres (not necessarily of all, because their load – resistance is random). Therefore, in such a case we actually do not know the precise level of the load causing the break of individual fibres. Moreover, we are not able to register the order in which they broke. So that, in the case of multiple fibres break, we know exact load causing the break of one fibre (we do not know which one, but in the case of 'identical' and independent fibres it is not important), and intervals of loads, which caused the breaks of the other fibres. From these considerations it is seen that the part of the data has a complicated interval-censored structure. Fortunately, if we observe a sufficient number of breaks, we register also a sufficiently large set of uncensored data (see [1]).

Let us first consider one individual fibre and the random variable U – its breaking strength. We assume that it has a continuous distribution on $[0,\infty)$ with a distribution function $F(u)$, density $f(u)$, hazard function $h(u) = f(u)/(1 - F(u))$ defined on $u \in [0,S]$ such that $F(S) < 1$. By $H(t) = \int_0^t h(u)\mathrm{d}u$ we denote cumulative hazard function. The 'fate' of a fibre during the increase of tensile strength u is described by two random processes, by the counting process $N^1(u)$ and identificator $I^1(u)$. $I^1(u) = 1$ if the load u affecting the fibre is observed, otherwise $I^1(u) = 0$. Specifically, $I^1(u) = 0$, if the fibre is already broken, if the experiment is terminated, and also for values of u during an abrupt step-wise increase of the load. We assume that trajectories of $I^1(u)$ are left-continuous. As regards $N^1(u)$, $N^1(0) = 0$and $N^1(u)$ jumps to 1 at the load level u_b causing the break of the fibre, provided $I^1(u_b) = 1$.

2.1. The model for bundle of fibres

Let us consider a bundle composed from m fibres. Let us assume, that the survival of fibres is described by independent identically distributed random variables $U_j, j = 1,\ldots m$, with distribution given by $f(u)$, $F(u)$, $h(u)$, $H(u)$ respectively. Now, we assume that at each moment the applied load is distributed equally among surviving (unbroken) fibres. Observed data has following structure: Let us imagine that the breaks of fibres occurred for three 'global' tensile strengths affecting the bundle, $0 < s_1 < s_2 < s_3 < S_{\max}$, that on levels s_1, s_2 the numbers k_1, k_2 of fibres broke and, finally, remaining k_3 fibres broke on level s_3, with $k_1 + k_2 + k_3 = m$. Therefore, just before the first break the load stretching each fibre was $u_1 = s_1/m$, while at the moment of the second break it was $u_2 = s_2/(m - k_1)$(naturally affecting only $m - k_1$ remaining fibres) and at the moment of the last break this 'individual' load affecting the last $m - k_1 - k_2$ fibres was $u_3 = s_3/(m - k_1 - k_2) = s_3/k_3$. As regards the 'observed' breaks (i.e. the breaks caused by a known load), we actually observed only three, caused by u_1, u_2 and u_3, respectively.

Other breaks were caused by unknown (unobserved) loads from intervals $(u_1, \overline{u}_1 = s_1(m - k_1 + 1))$, $(u_2, \overline{u}_2 = s_2(m - k_1 + k_2 + 1))$ and $(u_3, \overline{u}_3 = s_3)$, respectively for k_1-1, k_2-1, k_3-1 fibres. Moreover, if k_1 (or k_2, or k_3) > 1, we do not know the order in which the fibres broke. We can assume that the maximal load $S_{\max}$ is sufficiently large (e.g. $S_{\max} > S \cdot m$) in order not to terminate experiments too early.

Taking into account the assumption that the probability distributions of U_j are continuous, then there cannot be two breaks at the same level of tensile strength. In other words, fibres break one after another, not simultaneously (though we do not know their order). Then the intervals of breaking strengths can be specified even more precisely than $(u_k, \overline{u}_k)$ above. However, as it has been said, we do not intend to use the information about interval-censored strength values. That is why we are not going to discuss this aspect here.

2.2. Estimation of cumulated hazard rate

The first objective is to propose an estimator of cumulative hazard function $H(u)$ of distribution of breaking strength of one bundle. Let us consider that n 'identical' and independent bundles are tested. Denote by U_{ij} random variables (survivals), $N_{ij}(u)$, $I_{ij}(u)$ related individual counting and identificator processes for j-th fibre of i-th bundle ($j = 1,2,\ldots,m$, $i = 1,2,\ldots,n$). Further, denote

$$N_i(u) = \sum_{j=1}^{m} N_{ij}(u), \quad I_i(u) = \sum_{j=1}^{m} I_{ij}(u), \quad N(u) = \sum_{i=1}^{n} N_i(u),$$
$$I(u) = \sum_{i=1}^{n} I_i(u).$$

Based on those data, the most common estimator of cumulative hazard function, namely the Nelson–Aalen one, can be constructed:

$$\widehat{H}_n(u) = \int_0^u \frac{\mathrm{d}N(v)}{I(v)},$$

where we set $0/0 = 0$. It is seen that the ability of the estimator to approximate well the 'true' $H(t)$ depends on the identificator process, i.e. on observability of counting processes for all values of load u in the interval of interest $[0,S]$. More details on properties of this estimator in considered case can be found in [5].

2.3. Distribution of breaking strength

Let us now consider the 'reverse' problem. Namely, let us assume that we know the characteristics of survival distribution of individual fibres and our aim is to derive these characteristics for the whole bundle composed from m identical (and independent) fibres. More precisely, the question is how to estimate or compute the probability that the bundle will not survive the load s? Let this probability be given by the distribution function $F_R(s) = P(R < s)$, where R is the random variable describing the survival of the bundle. If we denote by $U_{(1)} < U_{(2)} < \ldots < U_{(m)}$ the order statistics created from $U_1, U_2, \ldots U_m$, then evidently,

$$P(R < s) = \left\{\cap_{k=0}^{m-1} U_{(k)} < \frac{s}{m-k}\right\}.$$

However, computation is not easy. For instance, for the simplest case $k = 2$ we obtain

$$P(R < s) = P\left\{U_{(1)} < \frac{s}{2}, U_{(2)} < s\right\} = 2\int_0^{s/2} \left\{\int_u^s f(v)\mathrm{d}v\right\} f(u)\mathrm{d}u$$
$$= 2\left\{F(s)F\left(\frac{s}{2}\right) - \int_0^{s/2} F(u)f(u)\mathrm{d}u\right\}.$$

Another and a quite simple approach to evaluation of distribution of random variable R consists in the simulation experiments. The following example illustrates such a simulation of survival of the bundle:

Example 1. Let us consider the bundle composed from $m = 20$ fibres and assume that the survival of each fibre (i.e. random variable U_{ij}) has the Weibull distribution, i.e. cumulative hazard function is

$$H(u) = \left(\frac{u}{\theta}\right)^{\beta}.$$

We simulated the breaks of $n = 1000$ such bundles. The results observed for one of them with parameters $\beta = 2$ and $\theta = 3$ are in Figs. 1(a) and (b). Naturally, the global load t under which the bundle broke was observed, too. We thus obtained a sample of $n = 1000$ realizations t_i of random variable R – the breaking strength of the bundle. The empirical distribution function

$$\widehat{F}_R(t) = \frac{1}{n}\sum I[t_i < t],$$

constructed from this sample is displayed in Fig. 2(b). Other empirical characteristics can be easily derived, too. For instance, the estimate of cumulative hazard function is given either as $-\ln(1-\widehat{F}_R(t))$ or directly from ordered sample: Let (i) be order of t_i in $t_1, t_2, ..., t_n$, then

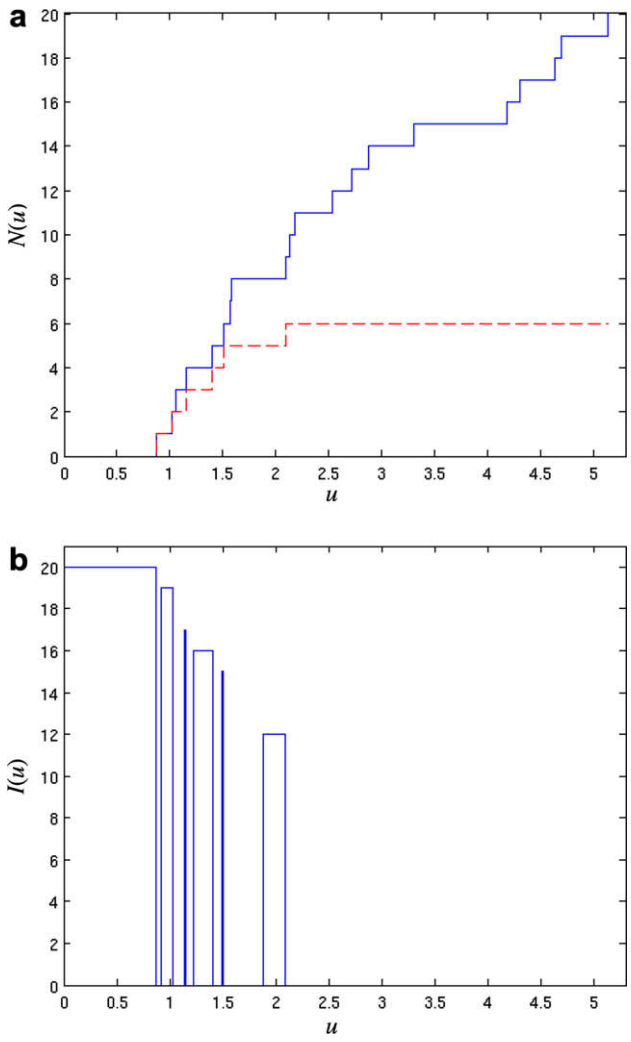

Fig. 1. (a) Process $N(u)$ of observed breaks (– – –) and process of all breaks (solid line), (b) process $I(u)$ of fibres in risk.

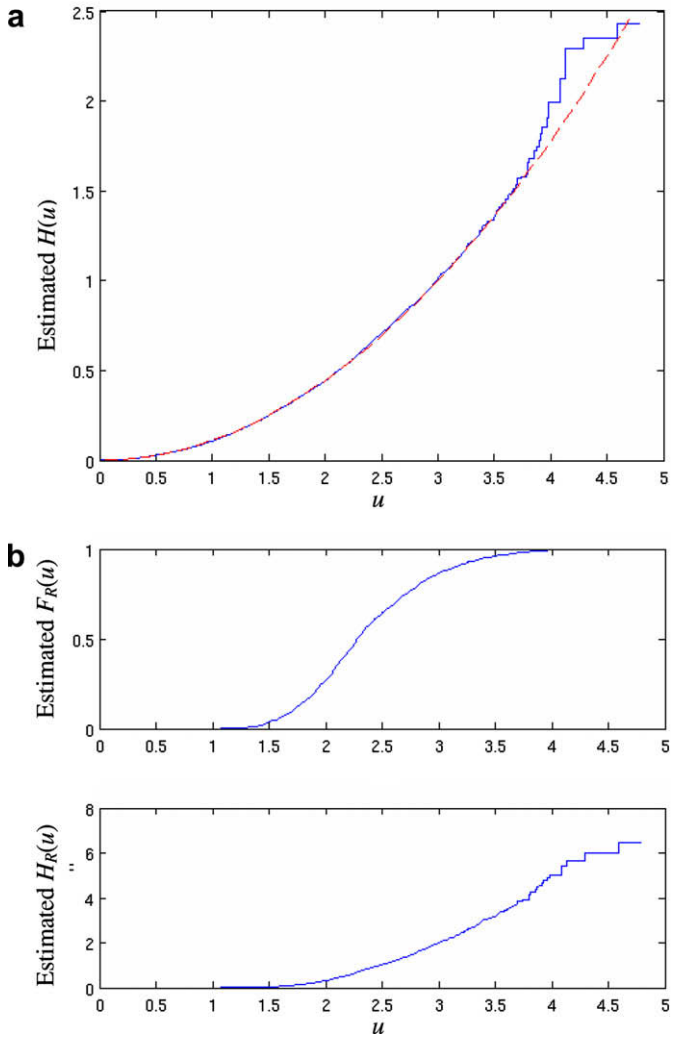

Fig. 2. (a) Nelson–Aalen estimator of $H(u)$ and its comparison with the cumulative hazard function of Weibull distribution with parameters $\beta = 2$ and $\theta = 3$, (b) empirical distribution function $F_R(u)$, estimator of $H_R(u)$, where $u = t/m$ is load per fibre.

$$\widehat{H}_R(t) = \sum_{i=1}^{n} \frac{I[t_i < t]}{n - (i) + 1}.$$

It actually is again the Nelson–Aalen estimator.

3. Simulation of a bundle of fibres stretching

While the objective of the preceding part consists in analysing hazard rates of fibres, of the whole bundle, and predicting its survival, the present method is aimed to the simulation of the process of bundle stretching and breaks. The objective is also to select such parameters of simulation algorithm to obtain results comparable with real cases. Such a comparison is than made through stress–strain curves. For simulation, let us imagine each (horizontal, say) fibre as a set of 'finite elements', nodes and arcs. In the simplest case – parallel set of fibres, no vertical connection exists between lines representing individual fibres. Each fibre breaks maximally once, when stretched.

In more advanced model we assume a friction between fibres – there is a resistance against shifts of one fibre against another, which actually is also another source of stress, when the whole bundle is stretched. In that case each fibre can break more than

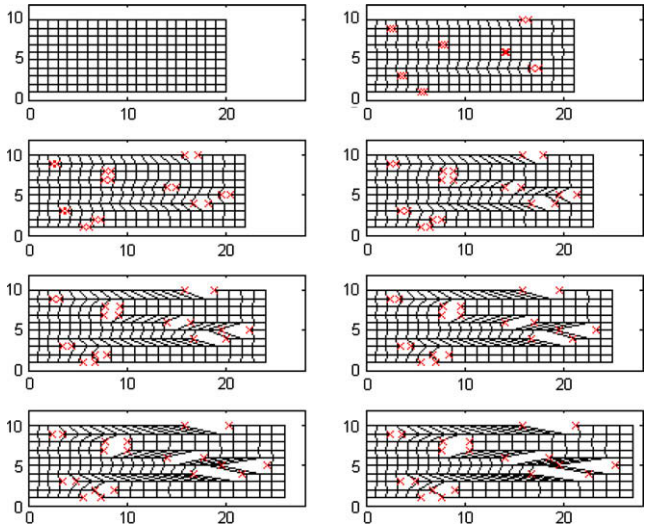

Fig. 3. Development of simulation from initial state to the state with all fibres broken.

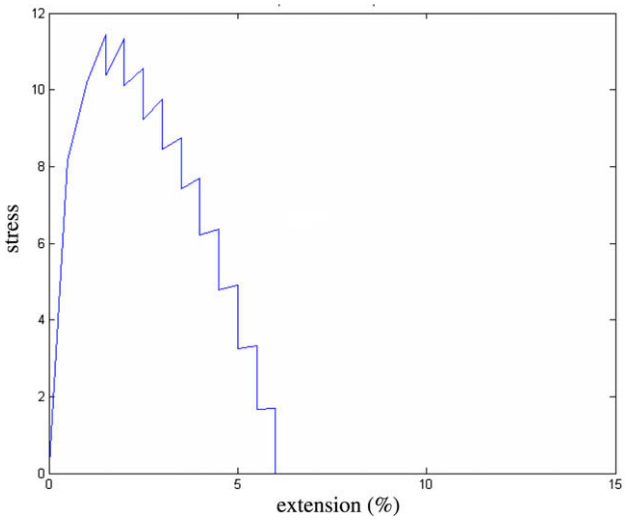

Fig. 4. Simulated stress–strain curve of 10 C wires.

once. Moreover, a real yarn is made (twisted) from pieces of fibres, of a random length and beginning, so that fibres are interrupted (it actually gives an effect similar to that of broken fibres sticking together thanks to friction).

The random generation proceeds in such a way that the changes of 'nodes' are proposed, in horizontal direction only. Total stress is the sum of stresses from their extension (stress is a power function of extension, with exponent larger than one) and from friction (here depending linearly on the shift of a fibre with respect to neighbouring ones). If total stress exceeds a certain (again randomised) level, the fibre breaks. Fig. 3 shows one such simulated experiment, while Fig. 4 displays corresponding stress–strain curve. The parameters for simulation were selected in such a way that obtained stress–strain curve corresponds to a real experiment with carbon fibres.

4. Simulations of a defect snag in a plain weave

This section shows an application of the modified Monte Carlo model introduced in previous part. Fig. 5 shows a grid consisting of a set of nodes (representing interlacing points) and flexible arcs (now representing real yarns), a simple model of fabric in a plain weave. Defect snag appears as the picks displaced out of alignment and sometimes also jammed, a lumpy fault occurs with locally displaced lines of weft yarns, i.e. the picks are not in alignment. The offending warp yarn is either broken or at least highly tensioned. Similarly, a defect hole is caused by a several absent yarns varying in form and size. These defects can arise when one or more picks are snagged on a rough or knotted warp and are shifted or broken. We assume that direction of stress is perpendicular to weft set of yarns and borders of simulated grid are fixed.

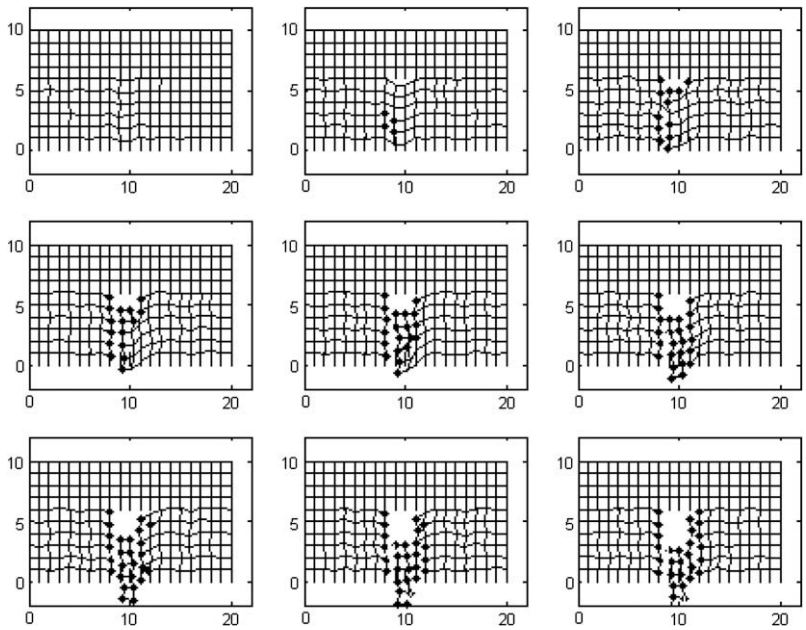

Fig. 5. Simulation example of consequence of vertical pressure, acting from above to central nodes of a grid, and results when the pressure increases gradually.

Stress is redistributed through grid, causes extensions and stresses in grid arcs. When it exceeds a certain (randomised) level, the arc breaks. Additionally, we consider also changes of angles of arcs connecting grid nodes and assume that when angle exceeds its critical magnitude, corresponding arc 'breaks', too. Different combinations of stress caused by change of length of arcs and by change of their angles, together with critical levels for breaks, enable us to generate cases corresponding to various real situations, different types of strain, and materials with different characters.

5. Conclusion

In order to study the process of composite reinforcement deformation we have analysed a standard stochastic load-sharing model and then, in the same setting, we have proposed Monte Carlo experiments simulating the influence of stress to a simplified model of composite reinforcement structure. We examined both the deformation of the fabrics as well as the process of extension and breaks of its fibres. Numerical results were obtained with the help of Markov Chain Monte Carlo computation, where joint combined distribution of grid node and grid arc was modelled as Gibbs distribution (Gibbs random field) of a special form. In example of part 3 it was also shown that a proper adjustment of procedure parameters, namely the nonlinear dependence of stress on deformation and random breaking strength level, could yield the results corresponding to real data cases.

Acknowledgements

This work was supported by the Czech Science Foundation under Grant No. 106/03/H150 and by the Projects of MSMT CR No. 1M06047 and No. LC06024.

References

[1] Belyaev YuK, Rydén P. Non-parametric estimators of the distribution of tensile strengths for wires. Research report. University of Umea; 1997.
[2] Crowder MJ, Kimber AC, Smith RL, Sweeting TL. Statistical analysis of reliability data. London: Chapman and Hall; 1991.
[3] Harthelius K, Carstensen JM. Bayesian grid matching. IEEE Trans Pattern Anal Mach Intell 2003;25:162–73.
[4] Sutherland LS, Guedes Soares C. Review of probabilistic models of the strength of composite materials. Reliab Eng Syst Saf 1997;56:183–96.
[5] Volf P, Linka A. On reliability of system composed of parallel units subject to increasing load. Int J Reliab Qual Saf Eng 2000;7(4):271–84.

Příloha 5

[5] Tunák, M., Bajzík, V., and Testik, M. Monitoring Chenille Yarn Defects using Image Processing with Control Charts. *Textile Research Journal*, **81**(13), 2011, 1344–1353. issn: 0040-5175. IF=1.102.

Original article

Textile Research Journal

Textile Research Journal
81(13) 1344–1353

DOI: 10.1177/0040517511402123
trj.sagepub.com

SAGE

Monitoring chenille yarn defects using image processing with control charts

Tunák Maroš[1], Bajzík Vladimír[1] and Testik Murat Caner[2]

Abstract

In this paper, a control chart is introduced for monitoring various defect types occurring on chenille yarns. To implement the control chart, a grey level image of chenille yarn is captured as an image matrix. Image preprocessing is applied and this involves thresholding to a binary image and a morphological opening operation for removing small objects from the image. The height of the pile yarn, measured from the processed images, is selected as the monitored quality characteristic. Since the monitored quality characteristic was highly autocorrelated, a first-order autoregressive AR(1) model was found to be appropriate for modelling the autocorrelation structure. Due to estimation of the AR(1) process parameters, a modified exponentially weighted moving average (EWMA) control chart for residuals is implemented as a tool for monitoring and detecting defects. It is shown that the modified EWMA control chart can be used successfully for monitoring different types of chenille yarn defects.

Keywords

Chenille yarn, exponentially weighted moving average, control charts, defect detection

Introduction

Quality control of textile products is an important part of production in the textile industry. Quality improvement of final products increases manufacturers' competitiveness as well as reducing costs. Consequently, automated methods for monitoring of quality characteristics based on computer vision are still in development. In the literature, several studies have dealt with the applications of digital image processing for fibrous materials. Various techniques and algorithms for the measurement of yarn hairiness have been proposed.[1,2] Measurement of yarn hairiness by an image analysis algorithm based on various edge detectors has been reported.[3] Assessment of yarn snarls with the aid of digital image processing and signal processing has been presented,[4] and image analysis and similarity based clustering method have been used for automatic determination of geometric parameters of slub yarn.[5]

The principal purpose of this paper is to describe an objective method for monitoring of chenille yarns' homogeneity and recognition of defects as an indicator of chenille yarns' quality. Statistical process control provides objective statistical methods for monitoring such quality characteristics. Furthermore, statistical process control combined with digital image processing technologies might eliminate the subjectivity of the human inspection process.

Methods that utilize control charts (the most widely used tool of statistical process control) for monitoring fabric defects have been proposed[6,7] in the literature. Based on image restoration, control charts were used in the automatic inspection of weaving density of woven fabric.[6] In this study, assessment of weaving density was obtained by using a spectral approach based on the 2D Fourier transform. Changes of weaving density value, relative to the expected value, were monitored with the aid of Shewhart control charts. This method was shown to be suitable for real samples with different structures.[6] On the other hand, multivariate control

[1]Department of Textile Evaluation, Faculty of Textile Engineering, Technical University of Liberec, Czech Republic.
[2]Department of Industrial Engineering, Faculty of Engineering, Hacettepe University, Turkey.

Corresponding author:
Tunák Maroš, Department of Textile Evaluation, Faculty of Textile Engineering, Technical University of Liberec, Studentska 2, Liberec 46117, Czech Republic
Email: maros.tunak@tul.cz

charts were also proposed when the quality of a process was characterised by multiple quality characteristics.[7] In this study, a vector of quality characteristics, based on second-order grey level texture features (obtained from grey level co-occurrence matrix), represented a multivariate observation. Hotelling's chi-squared chart, as a direct multivariate extension of the Shewhart chart, integrated multiple quality characteristics for monitoring regularity of a structure.

In the current study, we propose a method that uses image analysis followed by a control chart application for monitoring various types of defects occurring on chenille yarns. Image processing requirements and the control chart found to be suitable for this problem are explained. Homogeneity and height of pile yarns are important quality characteristics of chenille yarns. A control chart is used here as a tool for recognising places along the chenille yarn where there is an irregular structure. An easy and reliable automated procedure is demonstrated by using examples of real defect types. It is shown that the proposed approach can be useful in detection of various types of defects that may occur on chenille yarns during production.

Chenille yarns

Yarns called fancy yarns are the group of yarns that differ in their construction from single and folded yarns by deliberately produced irregularities in their construction.[8] Chenille yarn is a pile fancy yarn[9] that consists of two types of yarns – core and pile. Chenille yarns are manufactured by placing short lengths of yarns, called pile yarns, between two core yarns and then twisting the yarn together. The structure of a chenille yarn can be seen in Figures 1 and 2a. Core yarns provide the strength to the yarn, whereas pile yarns give soft and pleasant hand and also influence the volume and appearance of a chenille yarn. Chenille yarns can be found in a wide range of products from garments (sweaters, outerwear fabrics) to decorative fabrics, upholstery, bedspreads.[10,11] In addition to many desirable properties, a major undesirable property of chenille yarns that must be monitored is the high mass loss of pile yarns when the product is rubbed.

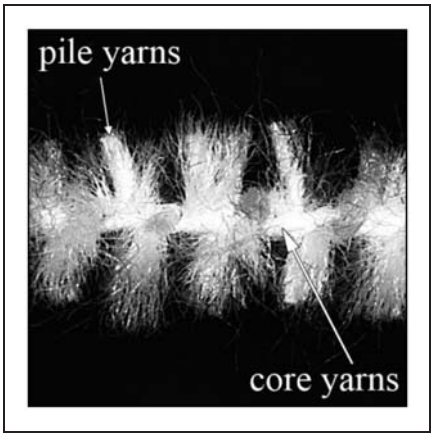

Figure 1. Structure of a chenille yarn.

Intensity of pile yarn shedding during abrasion is affected by friction forces between pile and core yarns. Chenille yarns with cotton pile yarns have a higher abrasion resistance than the ones produced from viscose and acrylic fibres.[11] The type of fibres, yarn twist, and pile yarn length are the most important characteristics influencing mass loss during abrasion.[10–14] In addition to material characteristics, the production parameters of machines also determine chenille yarn parameters, e.g. appearance, volume, and abrasion resistance.[15] Besides the influence of yarn construction on the abrasion resistance, dimensional stability of yarns and knits was also investigated in the literature. It was shown that the yarn construction affects dimensional stability after laundering or dry-cleaning[16] and shrinkage of yarns in boiling water.[17]

In the textile terminology, a defect is defined as any visible difference or change from expected standard or norm that causes quality reduction of textile products. Many different types of defects can be introduced during chenille yarn manufacturing and the presence of a defect can be attributed to many factors. Defects occurring in chenille yarns can be as a result of pile or core yarn imperfections, mistakes during manufacturing, dyeing or final finishing processes. From this standpoint, a thorough control of pile yarn homogeneity must be maintained after the manufacturing and subsequent finishing processes. Omission of this important step of production can cause quality reduction of the final article. Basic parameters describing structure of chenille were introduced by Çeven and Özdemir.[15]

The uniform height of pile yarn along the resultant yarn is an important parameter of chenille yarns. During chenille yarn manufacturing processes, some types of defects can occur:

- Knot – appears as a thick place caused by change in yarn thickness (Figure 2b)
- Empty place – appears as a result of pile yarns being absent in a certain region (Figure 2c)
- Sporadic yarn – appear as imperfections in the homogeneity with pile yarns missing in short sections (Figure 2d)
- Fly – appear as outstanding yarns in some places (Figure 2e)

Low abrasion resistance of chenille yarns causes problems in applying classical measurement instruments for detecting yarn defects. These problems arise

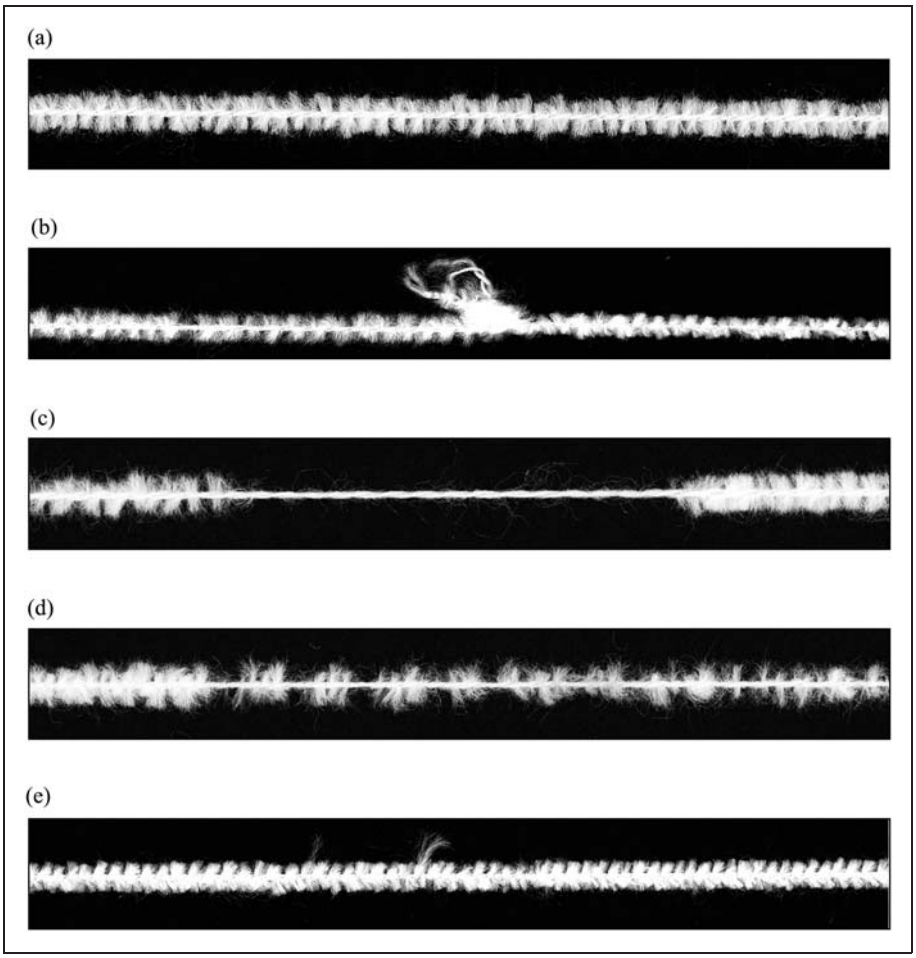

Figure 2. Chenille yarn defects, (a) non-defect, (b) knot, (c) empty place, (d) sporadic yarn, (e) fly.

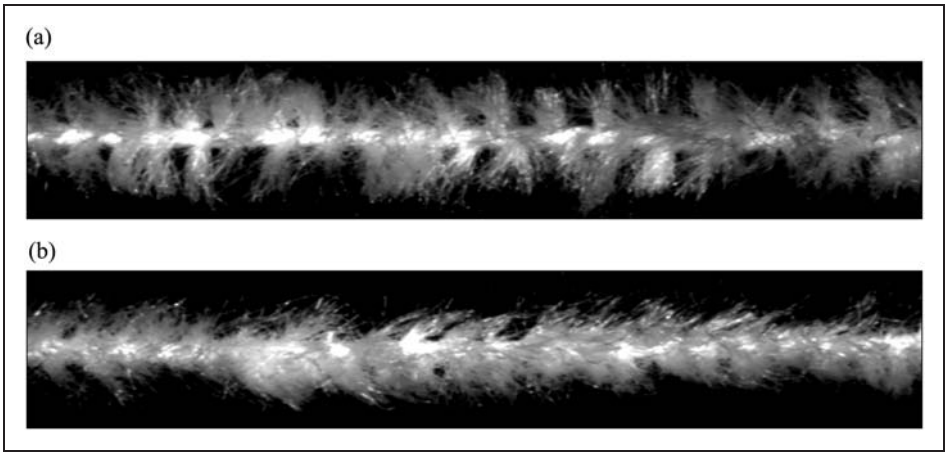

Figure 3. Chenille yarn (a) before and (b) after measuring on Uster Tester, where the yarn was pulled from right to left.

due to contact with, either the measuring equipment or the guiding parts that move the yarn into the measuring device. During measurements, the pile yarn can be pulled out or the 'direction' (orientation of pile yarn, relative to long axis of the core yarn) of the rest of the pile yarn can be changed (Figure 3). Measurement of uniformity of pile yarn height is also not possible once the pile has acquired a 'direction'.

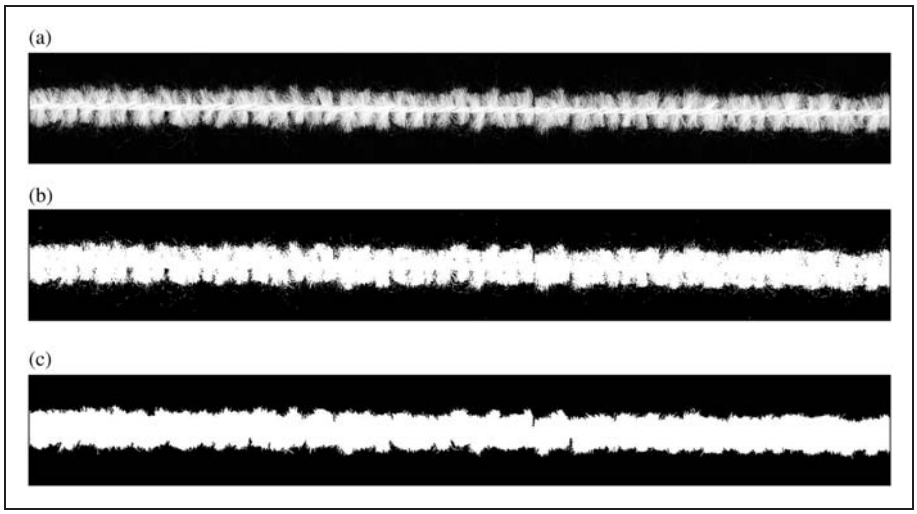

Figure 4. Image preprocessing, (a) grey level image, (b) binary image, (c) morphological opening.

In this study, digital image analysis followed by statistical data analysis are performed to implement a modified exponentially weighted moving average (EWMA) control chart of Testik[18] for monitoring the defects on a folded chenille yarn. The width observations obtained from the image of the yarn follow an autoregressive process of order 1 (AR(1)). Hence, the modified EWMA control chart is specifically designed for monitoring an AR(1) process. Since the process parameters are unknown, these are estimated from a training dataset. Details are discussed in the following.

Digital image processing

In this study, 100% acrylic chenille yarns of fineness 4.0 Nm with twist level 875 T/m and pile length 1.2 mm were used. Images of the chenille yarn were obtained by using a digital desktop scanner HP ScanJet 8270 with a resolution of 600 dpi to give a uniformly illuminated surface of chenille yarns and sufficient resolution of resulting images. Chenille yarns were stretched on a black base plate, which ensures sufficient contrast between yarn and background for the following image preprocessing. Note that a very important part of image capturing is to ensure a uniform illumination of chenille yarns. This would significantly reduce requirements for preprocessing of resulting images.

Images were captured as image matrices in 8-bit grey level range (Figure 4a). The binary image (Figure 4b) was converted from greyscale by using a threshold (level 0.2), where background is displayed by black (level – 0) and object is displayed by white (level – 1). Note that segmentation to a binary image simplifies and accelerates subsequent image operations due to the application of binary logical operations. In such prepared images, it is easier to carry out subsequent operations such as measurements of sizes, areas, orientations etc. of objects since they have exactly defined borders in contrast to grey level images. Small objects may also be visible around the image of the yarn. These objects can be caused by dust particles; fragments of fibres, random noise etc., and represent undesirable parts of the image. Hence, it is necessary to remove these from the image for a better representation. The morphological opening of the binary image is used to remove these small connected objects (connectivity 8) that consist of fewer than 50 pixels (Figure 4c) without failure of regions of interest, i.e. the yarn shape. Note that the images illustrated in Figure 4a–c belong to the same yarn.

The binary images of chenille yarns were captured in the resolution of 1000×7500 pixels. To monitor the height of the pile yarns along the length of the yarn, the width, measured as the number of white pixels from the first to the last white pixel in the y-axis of the image, is selected to be the monitored quality characteristic. Note that there is a width measurement corresponding to each of the 7500 pixels along the length, i.e. the x-axis of the image. To smooth these width measurements, the 7500 pixels along the x-axis of the image were divided into sequential and disjoint sets of 5 pixels each and the averages of the width measurements in each set were used in defect monitoring (i.e. 1500 average values of the width were treated as the observations).

Although it is the scope of a follow-up study for implementation, it is important to mention that a contactless image capturing device (for example a line scan camera) would be necessary in the case of online monitoring of chenille yarn quality at real production settings. In such cases, the image camera would be static

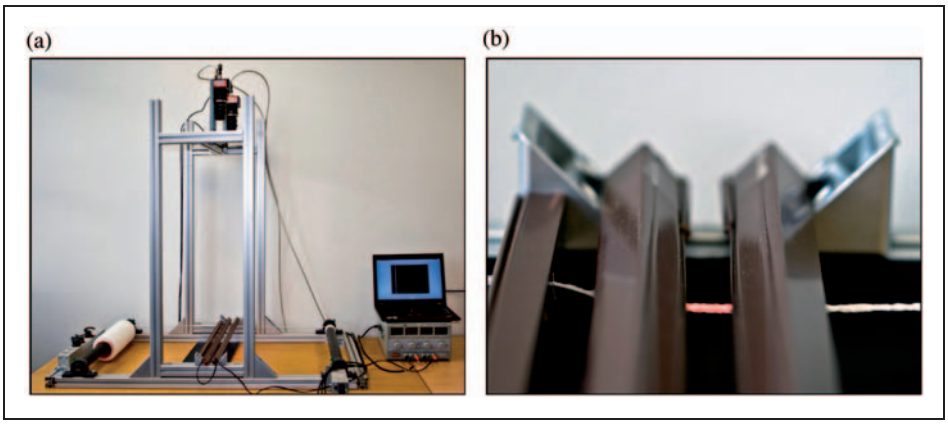

Figure 5. Detection system, (a) laboratory machine for online monitoring, (b) detail of monitored chenille yarn.

while the chenille yarn is moving. Hence, a prototype machine is also designed for simulating online quality monitoring settings (see Figure 5a and b), where the images are captured by a line scan camera.

The prototype machine consists of an aluminium frame, a DC motor, LED illumination and a line scan camera. This prototype machine is intended for winding of chenille yarn and thus to represent the behaviour of a continuous process. Characteristics of the prototype machine are provided below:

Yarn delivery: There are two rollers on the sides that straighten the yarn to stay straight. One of the rollers is driven by a *Maxon MCD EPOS 60W* motor, which offers the controls of acceleration, break, velocity, and the cycle count.

Illumination and image capture: Two lines of high bright red LEDs were built into the latch (Figure 5b). Picture acquisition is performed by using a *Basler L401k* monochrome line scan camera with resolutions 4080 px, i.e. about 8 px/mm.

Analysis system: Maximum line rates of 7.2 kHz would yield the top speed of about 54 m/min. However, real winding speed here is limited by the lighting conditions, yarn properties, and mostly by the complexity of successive processing, rather than by technical parameters of the hardware components.

Process modelling

A yarn without any defects was selected by a visual inspection and the measurements on it were used as the training dataset. The training dataset was first analyzed to define the in-control settings of the control chart. In this phase I analysis, the observations (1500 averages of the yarn width measurements) were found to be highly autocorrelated and also note that the traditional control charts have the assumption of serially independent observations. Autocorrelation has been shown to significantly distort the performance of a control chart and often an appropriate time series model (for example, an autoregressive integrated moving average (ARIMA) model) is first used to model the autocorrelation structure of observations and then a control chart is used to monitor the residuals from the time series model.[18,19]

To fit an appropriate ARIMA model, often autocorrelation and partial autocorrelation plots are useful.[20] It can be observed from Figure 6a and b, respectively for the sample autocorrelation plot and the sample partial autocorrelation plot of the training dataset, that an AR(1) model is an appropriate fit in this study (depending on the application, other ARIMA models can also provide a better fit to the data). The vertical axis in Figure 6a and b are the autocorrelation and partial autocorrelation coefficients, respectively. The horizontal axis corresponds to the lag between the observations. The significant autocorrelations and partial autocorrelations are the points exceeding the 95% confidence limits (horizontal lines) in the Figure 6a and b. Note that the strongly significant autocorrelations slowly decay and only the first-order partial autocorrelation is significant for an AR(1) process.

Suppose that the yarn data can be modelled by an AR(1) model

$$x_t = c + \varphi x_{t-1} + a_t \tag{1}$$

where c is a constant, $-1 < \varphi < +1$ is the autoregressive parameter, t is the index, and a is an independent and identically distributed normal random sequence with mean zero and variance σ_a^2. The minimum mean squared error forecast[20] of this process at index value t for index value $t+1$ is

$$\hat{x}_{t+1|t} = \varphi x_t. \tag{2}$$

Hence, the residuals e_t may be calculated as

$$e_t = x_t - \hat{x}_{t+1|t} \tag{3}$$

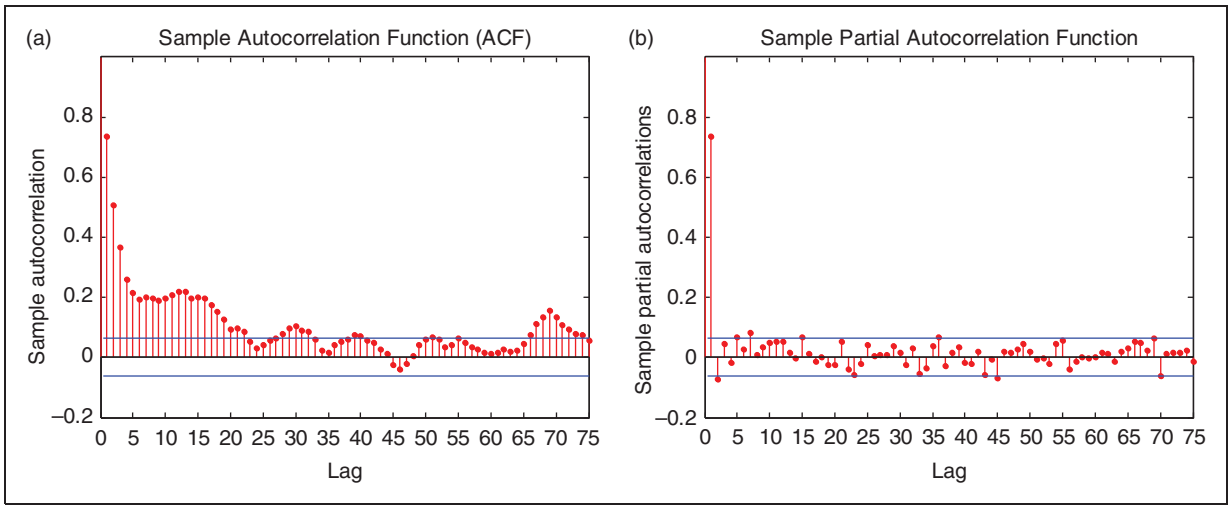

Figure 6. (a) Autocorrelation function, (b) partial autocorrelation function for chenille yarns data with 95% confidence limits.

Table 1. Estimates of parameters

Type	Coefficient	Standard error	t-value	p-value
AR(1)	0.74	0.0215	34.22	0.000
Constant	18.53	0.1211	152.95	0.000
Process mean	69.80	0.4563		
Residuals	SS = 14668.4	MS = 14.7	*d.f.* = 998	

Since the process parameters are unknown, these parameters can be estimated[20] from the training dataset. To estimate the AR(1) parameters, the middle 1000 observations in the training dataset were used and the obtained model was validated by using the remaining 500 observations. The AR(1) model obtained is

$$x_t = 18.53 + 0.74x_{t-1} + a_t \tag{4}$$

with the AR(1) process mean being 69.80. The estimates of the parameters along with the standard errors, t-values, and p-values are provided in Figure 7a and Table 1. The first-order autocorrelation coefficient is 0.7345. Furthermore, the histogram of the residuals (Figure 7b) indicates that the normal distribution would fit well to model the residuals.

An AR(1) model has the same form as a simple linear regression model, where the observation at index value $t+1$ is the dependent and the observation at the index value t is the explanatory variable. Here, the positive correlation between consecutive observations (the first-order autocorrelation) occurs due to the tendency for the piles to remain at the same height from one observation to the next.

Using the fitted AR(1) model, the residuals and the corresponding autocorrelation function and partial autocorrelation function were calculated (Figure 8a and b). In Figure 8, again the 95% confidence limits are provided. Since all the points plot inside the confidence limits, we conclude that the AR(1) model explains the autocorrelation structure well and the residuals are independently distributed.

Yarn quality monitoring using the modified EWMA control chart

The EWMA control chart for the yarn width data was constructed based on the suggestions of Testik.[18] Note that Testik[18] recommends a modification of the standard EWMA control chart applied to residuals of a time series model, when the time series process parameters are unknown but estimated. This practical modification might reduce the signal probability of a control chart for a false defect since process parameters are often unknown but estimated in practice. The EWMA control statistic, which is plotted on the control chart over time, for monitoring the residuals is defined as

$$z_t = (1-\lambda)z_{t-1} + \lambda e_t \tag{5}$$

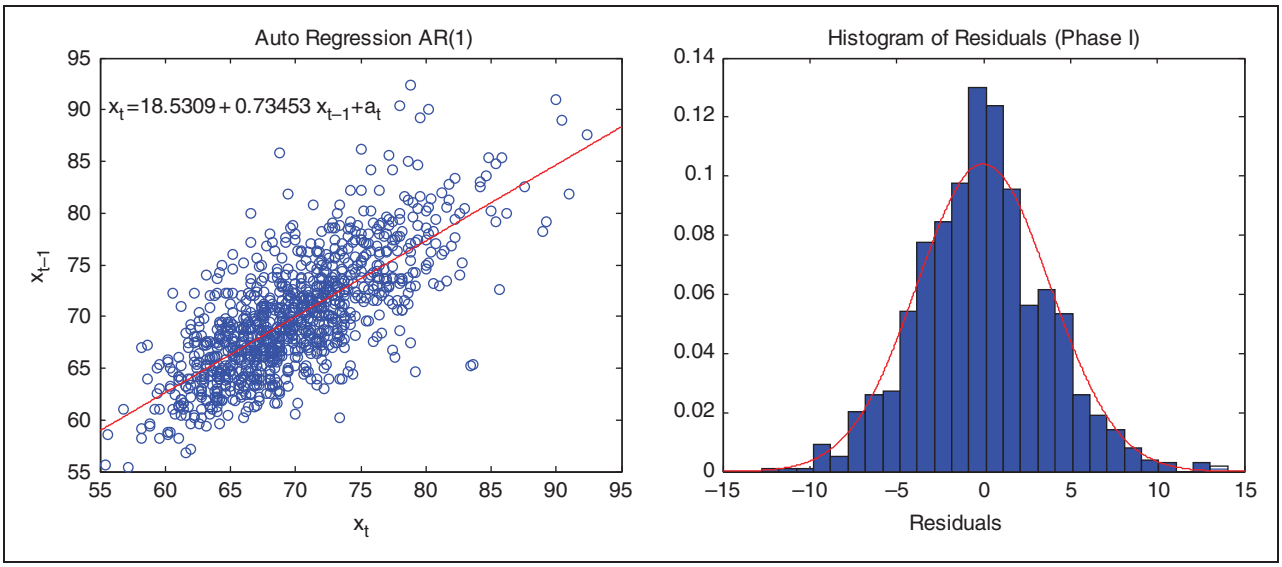

Figure 7. (a) AR(1) model, (b) histogram of residuals.

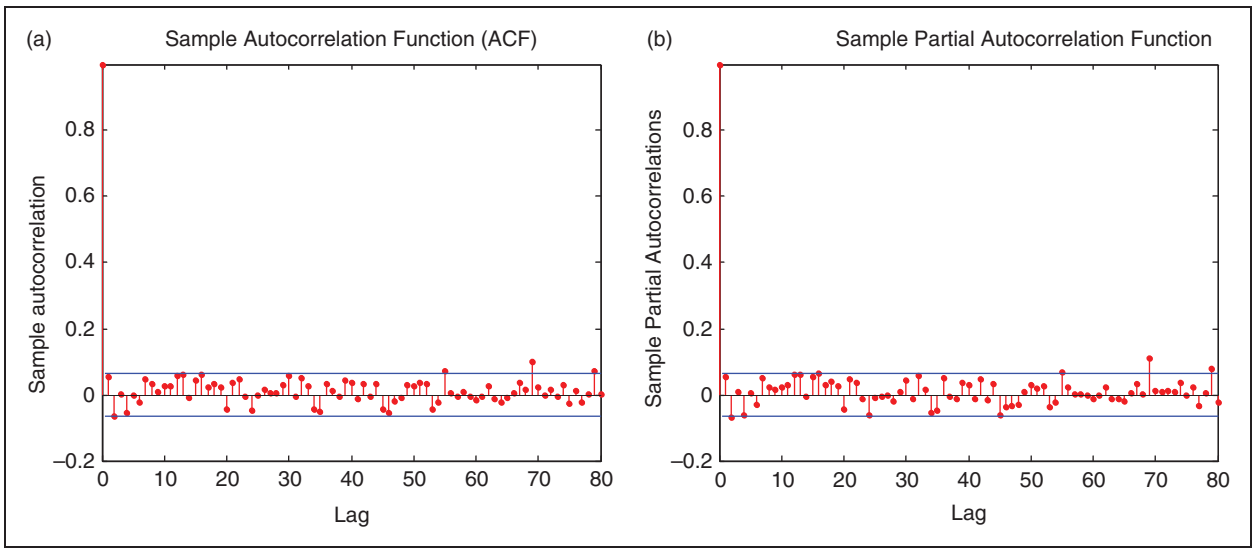

Figure 8. (a) Autocorrelation function of residuals, (b) partial autocorrelation functions of residuals with 95% confidence limits.

where $0 < \lambda \leq 1$ is the smoothing parameter and the starting value is $z_0 = 0$ since residuals are expected to have a mean zero.

Pairs of control limits are also plotted on the control chart to facilitate decision making with regard to the status of the process. A plotted point on the control chart that exceeds either of the control limits is taken as an indication of the existence of a defect. The control limits of the chart are set to

$$\pm L\sigma_z \tag{6}$$

where L is the control limit width and σ_z is the standard deviation of the EWMA statistic. In designing the modified EWMA control chart, the smoothing parameter λ was selected to be 0.2 and control limit width L was selected as 3. For the in-control data, variance of the residuals is 14.67 (standard deviation is 3.83). Therefore, the variance of the EWMA statistic can be computed as (see[18] for details)

$$\sigma_z^2 = \sigma_a^2 \frac{(1-\nu)}{(1+\nu)} \left\{ 1 + \frac{6\nu\sqrt{(1-\phi^2)/n}}{(1-\nu\phi)} + \frac{1+\nu\phi}{n(1-\nu\phi)} \right\} \tag{7}$$

where, $\nu = 1 - \lambda$ and n is the number of observations in the training dataset that are used in estimating the

AR(1) model parameters. The variance of the residuals e_t in equation 3 is used as an estimate of the term σ_a^2 in equation 7. In the chenille yarn monitoring study considered, the variance of the EWMA statistic, σ_z^2 is found to be 2.79 (standard deviation is 1.67) by using the values; 0.74 for ϕ, 3.83 for σ_a^2, 0.8 for ν, and 1000 for n, in equation 7. Hence the upper and lower control limits, UCL and LCL, were set at ± 5 by using the equation 6.

First, consider the EWMA control chart for the training dataset, which is known to be free of defects (Figure 9a). An observation exceeding either the UCL or the LCL (obtained from equation 6) normally signals a defect. Since it is known that the chenille yarn is defect free here, the signal can be classified as a 'false defect'. A control chart always has a probability of a false signal for a defect. However, by appropriate selection of the control limits, this false signal probability can be significantly reduced. In our design, the control chart is expected to signal a false alarm about once in 10000 observations, on average. Note that the values of the control limits calculated here also depend on the process model and the yarn characteristics of the manufacturer; hence, different applications might necessitate other designs.

After the phase I study to construct the control chart, the chart designed is used to monitor chenille yarn defects. The modified EWMA control charts for detecting different types of defects are provided in (Figure 9b–d). The control charts are very effective for detecting defects (points on the control chart that exceed the UCL or LCL indicate presence of defects) on the chenille yarns. Furthermore, the points exceeding the control limits in these control charts also

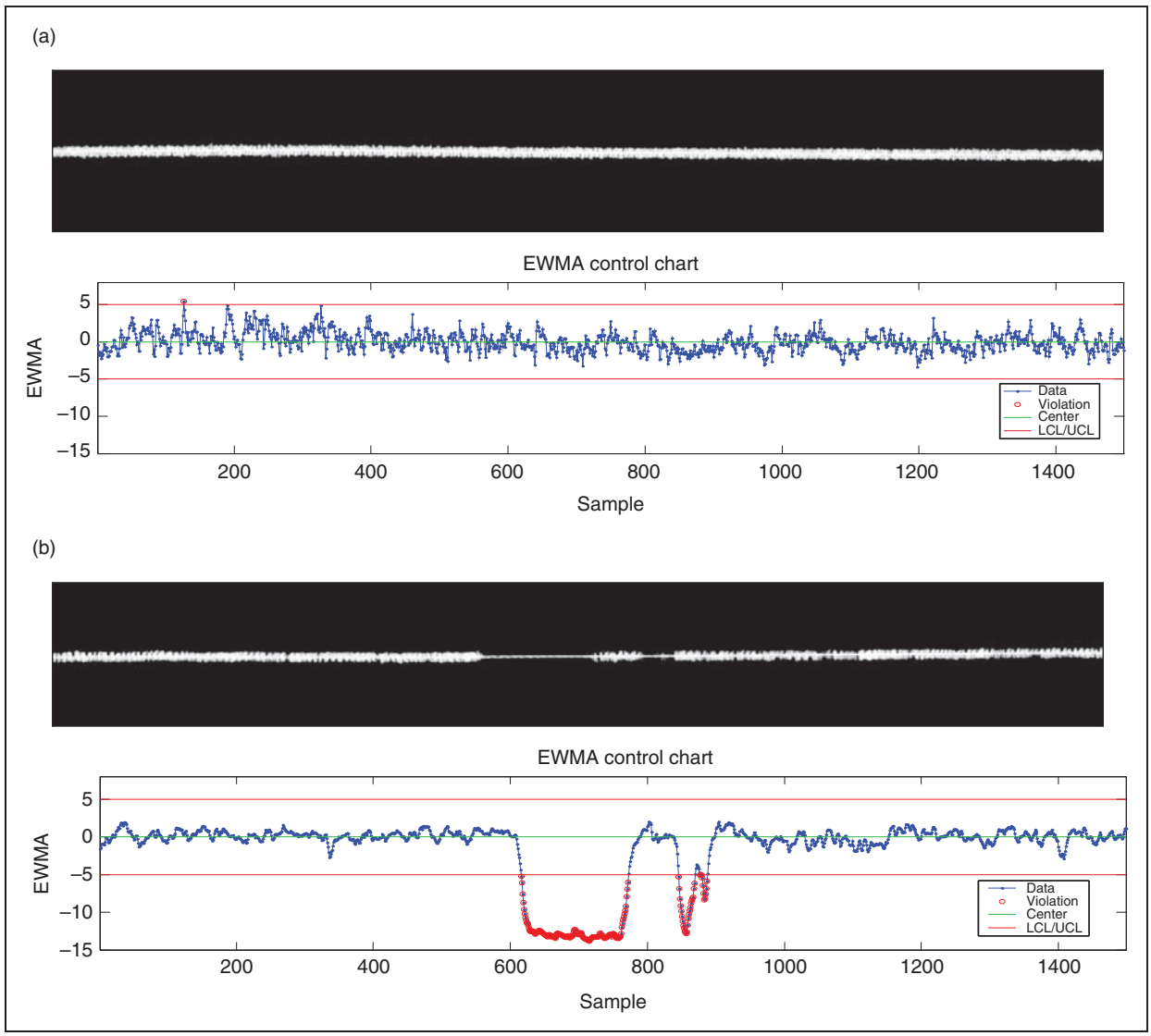

Figure 9. EWMA control chart of residuals, (a) non-defect, (b) empty place, (c) knot, (d) sporadic yarn.

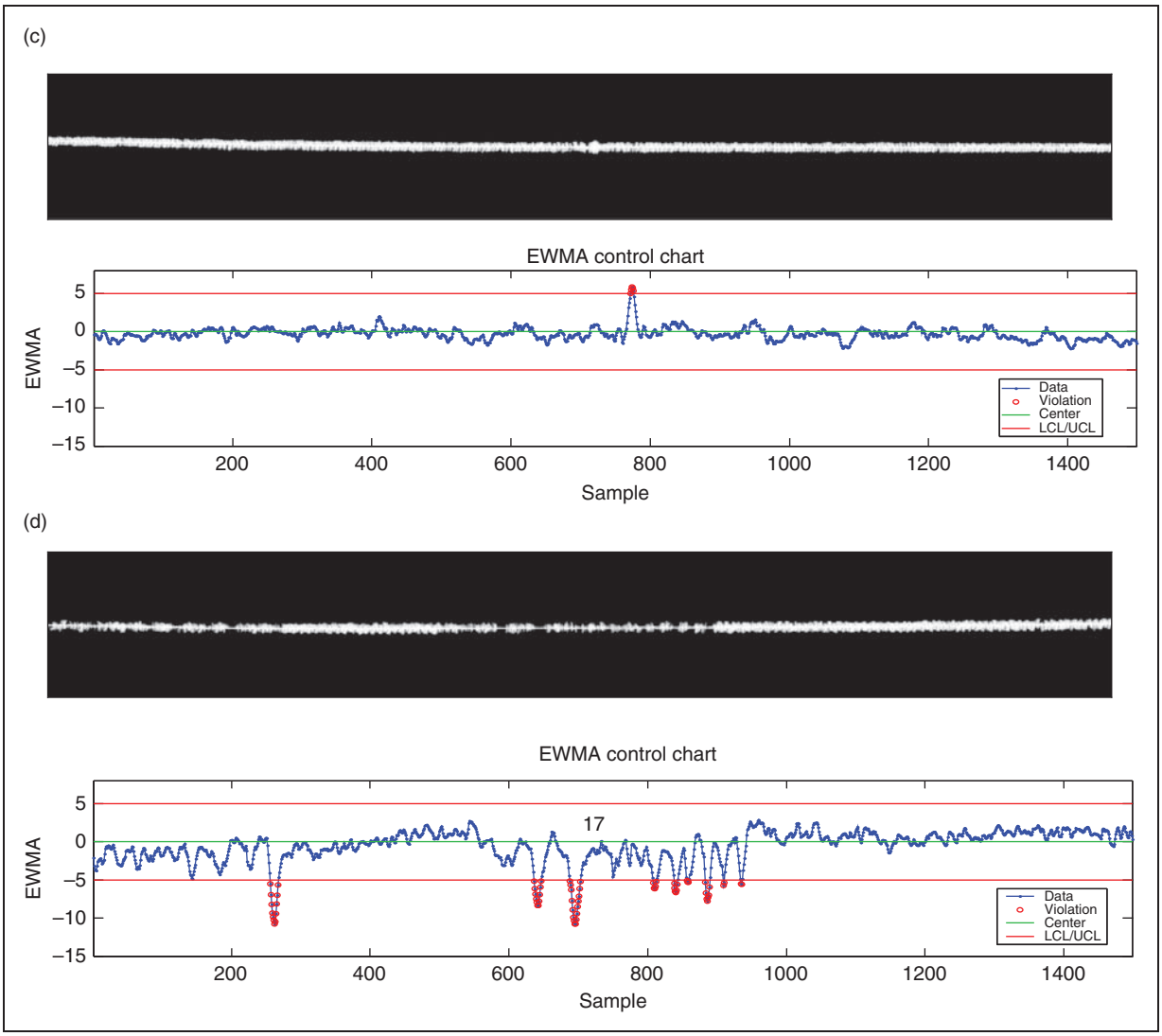

Figure 9. Continued.

provide some information on the location and type of defect encountered.

Conclusions

The proposed approach of monitoring chenille yarn defects is based on image processing followed by methods of statistical process control. The height of pile yarn was selected as the monitored quality characteristic. An autocorrelation analysis showed that the width measurements along the yarn image are highly autocorrelated and classical control charts (such as a Shewhart type chart) cannot be successfully implemented since too many 'false defects' may be encountered. An AR(1) model was found to represent the autocorrelated observations well and is used to remove autocorrelation from the observations. The modified EWMA control chart proposed by Testik[18] is used to monitor the residuals of the fit AR(1) model. Effectiveness of the control chart in detecting various types of defects on chenille yarns was illustrated, where violation of control limits pointed out the defective region of the yarn. It can be concluded that the modified EWMA control chart is suitable for detection of defects occurring in chenille yarns or monitoring of the homogeneity of pile yarns.

The pile distribution in chenille yarns is in 3D and a projection from the 3D space to 2D image may cause false signals for defects. False signals for defects can be reduced, for example, by use of two devices for capturing images in two directions and the proposed analyses could proceed separately. Here, only the methodology, which is based on image analysis for monitoring irregularities of pile yarns, has been proposed. The algorithm is computationally simple and fast for computer implementation and it only requires autocorrelation

model parameters to be determined from a training dataset and setting up the control chart as recommended in Testik.[18] In order to increase the computation speed, the proposed algorithm could also be implemented in C++ programming language with the use of OpenCV library. Further research is being planned for investigating the proposed approach in production settings and development of a computer software program for implementation. For this purpose, a prototype machine is developed to simulate real production settings.

Funding

This work was supported by the project Center of Quality and Reliability of Production MŠMT ČR (grant number 1M06047).

Acknowledgements

The authors would like to thank the referees for carefully reading the paper and for their comments, which greatly improved the paper.

References

1. Barella A. Yarn hairiness. *Textile Progress* 1983; 13(1): 1–57.
2. Barella A. The hairiness of yarns. *Textile Progress* 1993; 24(3): 1–46.
3. Guha A, Amarnath C, Pateria S and Mittal R. Measurement of yarn hairiness by digital image processing. *J Textile Inst* 2010; 101(3): 214–222.
4. Xu BG, Murrells CM and Tao XM. Automatic measurement and recognition of yarns snarl by digital image and signal proscessing methods. *Textile Res J* 2008; 78(5): 439–456.
5. Liu J, Xie Z and Gao W. Automatic determination of slub yarn geometrical parameters based on an amended similarity-based clustering method. *Textile Res J* 2010; 80(11): 1075–1083.
6. Tunák M, Linka A and Volf P. Automatic assessing and monitoring of weaving density. *Fibres and Polymers* 2009; 10(6): 830–836.
7. Tunák M and Linka A. Directional defects in fabrics. *Res J Textiles Apparel* 2008; 12(2): 13–22.
8. McIntire JE and Daniels PN. *Textile Terms and Definitions*. 10th ed. Manchester: The Textile Institute, 1995.
9. Ulku S, Ortlek HG and Omeroğlu S. The effect of chenille yarn properties on the abrasion resistance of upholstery fabrics. *Fibres & Textiles in Eastern Europe* 2003; 11(3): 38–41.
10. Kalaoğlu F and Demir E. The effect of chenille yarn properties on the performance of chenille upholstery fabrics. *Textile Asia* 2001; (3): 37–40.
11. Özdemir Ö and Çeven EK. Influence of chenille yarn manufacturing parameters on yarn and upholstery fabric abrasion resistance. *Textile Res J* 2004; 74(6): 515–520.
12. İlhan İ and Babaarslan O. A theoretical approach to pile yarn-shedding mechanism of chenille yarn. *J Textile Inst* 2007; 98(1): 23–30.
13. Çeven EK and Özdemir Ö. Evaluation of chenile yarn abrasion behavior with abrasion tests and image analysis. *Textile Res J* 2006; 76(4): 315–321.
14. Babaarslan O and Ilhan I. An experimental study on the effect of pile length on the abrasion resistance of chenille fabrics. *J Textile Inst* 2005; 96(3): 193–197.
15. Çeven EK and Özdemir Ö. A Study of the basic parameters describing the structure of chenille yarns. *Fibres & Textile in Eastern Europe* 2006; 14(2): 24–28.
16. Nergis BU and Candan C. Properties of plain knitted fabrics from chenille yarns. *Textile Res J* 2003; 73(12): 1052–1056.
17. Özdemir Ö and Çeven EK. Effect of chenille yarn parameters on yarn shrinkage behavior. *Textile Res J* 2005; 75(3): 219–222.
18. Testik MC. Model inadequacy and residuals control charts for autocorrelated processes. *Qual Reliability Eng Int* 2005; 21: 115–130.
19. Montgomery DC. *Statistical quality control*. 6th ed. NJ, USA: John Wiley and Sons, 2009.
20. Box GEP, Jenkins GM and Reinsel GC. *Time series analysis*, 3rd ed. NJ, USA: Prentice Hall, Inc., 1994.

Příloha 6

[6] Tunák, M. and Linka, A. Methods for Recognition of Woven Structure Defects. *World Journal of Engineering*, **5**(1), 2008, 2 pages. ISSN: 1708-5284.

METHODS FOR RECOGNITION OF WOVEN STRUCTURE DEFECTS

Tunák Maroš, Linka Aleš

Dept. of Textile Materials, Technical university in Liberec, Hálkova 6, 461 17 Liberec 1, Czech Republic

Introduction

In the textile industry the current inspection process of quality of textiles still depends on human visual inspection. It is a time consuming and repetitive activity requiring permanent attention in order to detect defects. According to all that, there is many human mistakes in this process. Therefore, textile industry takes concern in replacing human visual inspection with a suitable automated visual inspection.

In this paper, we will introduce automated visual inspection based on the statistical approach and we will show usage for the directional defect detection. Woven fabric is normally composed of two sets of mutually perpendicular and interlaced yarns. The weave pattern or basic unit of the weave is periodically repeated throughout the whole fabric area with the exception of the edges, thus images of woven fabric are homogenously structured and can be consider as textured images. These periodicities correspond to periodicity of second-order grey level statistic features. We especially focus on recognition of common directional defects associated with the change of weaving density or defects that appear as a thick place distributed along the width or high of an image. In this paper we will test algorithm for recognition of simulated defects and finally we will show a few examples of recognition on real samples, too.

Second order grey level statistics

Texture statistics are frequently classified into first-order, second-order and high-order statistics. First-order statistics refer to the marginal grey level distribution and can be derived from the grey level histogram, e.g. mean, variance, skewness, energy etc. The first-order statistics are highly dependent on the lighting conditions and in common practice should be eliminating the influence of first-order statistics in texture analysis by making the grey level histogram match a specific distribution. This approach destroys any spatial information of textures pattern and only retains their brightness information. Second-order grey level statistics refer to the joint grey level distribution of pairs of pixels and it is based on grey level co-occurrence matrices. The grey level co-occurrence matrices (GLCM) are full representation of the second-order grey level statistics and retain both spatial arrangement and relative brightness information.

Grey level co-occurrence matrices

The size of textured digital image $f(x,y)$ is mxn and its grey level resolution is G. A GLCM, $\boldsymbol{c}$, is a square matrix with size equal to number of grey levels G contained in textured image and is defined with respect to two parameters, d, the distance between two pixels, and θ, the position angle between two pixels (x_1, y_1) a (x_2, y_2). An element of GLCM, c_{ij}, is the number of times a point having grey level i occurs in position given with respect to parameters d, θ to a point having grey level j. Normalized GLCM, $\boldsymbol{C}$, is the joint probability occurrence of pixel pairs with a defined spatial relationship having grey level values i and j in the image. A lot of features can be computed from the normalized GLCM, in this contributions we extracted a set of four features. For example, measure of the intensity contrast between a pixel and its neighbour over the whole image is given by [1], [2]:

$$I = \sum_{i=0}^{G-1} \sum_{j=0}^{G-1} |i-j|^2 C_{ij} \cdot \qquad (1)$$

Defect detection in simulated structures

The algorithm was tested first for simulated structures of woven fabric (size 500 x 500 pixels) in a plain weave with randomly generated defects. The simulated output image of a periodic structure in a plain weave can be simulated as a convolution of an elementary unit (pattern repeat) by an input image of pattern of repetition. Images of a plain weave contained common directional defects were modelled by using algebraic operations on simulated images of plain weave structure, in some cases with removing some rows or columns. Position, size and shape of defects were randomly generated from uniform distribution, see [3]. We evaluated a set of eight features for m = 1000 randomly placed windows of size 50 x 50 pixels in image of simulated structure without defects. Four features extracted from GLCM with parameters d = 1 and θ = 0° (weft direction) and four features from GLCM with parameters d = 1 and θ = 90° (warp direction). We obtained m samples of p – dimensional normal distribution. Then we evaluated a multivariate

Shewhart control charts for the process mean with upper control limit [4]:

$$L_u = \frac{p(m+1)(m-1)}{m(m-p)} F_{1-\alpha,p,m-1}, \qquad (2)$$

where m is number of multivariate observation and p is number of variables. Then we applied algorithm to detection of defects in simulated structure with defects. We counted the test statistic for ith individual observation of features extracted from sliding window moved over the whole image and compared against control limit in the form:

$$D_i^2 = (x_i - \bar{x}_m)' S_m^{-1} (x_i - \bar{x}_m). \qquad (3)$$

where S_m is a variance-covariance matrix. If any observation was outside the limit, for a given level of significance a, the window was considered as the window containing defect. Size of images was set to 500 x 500 pixels; Gaussian noise of mean 0 and variance 0.0025 was added to images. Sliding window of size 50 x 50 pixels was moved by the step of size 25 pixels. Windows with detected defect or imperfection remained in image and were displayed with red colour. Fig. 1 show plot of individual observation against control limit, red windows are outside the control. Figure 2 (a) – (c) display result of applied algorithm to some few simulated images of common directional defects: broken pick, warp yarn defect, irregular weft density (insufficient). As we can see from figures, process is suitable for simulated images of directional defects.

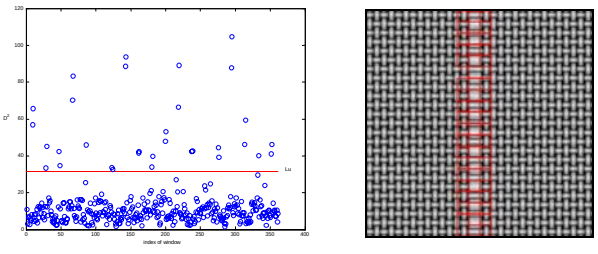

Fig. 1. Plot of individual observation against control limit.

Directional defect detection

The same algorithm was tested for the defects in real samples in a plain and twill weave. Images were captured by flat scanner with resolution 400 dpi in 256 grey levels and stored in an image matrix of size 500 x 500 pixels. Equalization was used for contrast enhancement. Figure 2 (d) – (f) show a few examples of recognition of defects in real structures. Examples represent real directional defects. Sliding window was setting to 50 x 50 pixels.

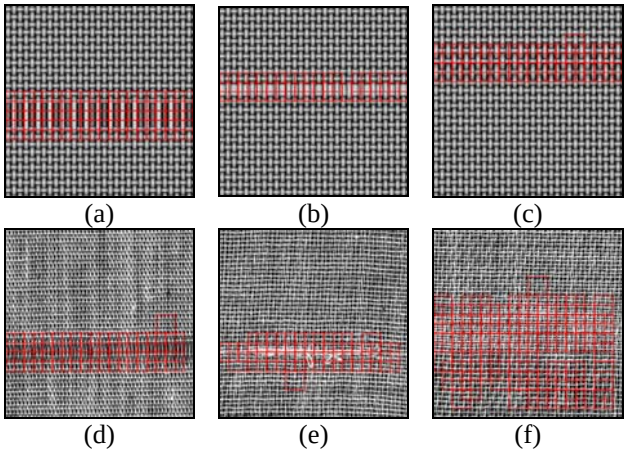

Fig. 2 Result of the applied algorithm, (a)-(c) in simulated samples, (d)-(f) in real samples, where red window indicate defect, imperfection.

Conclusion

Recognition algorithm based on second-order statistical features extracted from grey level co-occurrence matrix is useful for simulated samples of common woven fabric directional defects. By using this method we can detect defects associated with change of weaving density or defects that appear as a thick place distributed along the width or height of an image and for no directional defects too. The advantages of automated visual inspection are objectivity and independence on the human inspectors. This method is relatively fast and it could be used as online visual inspection of quality.

Acknowledgement: This work was supported by the project of MSMT CR No. 1M06047 and by the Czech Science Foundation under grant No. 106/03/H150.

References

[1] Haralick, R. M., Shanmugam, K., Dinstein, I.: Textural Features for Image Classification. *IEEE Transaction on Systems, Man. and Cybernetics*. Vol. 3 (6): 610 – 621. 1973..

[2] Carstensen, J. M.: Description and Simulation of Visual Texture. Ph.D. Thesis. Lyngby, Technical University of Denmark. 1992.

[3] Linka, A., Tunák, M.: Simulation and recognition of common fabric defects. *13. International Conference on Structure and Structural Mechanics of Textiles (STRUTEX 2006).* Liberec, 27.11.-29.11. 2006, pp. 363-370, ISBN 80-7372-135-X.

[4] Bersimis, S., Psarakis, S., Panaretos, J.: Multivariate Statistical Process Control Charts: An Overview. *Quality and Reliability Engineering International*. Published online in Wiley InterScience (www.interscience.wiley.com). 2006.

Příloha 7

[7] Kula, J., Tunák, M., and Linka, A. Real-time Quality Control of Fabrics based on Multivariate Control Charts. *World Journal of Engineering*, **7**(1), 2010, 9 pages. ISSN: 1708-5284.

Inspection system of fabric based on texture segmentation utilizing Gabor filters

Jiri Kula, Maros Tunak and Ales Linka

Abstract

In presented contribution we talk about our implementation of Gabor filters that we use for texture description and subsequent texture segmentation in order to obtain efficient method for detection of dissimilarities of fabric during its quality inspection process. Design of Gabor filter is presented both in spatial and frequency domain.

Introduction

There are many approaches in the development of automated system for quality evaluation of surface properties. In textile industry, one can most often see manual methods of inspection of quality of fabrics. This process involves human operator to watch the surface of material and mark the faulty areas by hand. Advanced loom machines are able to detect some faults by itself, however, there is still significant amount of defects, that needs to be inspected later, after the weaving stage. Those defects, that can not be detected on the loom, are particularly certain variations in the appearance of the product. Defects like broken pick or coarse yarn are sort of defects that can be detected directly on the loom. In contrast, those defects like appearance fault, a stain, a hole or a weft kinks, belong to class of defects that remain unnoticed by any other systems than the visual.

Gabor filter

Gabor filter is a finite impulse response filter first proposed by Gabor [2]. Generalized 2D filters are widely used in image processing for line and edge enhancement. Filters impulse response in spatial domain is defined as Gaussian envelope modulated by periodic function

$$g(x, y, \xi, \eta, \sigma, \theta, \lambda, \varphi) = e^{-\frac{X^2+\left(\frac{Y}{\gamma}\right)^2}{2\sigma^2}} \cdot e^{i\left(2\pi\frac{X}{\lambda}+\varphi\right)} \tag{1}$$

$$\begin{aligned} X(x, y, \xi, \eta, \theta) &= (x-\xi)\cdot cos(\theta) - (y-\eta)\cdot sin(\theta) \\ Y(x, y, \xi, \eta, \theta) &= (x-\xi)\cdot sin(\theta) + (y-\eta)\cdot cos(\theta), \end{aligned}$$

which means that the filter consists of real and imaginary parts, each of which is phase shifted by $\pi/2$.

Let's explain parameters of equation [1]. Since this article talks about digital implementation of filter, each of variables here are of discrete nature. The x, y refers to spatial domain, while ξ and η respectively, denote position of filter origin in (x, y) plane. The extent of Gaussian envelope is defined by σ for both axes, it's circularity is expressed with γ parameter that adjusts the

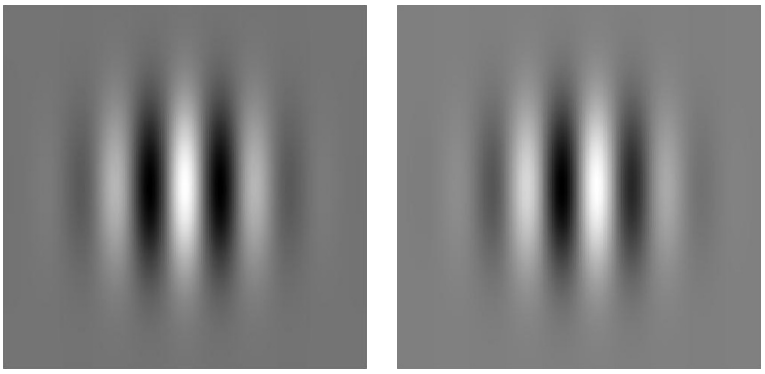

(a) (b)

Fig. 1: Gabor filter in spatial domain; (a) real (b) imaginary part.

extension of the filter along y axis. Another two properties of filter orientation and harmonic function phase are expressed by θ and φ value respectively. Phase offset explains the relationship between real and imaginary part of the filter. It is natural to write equations for both parts as equations [2] and [3]. Last parameter, λ refers to wavelength of harmonic function. Selected examples of filters built using various parameters are shown in Fig. 2. The sample images differ from image shown in Fig. 1.

$$g(x, y, \xi, \eta, \sigma, \theta, \lambda, \varphi) = e^{-\frac{X^2 + \left(\frac{Y}{\gamma}\right)^2}{2\sigma^2}} \cdot cos\left(2\pi\frac{X}{\lambda} + \varphi\right) \tag{2}$$

$$g(x, y, \xi, \eta, \sigma, \theta, \lambda, \varphi) = e^{-\frac{X^2 + \left(\frac{Y}{\gamma}\right)^2}{2\sigma^2}} \cdot sin\left(2\pi\frac{X}{\lambda} + \varphi\right) \tag{3}$$

Spatial filter is used for image convolution. However, this work deals with filtering images in frequency domain. In accordance to convolution theorem, filtering in frequency domain and convolution in spatial domain produce equivalent results, though. Operation of spatial convolution of digital image and its relation to convolution theorem is expressed in equation [4], in which symbols $f(x, y)$, $g(x, y)$, $h(x, y)$ denote input image of size $M \times N$ pixels, Gabor kernel of size $R \times C$ pixels and result of their convolution respectively, that is of 1×1 in size at (x, y) position. Also note, that lower case letter refers to spatial domain while capital denotes it's frequency representation using frequency coordinates u, v.

$$h(x, y) = f(x, y) * g(x, y) = \sum_{r=-\frac{R-1}{2}}^{\frac{R-1}{2}} \sum_{c=-\frac{N-1}{2}}^{\frac{C-1}{2}} g(c, r) \cdot f(x - c, y - r) \tag{4}$$

$$f(x, y) * g(x, y) \sim F(u, v) \cdot H(u, v) \tag{5}$$

Convolution of two signals can thus be obtained by multiplying the corresponding components of frequency representation of these signals. Gabor filter in frequency domain is defined by equation [6].

$$G(\Omega, \Theta) = e^{-(\frac{\theta - \Theta}{2\sigma_r})^2 - (\frac{\omega - \Omega}{2\sigma_t})^2} \tag{6}$$

Gabor kernel in frequency domain is a bandpass filter. The principle of using the filters in frequency domain consists of multiplying the spectrum of input image by a set of (non overlapping)

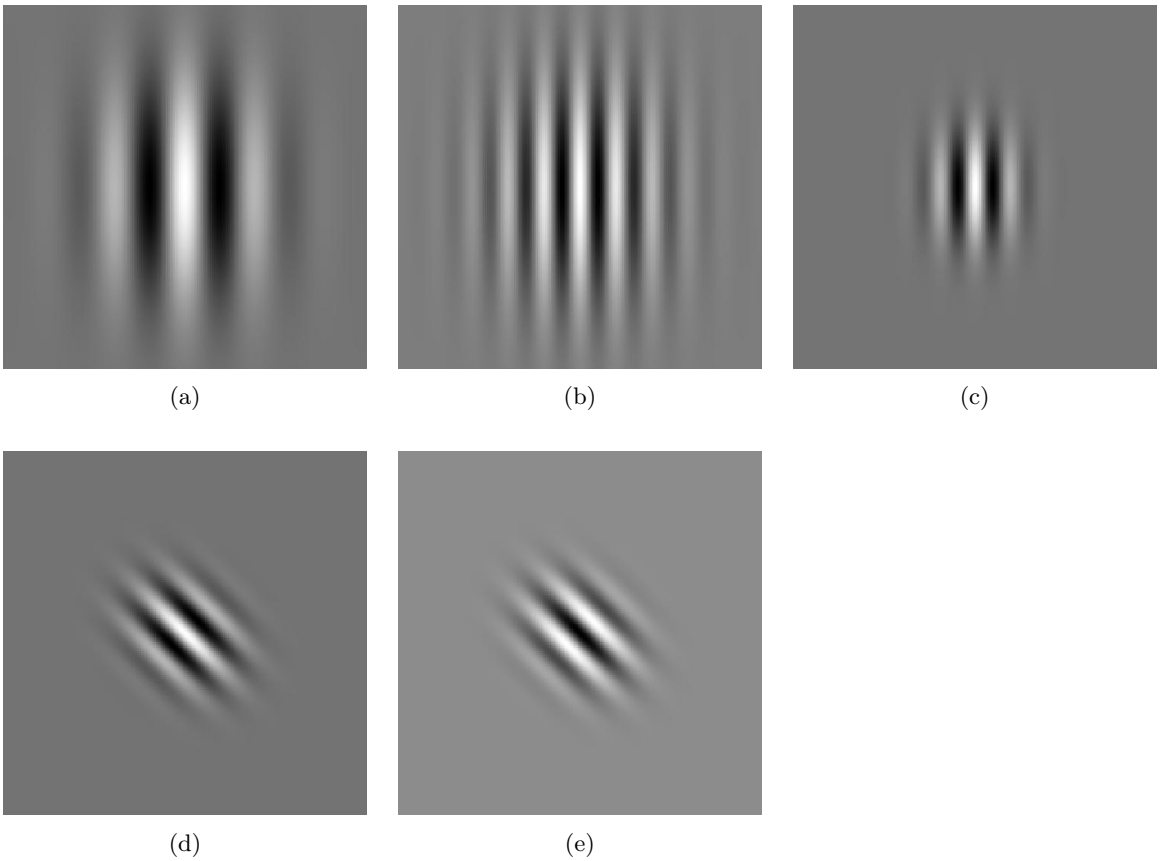

Fig. 2: Influence of various parameters; (a) increased aspect ratio γ ($\gamma > 1$), (b) reduced wavelength λ, (c) reduced extent σ, (d) non-zero rotation angle θ, (e) phase offset φ.

kernels that together cover the entire area of the spectrum. The frequency representation of spatial input image is obtained by Fourier transform with DC component shifted to the center of frequency space. It is appropriate to carry out the design of kernels in polar coordinates, which is consistent with the previous definition of the filter in equation [6]. Here the symbols ω, Ω denote frequency - while describing spectrum in polar coordinates - Ω equals the distance from center of the frequency space ω; Θ refers to angular distance of the origin of the kernel measured relatively to the horizontal axis; σ_a and σ_r denotes axial (frequency) and radial (orientation) bandwidths of the kernel. Construction of Gabor filter in frequency domain is illustrated in Fig. 3(a). Note that this illustration shows only the 1^{st} quadrant of frequency space.

Filters, like the one shown at Fig. 3, are constructed to cover the whole frequency space in such a way that meet certain criteria. There is considerable redundancy when adjacent filters overlap [3], which can be reduced by means of following filter design. Radial (angular) bandwidth σ_r is a constant value for the entire set of filters. Axial bandwidths of the filters are set one octave wide depending on the distance Ω of the filter from the origin O. Let's consider two different frequencies ω_0, ω_1 such that $2\omega_0 = \omega_1$. Then, the distance between these two frequencies is called to be one octave wide. Let's take the third frequency ω_2, which is twice as high as the second frequency: $\omega_2 = 2\omega_1 = 2 \times 2\omega_0 = 2^2\omega_0$. The distance between frequencies ω_0 and ω_2 is two octaves wide. It follows that the number of octaves k, that spread between two different frequencies ω_{min}, ω_{max}, is given by equation [7].

$$k = log_2 \frac{\omega_{max}}{\omega_{min}} \tag{7}$$

The value of i-th bandwidth $B_{a,i}$, in axial direction, equals to its lower frequency limit ω_i, as show in Fig. 4. The center of each filter is placed in the middle of i-th octave. In order to

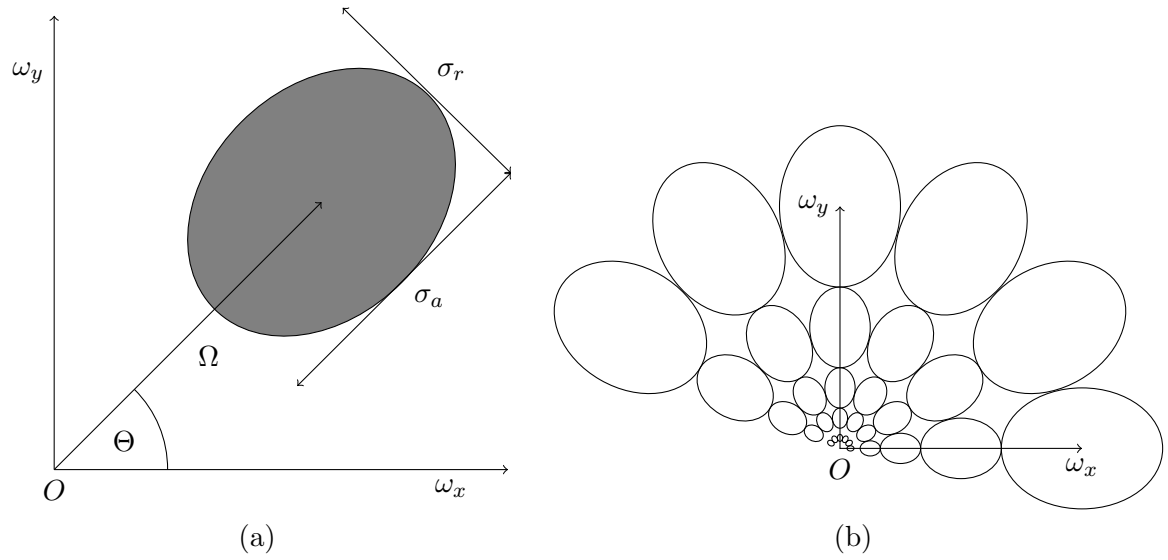

(a) (b)

Fig. 3: The design of Gabor filter in polar coordinates; (a) only the first quadrant of frequency space is visible, so that O is placed at the center of frequency space; (b) the frequency space is distributed into multiple channels by the set of Gabor filters.

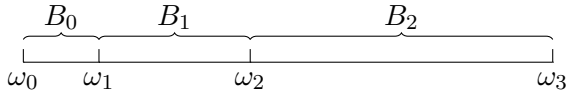

Fig. 4: Explanation of octave; w_i denote increasing frequency, B_i vales denote band width of respective octave. The width B_i or width of i-th octave equals w_{i-1}.

avoid redundancy produced by overlapping adjacent filter, their extents are designed so that neighbouring filters touch at half of filters peak value Filters take values between $< 0, 1 >$; the peak stands in the center of Gaussian and decreases outwards. The size of standard deviation in axial direction σ_a can be derived from Fig. 4, where the width of the i-th band is denoted B_i. Following equation (6) we get $e^{(-\frac{B_{a,i}/2}{2\sigma_a})^2} = 0.5$, thus, the i-th standard deviation in axial direction is given by $\sigma_a^i = \frac{B_{a,i}}{2\sqrt{2ln(2)}}$. The number n of filters is a constant value for all bands and it defines the bandwidth of the filter in radial direction $B_r = \frac{2\pi}{n}$. The size of the standard deviation in the angular direction is therefore also a constant, $\sigma_r = \frac{B_r}{2\sqrt{2ln(2)}}$.

Thanks to the symmetry of the Fourier spectrum about the origin, it is sufficient to perform the processing on only the half of the domain. At the moment of preparing bank of filters, it is therefore sufficient to include only the filters at angles between $< 0, (\frac{\pi}{2} - B_r) >$. Resulting filter bank for $B_r = 30°$ and octave count $k = 7$ is shown in Fig. 5. It is worth to mention how the filter bank is used during the process of texture description and segmentation. In textile industry, the inspection system has to deal with large images. In order to analyse them, the approach of local analysis is used instead of capturing global information about the input image that is acquired from the surface of fabric. Local analysis is carried out by means of dividing the area of input image into two dimensional rectangular sub ranges. The later analysis is performed within each range independently. This process is also called a tessellation of spatial domain. Within each range, the Fourier transform is carried out and then shifted so that the DC components appears in the center of spectrum domain. After that, each filter from the bank is used as a mask of given spectrum, in order to perform band pass filtering. In frequency domain, filtering is carried out by multiplying corresponding pixels of the spectrum and the filter. There are certain examples of filtering the input image by Gabor filters of various settings shown at Fig. 6. There are both the spectrum and the filter superimposed in odd rows and the result of filtering on even rows. The result here is presented as the inverse Fourier transform

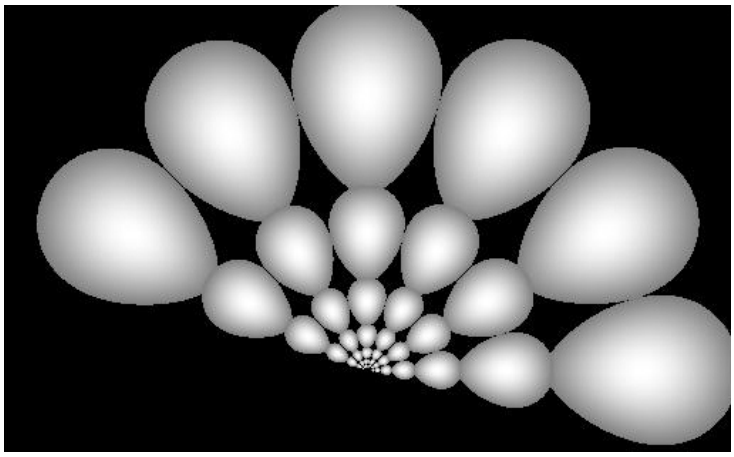

Fig. 5: A bank of Gabor filters.

of filtered spectrum. The special feature of Gabor filter, which lies in the fact that it gives information about certain frequency at specified orientation, is perfectly usable in conjunction with patterned textiles.

Gabor filters are used in this work for the task of detection of defects in woven fabric. The detection is based on principle of comparison of similarity between the reference texture and the texture being processed. The degree of similarity is expressed by calculating Euclidean distance between two vectors, each of which is describing features of the texture. Let's assume that there is a bank of 30 filters. When processing given spectrum, each of these filters is multiplied with this spectrum, resulting in 30 filtered planes. If we take the mean μ and standard deviation σ of the spectrum coefficients that remained after the filter was applied, we get two vectors $\vec{\mu}$, $\vec{\sigma}$. These two vectors, combined together so that their elements interlace, constitute a single vector that is treated as texture descriptor $\vec{v}$. The algorithm of detection takes two phases. The first phase consists of dividing the reference texture into multiple regions and determining the descriptor for each of these sub images. In case there is low variability in reference texture, which should be, we are able to calculate the mean of these vectors and treat it as a reference vector $\overline{r}$. A reference texture and its vector denote the texture that does contain no visible defect, and its vector respectively. There has to be a supervisor, that is responsible for definition of such reference area. The second stage consists of processing another texture while comparing its descriptor with the reference one. Reusing last example, there is a set or a bank of 30 filters, each of which has its Ω, Θ, σ_a, σ_r parameters. Filtering with this set of filters, we get vector $\vec{u} = (\mu_0, \sigma_0, \mu_1, \sigma_1, ..., \mu_{29}, \sigma_{29})$. Comparison of vector u with vector r yields the measure of similarity between the two textures. Elements of both vectors $\vec{u}$, and $\vec{r}$ are scaled into interval $< 0, 1 >$, thus the dissimilarity measure defined by equation (8) reaches zero for the similar and one for completely different textures.

$$s = \frac{1}{K}\sqrt{\sum_{i=0}^{K-1}(r_i - v_i)^2} \tag{8}$$

It becomes obvious that the similarity measure, defined by equation (8), of fabric texture that meets the specified visual appearance parameters, does not rise up from zero as much as the value that comes from defective area. The texture segmentation proposed in this paper is therefore based on the principle of thresholding. The threshold value for specific texture is set in the first phase also. After the reference vector was found, the area of reference image is divided again. The division into sub windows is random and maximum dissimilarity value found over these windows is taken as threshold value in later inspection.

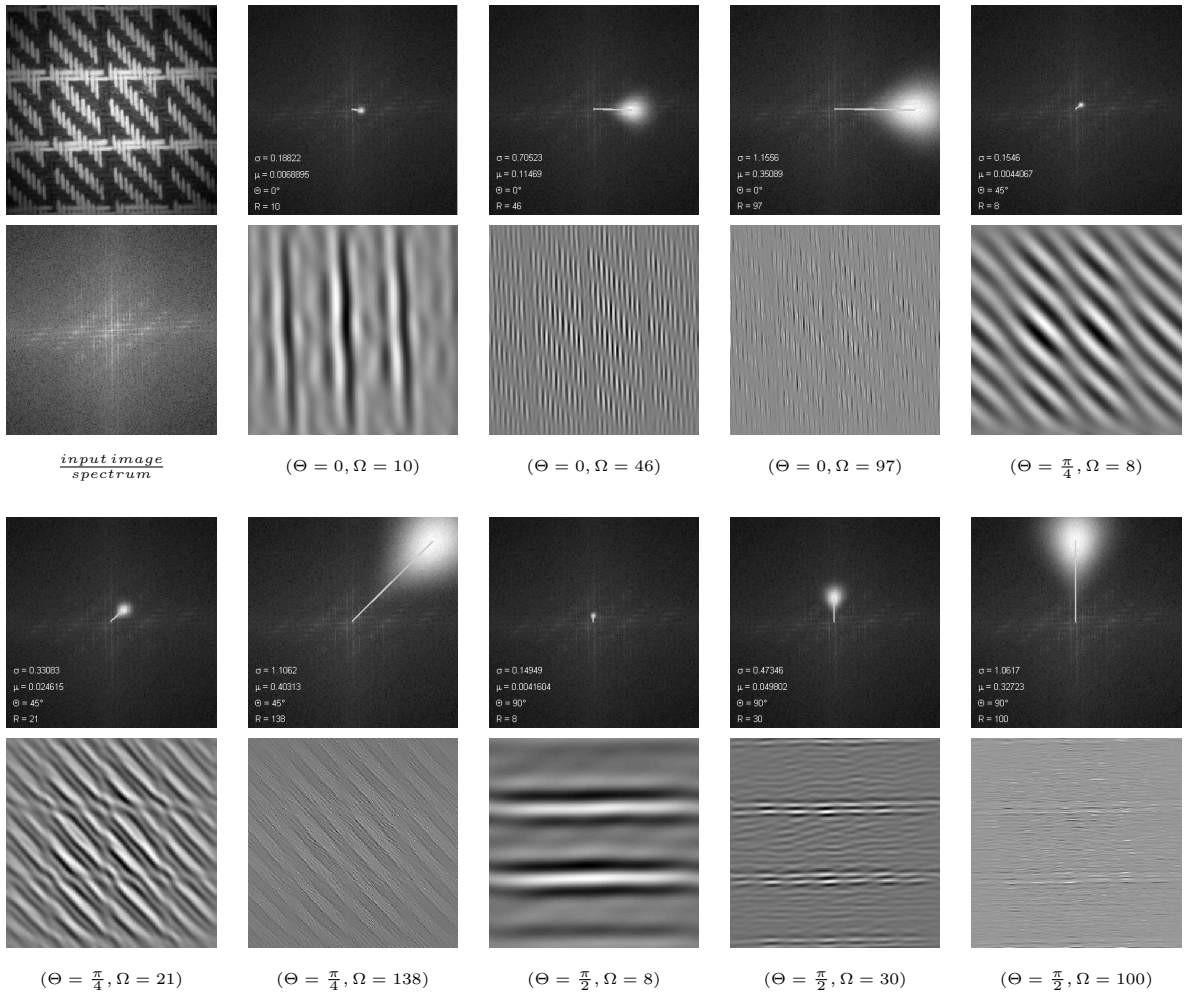

Fig. 6: Output of filtering the spectrum of an input image (see upper left corner) by various Gabor filters. Superimposed spectrum with the filter is show in the 1^{st} and the 3^{rd} row. There is also a radius vector printed on each image that connects the center of the spectrum plane with the origin of the filter. Pictures below show inverse Fourier transform of filtered spectrum.

Implementation

The performance of an algorithm, in the manner of accuracy, false alarm rate or speed, may differ significantly during a development process and under real world environment. In order to see how the system would work when deployed, it is implemented in software and it undergoes various tests on dedicated laboratory machine. There is no doubt that interpreted computer languages offer great productivity to software developers. However, these languages does not necessarily bring such great leap in productivity to applications themselves. It is reasonable to begin the development using a robust software tool like Matlab. Writing an application in Matlab will, in fact, result in managed application. Although the time spent on developing managed applications is relatively short, this is compensated by the slow behavior of programs during runtime, due to large number of idle operations and just-in-time compilation.

For manipulation with hardware devices and large sets of data that we encounter in image processing, it is suitable to implement the software with native programming language that is compiled directly into processor instructions. Such a program runs directly on the architecture, for which it is built for, without unnecessary overhead. Besides implementing the Gabor filter with *C++* language, we have built a special machine that consists of endless strap of inspected fabric, DC motor and array of line scan cameras. In order to handle all aspects of relatively

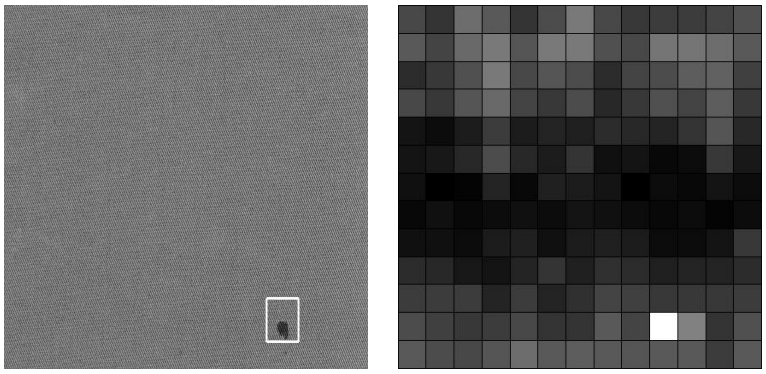

(a) (b)

Fig. 7: Implementation of texture segmentation utilizing Gabor filters; (a) image of woven fabric which shows a defect, (b) rectangular grid responses the filtering at each sub range, dissimilarity is displayed with gray level scope in which the dark areas denote high similarity whereas white rectangle highlights significant dissimilarity between the reference texture and the texture at the current rectangle.

complicated system of hardware synchronization, data acquisition, image processing and result presentation, while maintaining the platform sufficiently modular, we based our software solution on *DirectShow*, *COM* and *ATL* architectures. The solution we develop is standard Windows application that serves as a host for independent software components. The host application allows for connecting components in various orders, thus constituting form of a graph, a chain or a diagram. Each component is also called a filter and it shows itself as blocks in the graph, bearing connection points called pins. Through these pins the filters connect. After the connection is established, it represents a video and or arbitrary data pathways. Presented approach allows almost infinite number of ways to design the algorithm of image processing during runtime without the need to modify source code and re-compile. Finished topology also gives a visual picture of the operations that are applied to the data. Changing one filter does not have any influence on the rest of the graph. Most of these features are inherited from the *DirectShow* architecture. Filters themselves are *COM* components. The *COM* stands for Component Object Model, a binary protocol for language independent, location transparent, object oriented architecture that allows for cooperation among various pieces of software. Neither the programming language, nor the physical location of the binary is important when programming for this model. Active Template Library, or ATL, simplifies COM development by providing a set of template classes, thus reducing the amount of code that would otherwise be necessary to write by hand.

Current implementation allows for displaying the plot of dissimilarity index over entire input image. An example of such plot is shown in Fig. 7. There is a woven fabric show on the left. The defect of oil staining appears as a dark spot in lower right corner of Fig. 7(a). It is automatically detected and market in accordance with the proposed procedure of texture segmentation. Taking a look inside of the procedure, we can extract the dissimilarity values over the inspected area, which is shown in Fig. 7(b). Main window of application is depicted in Fig. 8(a). It contains a typical graph in which acquired images of whole fabric are taken by the array of line scan cameras. As the acquisition completes, these separate images are merged into a single one by Multiplexor filer. Merged data are delivered downstream to the Gabor filter component. Gabor filter outputs the video unchanged and adds the information about locations of detected defects on separate pin. Another downstream filter accepts both of these types of data and it draws rectangular markers around each defect. These markers are displayed as a result on computer display. Additional option is to insert data into database and explore them off-line. Fig. 8(b) shows three examples of certain components . Input pins are placed on the left, whereas output pins occupy the right side of the filter.

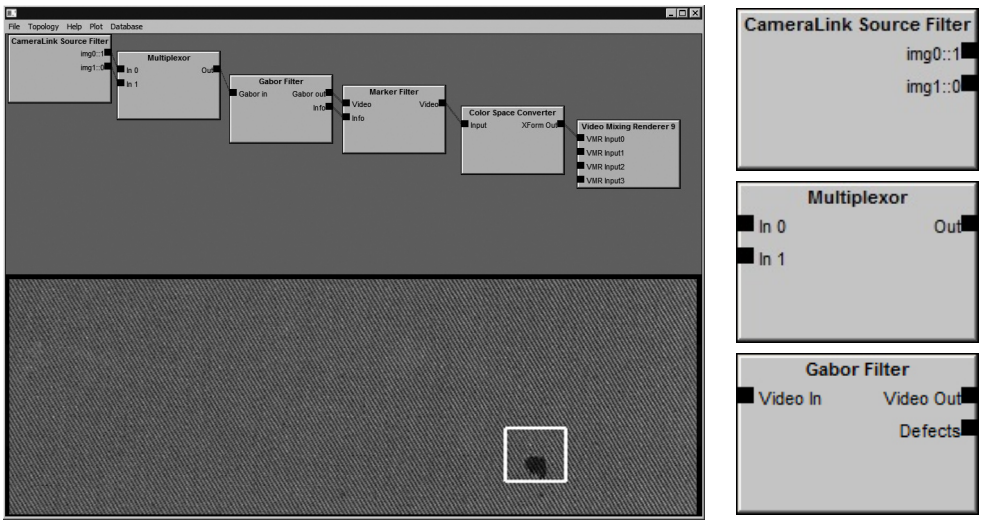

(a) (b)

Fig. 8: Software implementation of inspection system for fabric; (a) application's main window is horizontally divided into two parts that display the data flow of current processing pipeline and the result of detection, (b) selected filters show general design of processing components.

Conclusion

Gabor filters were implemented both in spatial and frequency domain. Application of filters in frequency domain was used for calculation of similarity between a set of different textures. The principle of similarity estimation was also used for inspection of woven textiles in terms of defect detection and localization. In order to evaluate the possibility of deploying Gabor filters for surface inspection under real conditions, we built dedicated laboratory device. The device acquires digital image of moving fabric surface with an array of line scan cameras. Image is provided to software and processed in real-time. The application provides a robust platform for high performance software component, which implement specific task and allows connection of these components into comprehensive processing pipeline. Gabor filters, implemented in such environment, proved itself to be suitable method of inspection in real-time with sufficient accuracy on certain types of visible defects.

References

[1] Teifelova, M., Detection of defects of woven fabric using Gabor filters. Dimploma thesis, Technical University of Liberec, Faculty of Textile Engineering, 2010.

[2] Gabor, D., Theory of communication. In *J. IEE*, Vol. 93, London, 1947, pp. 429-457.

[3] Bianconi, F., Fernández, A., Evaluation of the effects of Gabor filter parameters on texture classification. *Pattern recognition*, Vol. 40, 2007, pp. 3325-3335.

[4] Bodnarová, A., Bennamoun, M., Latham, S., Optimal Gabor filters for textile flaw detection. *Pattern recognition*, Vol. 35, 2002, pp. 2973-2991.

[5] Petrou, M., Sevilla, P., *Image Processing Dealing with Texture*, 1 st ed.; Wiley, England, 2006.

[6] Gonzalez, R., Woods, R., Eddins, S., *Digital Image Processing using Matlab.*, 1 st ed.; Pearson Prentice Hall, USA, 2004.

Příloha 8

[8] Kula, J., Tunák, M., and Linka, A. Inspection System of Fabric based on Texture Segmentation utilizing Gabor Filters. *World Journal of Engineering*, **7**(1), 2010, 8 pages. ISSN: 1708-5284.

REAL-TIME QUALITY CONTROL OF FABRIC BASED ON MULTIVARIATE CONTROL CHARTS

Jiri Kula, Maros Tunak and Ales Linka

Faculty of Textile Engineering, Technical University of Liberec
Studentska 2, 461 17 Liberec, Czech Republic
E-mail: jiri.kula@tul.cz / maros.tunak@tul.cz / ales.linka@tul.cz

Abstract

This contribution deals with a procedure of monitoring fabric production process in terms of defect detection. Detection algorithm is based on spectral approach with 2D Fourier transform, which has shown to be suitable method of describing periodic and almost periodic structure of fabrics. Multivariate control charts are used as a tool for monitoring several quality variables. In order to make an off-line and on-line quality monitoring of fabrics possible, we built up a prototype machine, which consists of aluminium frame, DC motor, LED lights and a line scan camera. Fabric width is $50cm$ and maximum winding speed of about $16m/min$ can be achieved. The core of detection algorithm utilizes relatively time consuming Fourier analysis, so we split an acquired image into independent parts and let the work be done concurrently. Writing native, multi-threaded and scalable code, that takes advantage of modern multi-core machines, is one of our main objectives. Based on *Visual C++* language and additional libraries, we are able to to check $1m^2$ of fabric in about 1.5 second on *Intel Core2 Quad CPU*. We use *OpenCV* library together with *Intel Threading Building Blocks* templates for the most part.

1 Introduction

Quality control has gained major importance in today's manufacturing process. In textile industry especially, the monitoring is still performed by human observation. This process involve a group of workers repeatedly checking the product many times again. The human visual inspection makes the final product much more expensive, moreover, such way of control does not achieve more than 70% of all defects to be detected. Goal of our research is to investigate and develop new algorithms for the detection of defect in textured materials (textiles) using automated visual inspection. These algorithms are expected to offer high detection rate with low level of false alarm.

Fabric is, as a rule, composed of two sets of mutually perpendicular and interlaced yarns. The weave pattern of basic unit of the weave is periodically repeated throughout the whole fabric area with the exception of the edges. Due to the periodical nature of woven fabrics, their images are homogeneously structured and can be considered as texture images. Considering the periodic nature of fabric, we are able to describe the relationship between the regular structure of woven fabric in spatial domain and its Fourier spectrum in the frequency domain. The directional feature of periodical structure of woven fabric correspond to high energy frequency component in the Fourier spectrum. Therefore, the Fourier transform seems to be appropriate for graphical representation of planar anisotropy of images in spatial domain, as it is shown *Tunak & Linka (2007)*. A presence of defect in this periodical structure causes changes in periodicity and consequent changes of spectral features.

In his paper, we especially focus on recognition of common directional defects associated with the change of weaving density or defects that appear as a thick place distributed along the width or height of an image. The method will be illustrated by certain examples of analysis of real fabrics with various defects. The basic principle of detection method lies in estimation of periodic characteristics over the entire fabric sequentially by a concept of sliding window. At each step, statistical comparison is performed in order to recognize those parts that contain defects. Multivariate statistical process control is used to

make such decision. Other approach, e.g. statistical approach based on second-order statistical features extracted from a grey level co-occurrence matrix for automatic detection of defects in woven fabrics can be found in *Tunak & Linka (2008)*.

Aim of the final quality inspection of woven fabric is efficient detection and localisation of defective regions. Multivariate statistical process control as a technique for monitoring of multiple quality variables simultaneously, with the aid of Hotelling's multivariate control charts, is used for automatic detection.

In addition to development of algorithms for defect detection in textiles, we constructed a special laboratory device that allows us to acquire the image of moving fabric. This device, among the other parts, consists of line scan camera, step motor and associated PC that takes care about the control of these devices and that performs overall data processing. In this article, we also explain some fundamental concepts that make the on-line process control possible.

2 Two Dimensional Discrete Fourier Transform

The spectral approach is based on two-dimensional discrete Fourier transform (2D DFT). The Fourier spectrum is ideally suited for describing the directionality of periodic or almost periodic patterns in grey level images of textures. Let $f(x, y)$ be a two-dimensional function, where $x = 0, 1, 2, ..., m - 1$ and $y = 0, 1, 2, ..., n - 1$, are the spatial coordinates and the amplitude f at any pair coordinates is the grey level of the image of size *m* x *n*. The 2D DFT of $f(x, y)$ is given (*Gonzales & Woods (2002)*)

$$F(u, v) = \sum_{x=0}^{m-1} \sum_{y=0}^{n-1} f(x, y) e^{-j2\pi(\frac{ux}{m} + \frac{vy}{n})} \tag{1}$$

where $u = 0, 1, 2, ..., m-1$ and $v = 0, 1, 2, ..., n-1$ are frequency variables. The *dc* (direct current) component is the origin of frequency domain $F(0, 0)$ and represents the origin of the system of frequency coordinates. If $f(x, y)$ is real, its transform is, in general, complex. The *power spectrum* is defined as the square of magnitudes

$$P(u, v) = |F(u, v)|^2 \tag{2}$$

In order to display and analyse the *power spectrum* visually, it is convenient to reduce dynamic range of coefficients by *logarithmic transformation*

$$Q(u, v) = log(1 + |F(u, v)|^2) \tag{3}$$

A typical woven fabric consists of two, mutually perpendicular arrays of yarns. The resulting periodic structure can be nicely seen in both an image of spatial domain, even in an image of frequency domain. It is also true, that any defect in weft or warp direction causes serious disorder in such periodic structure, and as a consequence, takes significant effect in distribution of Fourier spectrum coefficients.

3 Anisotropy of Fiber Systems

One of the common operations of image analysis is called a segmentation. The purpose of segmentation is to split the information captured by the image into logical parts that have close relation to objects of a real world. These objects are either randomly distributed on the image background or they prefer certain directional placement. In textile experience, the objects are considered to be fibers, threads and cross-sections of fibers. Complex systems built of these basic objects can be represented by webs, fibre layers, woven fabrics, knitted fabrics, non-woven textiles etc.

In our implementation, we consider a grey scale image to be a square matrix of size *m* x *m*. It is convenient to let *m* be an odd number for correct definition of the center of the Fourier spectrum. All

frequency components from the Fourier spectrum are summed in the directional vector of certain angle α. Since the transformation of real image function $f(x, y)$ results in complex coefficients, the absolute magnitudes of frequency components $|F(u, v)|$ are obtained according to relation (**??**). The sum of frequency components S_α in the directional vector is given by

$$S_\alpha = \sum_{i=1}^{(m+1)/2} |F(u, v)|_i \tag{4}$$

where α forms an angle between the directional vector and u axis, $|F(u, v)|$ is a frequency component of the directional vector at the coordinates (u, v) and m is the size of the image. The Bresenham's line algorithm is used to estimate coordinates of corresponding matrix elements.

4 Defect detection

4.1 Multivariate control charts

The objective of our work consists of efficient detection and localization of defective regions in the image of fabric, which is important part of quality control. Because exploring each quality feature individually could lead to inadequate results, we decided to keep track of multiple variables simultaneously. The process of observing several quality features together is known as multivariate statistical process control. Hotelling's multivariate control charts, which are a direct multivariate equivalent of the Shewhart $\overline{X}$ charts (based on Mahalanobis distance) for the process mean, are useful tool that integrates multiple texture features and help judge the presence of defects.

We assume, that the observations come from p-dimensional normal distribution with known mean vector $\boldsymbol{\mu}$ and known variance-covariance matrix $\boldsymbol{\Sigma}$. Then the test statistic D^2 for i-th individual observation has the form (*Bersimis et al. (2007), Zamba & Hawkins (2006)*)

$$D_i^2 = (\mathbf{X}_i - \boldsymbol{\mu})^T \Sigma^{-1} (\mathbf{X}_i - \boldsymbol{\mu}) \tag{5}$$

where $\mathbf{X}_i$ is the i-th, $i = 1, 2, ..., m$, observation that comes from p-dimensional normal distribution $N_p(\boldsymbol{\mu}, \boldsymbol{\Sigma})$. In real situation we often face the problem, that mean vector $\boldsymbol{\mu}$ and variance-covariance matrix $\boldsymbol{\Sigma}$ are not known in advance. Therefore we obtain the data $\mathbf{X}_j$, $j = 1, ..., n$ while the process is in statistical control. We consider these data to be a random sample from a p-dimensional normal distribution $N_p(\boldsymbol{\mu}, \boldsymbol{\Sigma})$, where $\boldsymbol{\mu}$ and $\boldsymbol{\Sigma}$ are unknown. Sample mean and sample variance-covariance matrix of this distribution are defined

$$\overline{\mathbf{X}} = \frac{1}{n} \sum_{j=1}^{n} \mathbf{X}_j \tag{6}$$

$$S = \frac{1}{n-1} \sum_{j=1}^{n} (\mathbf{X}_j - \overline{\mathbf{X}})(\mathbf{X}_j - \overline{\mathbf{X}})^T \tag{7}$$

where $\overline{\mathbf{X}}$ and S are unbiased estimates of $\boldsymbol{\mu}$ and $\boldsymbol{\Sigma}$. Then the test statistic for an observed vector $\mathbf{X}_i$ is

$$D_i^2 = (\mathbf{X}_i - \overline{\mathbf{X}})^T S^{-1} (\mathbf{X}_i - \overline{\mathbf{X}}) \tag{8}$$

For later process control, that follows the initial calibration of control charts from a "learning sample", we define the upper control limit as

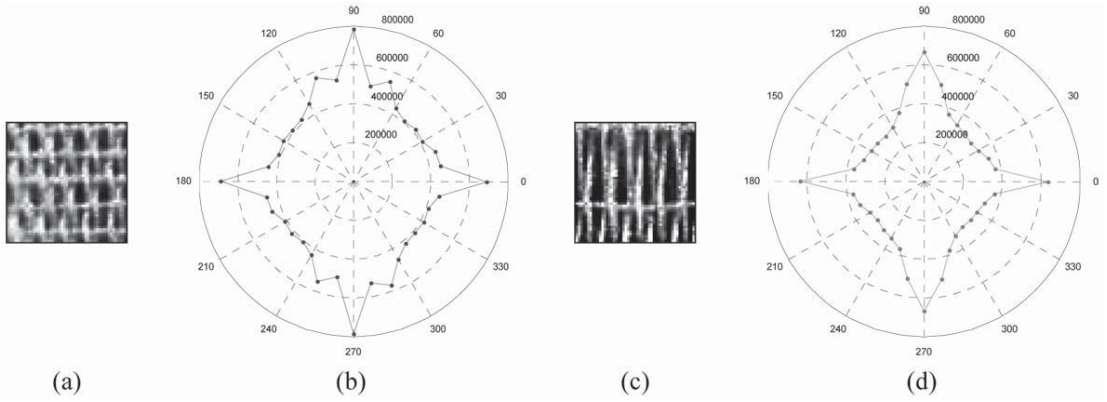

Fig. 1: (a) Window with non-defective area, (c) window with defective area, (b),(d) polar plots of S_α in 10 degree step.

$$UCL = \frac{p(n+1)(n-1)}{n(n-p)} F_{p,n-p}(1-\alpha) \tag{9}$$

where $F_{p,n-p}(1-\alpha)$ is the $(1-\alpha)$ percentile of the F-distribution with p and $(n-p)$ degrees of freedom. In case of D_i^2 statistic exceeds the upper control limit at specified level of significance α, then the observation is considered to be out of control.

4.2 Defect Detection using Multivariate Control Charts

We consider values of S_α obtained from image of fabric as a vector of features $\mathbf{X}_i$. These features can be used for evaluation of material homogeneity and searching for random imperfections in regular structure. Images of the same or identical structure would have similar shape of estimated rose of direction, i.e. almost the same values of S_α. On the other hand, image of structure with defective area would have different shape of polar plot of S_α. This idea, supported by multivariate control charts, can find its application of defect detection inside of a real structure.

Figures 1(a),(c) display windows of 50x50 pixels taken from regular and defective parts of the source image (see Figure 4(g). Corresponding polar plots of S_α with the 10 degree step obtained form equation (9) can be seen in Figure 1(b),(d). Difference in shape of these polar plots is obvious.

At the beginning, values of S_α are captured using 10 degree step over 1000 randomly selected sample windows in a defect free area. As a result we get data matrix with $n = 1000$ samples of $p = 18$-th dimensional normal distribution. Then the upper control limit given by formula (9) for a level of significance $\alpha = 0.001$ is evaluated. Monitoring of fabric area is based on sliding window moving systematically over the whole image area. The step between subsequent windows is half their size so they fully overlap. For every window, i-th test statistic is evaluated using Mahalonobis distance from equation (8). Then the distance is compared with given *UCL*. If any observation exceeds the limit, the window is considered to be at the position of significant defect.

Example in Figure 2(a) represents image of real woven structure containing defect, concretely insufficient weft density. Figure 3(c) shows the plot of *i*-th test statistic against the upper control limit. Result of detection algorithm can be seen in Figure 2(b), where the marker windows represent defective areas. In order to get even better idea, Figure 2(d) shows polar plots of S_α with the step of 10 degrees, where the dark curves represent the windows with regular structure and grey curves highlight the windows where the structure does not match given criteria. Similarity in shape of polar plots can be seen for

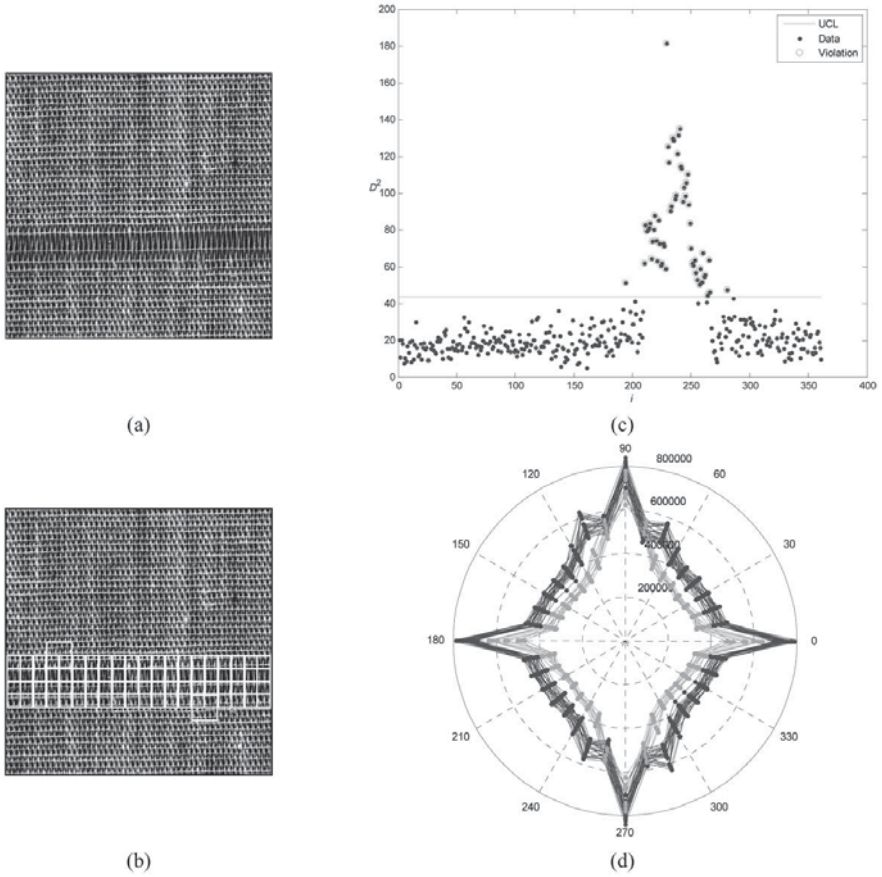

Fig. 2: (a) Defect in real structure, (b) results of detection algorithm, (c) plot of i-th test statistic, (d) polar plots in 10 step.

non-defective structure, whereas the shape of polar plots of defective structure differ significantly. More examples of defects in real structures after the application of detection algorithm can be seen in Figure 3, namely (a) foreign body, (b) double pick, (c) warp yarn defect, (d) snarl, (e) abrasion mark, (f) broken warp yarn.

It will be reasonable to devise an optimized method, which defines appropriate parameters for a given structure in terms of size of a sliding window. Figure 4(b)-(l) displays result of applied algorithm for detection of irregular weft density with various sizes of sliding windows.

5 Hardware

The algorithm that we talked about so far, was developed inside of Matlab using static images for purposes of fine tuning and testing. However, any algorithm that performs well in laboratory conditions may fail easily when applied in an industrial environment. For that reason we decided to build a laboratory device that would imitate production conditions by acquiring an image of moving fabric and applying the algorithms on-line. The experimental machine consists of aluminium frame, DC motor, LED illumination and a line scan camera. It's intended for repeated winding of endless strap of fabric, and thus to represent the behaviour of continuous process.

The apparatus is formed by a modular aluminium frame. A strap of a fabric can be up to $50cm$ wide

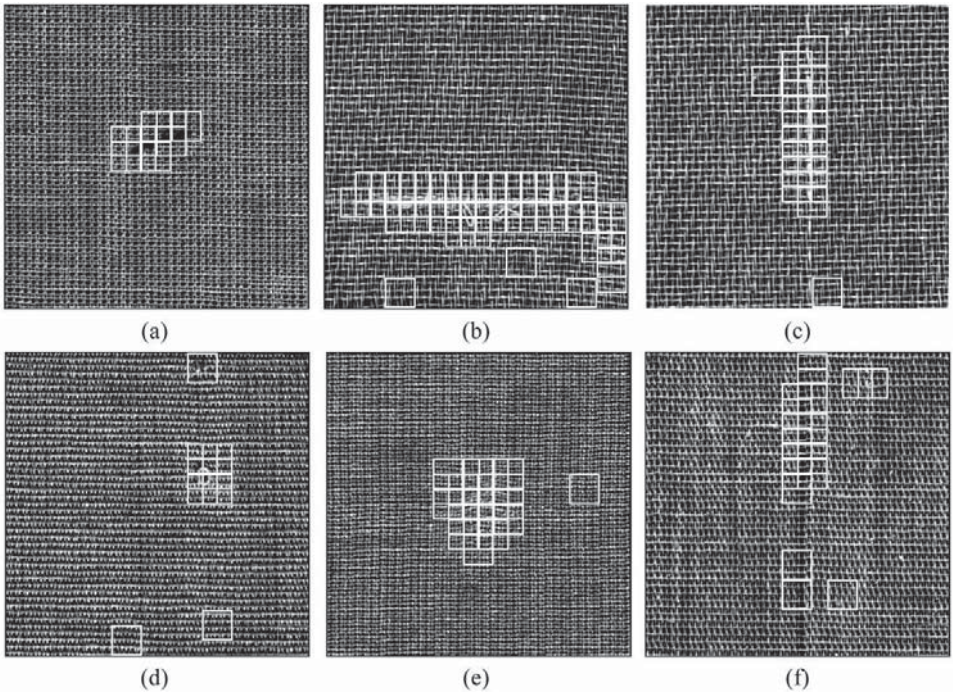

Fig. 3: Results of detection algorithm in real structures.

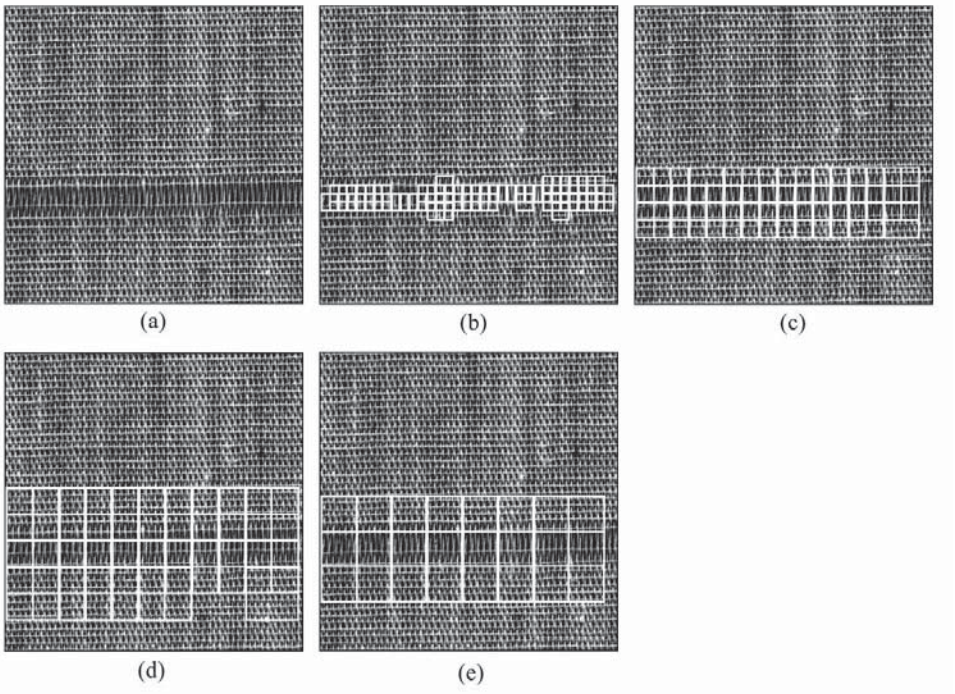

Fig. 4: Results of detection algorithm in real structures with different size of sliding window, (b) 30, (c) 60, (d) 90, (e) 120 pixels.

and over $2m$ long. There is a roller on each side that keeps the fabric straight. Thanks to the modular design of the frame, replacing the strap is quite easy, so various types of fabrics can be observed without too much effort. One major property of such design has its advantage that turning this laboratory device into industrial equipment consist only in mounting the camera on top of current inspection tables in the factory. No other modification would be necessary.

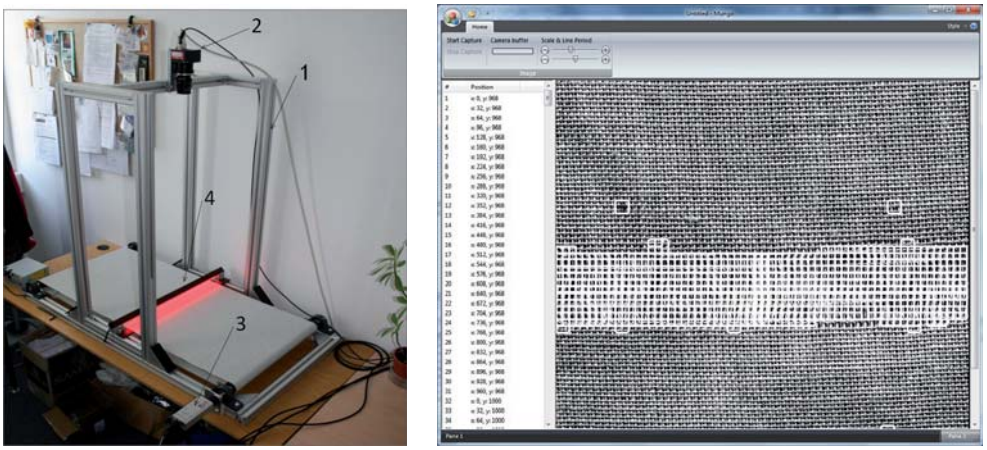

(a) (b)

Fig. 5: Laboratory device: (a) assembly; 1-frame, 2-line scan camera, 3-DC motor, 4-light array, (b) Application window.

One of the roller is driven by fully programmable *Maxon MCD EPOS 60W* motor. We use the cycle count property to track current position of the strap. The information about location of a defect is especially important for the serviceman who can make the appropriate correction short after the process has run out of control.

Image acquisition is performed using the monochrome *Basler L401k* line scan camera. It's line resolution is $4080px$, so that *8* pixels cover $1mm$ of fabric. Maximum line frequency $7.2kHz$ yields the theoretical top speed of about $46m/min$ with current optics and overall setup. However, real winding speed is limited by lightning conditions, fabric properties and mostly, by the complexity of data processing, rather than by technical parameters of each of hardware component. Camera's exposition time, line period, gain control and many other properties are exposed to the application and therefore can be modified on demand at runtime.

Although the on-line control has continuous nature, we have to divide the process into discrete portions by acquiring image into circular buffer. This concept comply with working principle of line scan cameras. By using line scan camera, one gets just a single row of the whole image at a time. In order to get the final image, subsequent rows need to be aligned into 2D array from capturing buffer. Ones we have a portion of a fabric acquired, we can run the image processing and analysis stage. Although this principle may involve serial processing, which would lead to serious problems in on-line control, there is a way not to waste the available computing resources, as described in Fig. 6. The image acquisition stage takes long time to complete. Specifically it takes image's *vertical resolution* multiplied by camera's *line period* seconds. Serial program would wait for that time idling and then, as the image buffer gets filled by data, it would perform the analysis. But the image acquisition would be forced to wait during analysis stage while the motor would need to stop as well. If the movement did not stop, the application

would leave some part of fabric undetected. There is relatively easy solution to this particular problem that splits an acquisition and a processing into separate tasks and allows them to run in parallel.

6 Software

From the software perspective, we develop a standard *Windows MFC* application. There have been a lot of approaches to implement an automatic machines for control of quality characteristics in fabric. Despite these attempts, most implementations are either too simple and week or extremely expensive. Algorithm that is based on Fourier transform takes a lot of time to complete, so one could say that it's not much suitable for on-line processing. Anyway we see this approach robust and promising enough. The programming language we use is purely native *Visual C++* that executes much faster than interpreted *Matlab* code. There is also a user interface that inherits from *Windows 7 Ribbon* design which allows quick and intuitive control over the on-line quality control process. The client area of the application's window is divided into two panes which logically relate to each other. There is a list of detected defect in the left side. Each item in this list contains an information about defect location and size. These items are references to the fabric preview pane on the right side of the window (Figure **??**). Here a user can see the image of the textile together with visually highlighted defects. The application takes care about the control of the two major devices - motor and camera. Since the camera is line scan, the velocity and the line period has to be synchronized carefully in order to get undistorted image. The *OpenCV* library is used widely for image manipulation, processing and matrix operations.

Our aim is to produce cheap and commonly available, yet powerful equipment for quality control in the factory of any size, so we build the system using standard PC. Despite of availability and low cost of these machines, their powerful processors come equipped with at least two or four computational cores these days. Our algorithm for defect detection is based on spectral analysis in such a way that the whole image is divided into mutually independent sub-windows. We find the 2D Fourier spectrum inside each of these separate parts and by summing the frequency components in different directions we get a vector of desired characteristics. Then, we estimate the Mahalonobis distance of these characteristics from the reference vector and consider the value as a measure of structure irregularity. Since all the computations within every window are mutually exclusive from other windows, it allows to run the computation in different locations concurrently. Although parallel programming is much more challenging than development of a traditional serial program, well designed algorithm is able to fully extract the computational power of multi core processor. We have obtained a linear speed up with respect to increasing number of available processor cores. *Intel Threading Building Blocks* templates were used for writing the parallel

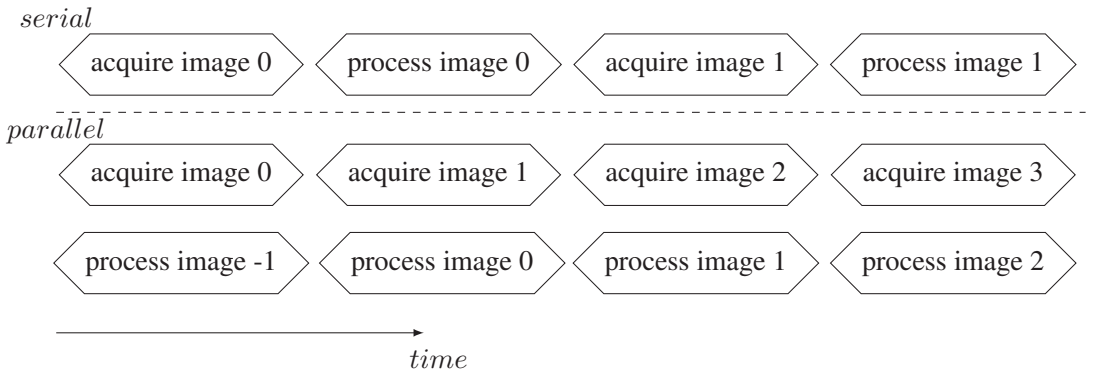

Fig. 6: Image acquisition and analysis cycle.

algorithm that can check $1m^2$ in about 1.5 second so far, running on *Core 2 Quad* processor.

7 Conclusion

Building a system of automatic visual quality control, that would support or even replace the quality control provided by human observation, is a complex problem that still provide enough topics for research. Although there are suitable control systems for paper, wood, steel and drug production industry, observation and reliable defect detection systems for textiles are still quite rare. There are two major aspects that make the inspection difficult for textiles. The first we mention lies in wide diversity of textile fabrics in terms of weaving and printing patterns. The products itself is of inhomogeneous structure that tends to tilt, stretch, etc. The algorithm has to be robust against the mistakes that can arise from such diversity. Together with robustness there comes complexity that affects the speed of execution, which is crucial in on-line quality control.

In our work we have implemented own algorithm for defect detection based on Fourier analysis. The algorithm was tested with woven fabrics that proved the algorithm to be highly sensitive to random irregularity in periodic structure. We also build a prototype machine that allows us to apply new algorithm under real conditions.

Acknowledgement

This work was supported by the project of MSMT CR No. 1M06047 (Center of Quality and Reliability of Production).

References

[1] Tunak, M., Linka, A. Directional Defects in Fabrics. *Research Journal of Textiles and Apparel*, 2008, Vol.12, No.2, pp.13-22.

[2] Gonzales, R.C., Woods, R.E. *Digital Image Processing*, 2002, 2nd edition, Prentice-Hall.

[3] Tunak, M., Linka, A. Analysis of Planar Anisotropy of Fibre Systems by using 2D Fourier Transform. *Fibres & Textiles in Eastern Europe*, 2007, Vol.15, No.5-6 (64-65), pp.86-90.

[4] Bersimis, S., Psarakis, S., Panaretos, J. Multivariate Statistical Process Control Charts: An Overview. *Quality and Reliability Engineering International*, 2007, Vol.23, No.5, pp.517-543.

[5] Zamba, K.D., Hawkins, D.M. A Multivariate Change-Point Model for Statistical Process Control. *Technometrics*, 2006, Vol.48, No.4, pp.539-549.

[6] Bradski G., Kaehler, A. *Learning OpenCV*, 2008, 1st edition, O'reilly

[7] Reinders, J. *Intel Threading Building Blocks*, 2008, 1st edition, O'reilly

Errata

str. 7 j - imaginární jednotka

str. 13 Obrázek 2.6 (c),(d)

str. 13 (Příloha 8)

str. 14

$$\overline{\mathbf{X}} = \frac{1}{m}\sum_{i=1}^{m}\mathbf{X}_i,$$

$$\boldsymbol{S} = \frac{1}{m-1}\sum_{i=1}^{m}(\mathbf{X}_i - \overline{\mathbf{X}})(\mathbf{X}_i - \overline{\mathbf{X}})^T$$

str. 14 UCL - Horní regulační mez
Data - data
Violation - překročení mezí

str. 22 Φ - autokorelační koeficient prvního řádu

str. 25 ... síla působící na každé vlákno ...